

SYNTHESIS AND OPTIMIZATION OF A MODEL SYSTEM
REPRESENTING THE NATURAL PRODUCT MARINEOSIN A AND
DISCOVERY OF VU0431316, A NEGATIVE ALLOSTERIC
MODULATOR OF THE METABOTROPIC GLUTAMATE RECEPTOR 5

By

Brittney Shaye Bates

Thesis

Submitted to the Faculty of the
Graduate School of Vanderbilt University
in partial fulfillment of the requirements
for the degree of

MASTER OF SCIENCE

in

Chemical and Physical Biology

December 2013

Nashville, Tennessee

Approved:

Craig W. Lindsley, Ph.D.

Gary A. Sulikowski, Ph.D.

Stephen W. Fesik, Ph.D.

*“For I know the plans
I have for you,” declares the Lord,
“plans to prosper you and not to harm you,
plans to give you hope and a future.”*
Jeremiah 29:11

ACKNOWLEDGEMENTS

First of all, I would like to thank my advisor Craig Lindsley for the opportunity to work in his lab. I am truly blessed for being able to work with Craig and am thankful for his continued support and help along the way. I would also like to give a special thanks to Kyle Emmitte, who has been a wonderful mentor and friend. I am grateful for all of your support and advice. Thank you to my committee members, especially Gary Sulikowski and Steve Fesik for your instruction and encouragement.

Next, I want to acknowledge all of my lab mates, past and present. A special thank you to Andrew Felts for training me in the lab and for, of course, always giving me a hard time. I value every relationship with my colleagues and want to thank all of you for your efforts to help me in my endeavors. I have made many life-long friendships, and for that I am forever grateful. A special thank you to the few of you who will ever actually read this document in its entirety.

Last, but certainly not least, thank you to my wonderful family and friends. You have all been through this with me, and I can't thank you enough for your continued love and support.

TABLE OF CONTENTS

	Page
ACKNOWLEDGEMENTS	iii
LIST OF TABLES	vi
LIST OF FIGURES	vii
LIST OF SCHEMES	ix
ABBREVIATIONS	xi
Chapter	
1. SYNTHESIS AND OPTIMIZATION OF A MODEL SYSTEM REPRESENTING THE NATURAL PRODUCT MARINEOSIN A	1
1.1. Introduction.....	1
1.1.1. Marineosins A and B	1
1.1.2. Prodigiosin Alkaloids	3
1.2. Significance.....	10
1.2.1. Towards the Total Synthesis of Marineosin A	10
1.2.2. Determining the Minimal Pharmacophore of Marineosin A and Optimizing Structure-Activity Relationships	11
1.3. Literature Review.....	11
1.3.1. Evaluation of Fenical's Biosynthetic Proposal	11
1.3.2. Snider's Alternative Biosynthetic Proposal and Spiroiminal Synthesis	14
1.3.3. Snider's Functionalized Model System and Progress Towards Marineosin A	18
1.4. Synthesis and Optimization of Model System.....	20
1.5. Conclusions.....	27
1.6. Future Directions	27
1.7. Experimental Section.....	31
1.7.1. Methods and Materials.....	31
1.7.2. Experimental Procedures	32
2. DISCOVERY OF VU0431316, A NEGATIVE ALLOSTERIC MODULATOR OF THE METABOTROPIC GLUTAMATE RECEPTOR 5.....	43
2.1. Introduction	43
2.1.1. Metabotropic Glutamate Receptors	43
2.1.2. Allosteric Modulators	48
2.2. Significance.....	49

2.3. Literature Review.....	50
2.4. Discovery of VU0431316.....	53
2.4.1. Development of Structure-Activity Relationships.....	54
2.4.2. Drug Metabolism and Pharmacokinetics.....	66
2.4.3. Behavioral Pharmacology.....	69
2.5. Conclusions and Future Directions.....	71
2.6. Experimental Section.....	72
2.6.1. Methods and Materials.....	72
2.6.2. Selected Experimental Procedures.....	72
Appendix	
A. SPECTRA RELEVANT TO CHAPTER 1.....	81
B. SPECTRA RELEVANT TO CHAPTER 2.....	108
REFERENCES.....	117

LIST OF TABLES

Table	Page
2.1. mGluR Group classifications.....	46
2.2. Heteroaryl core SAR.....	57
2.3. Northern fluoropyridine SAR.....	59
2.4. Northern pyrimidine SAR.....	64
2.5. CYP450 inhibition.....	67
2.6. Protein binding.....	67

LIST OF FIGURES

Figure	Page
1.1. Structures of marineosins A (1.1) and B (1.2)	2
1.2. Large-ring conformation of 1.1 suggested by the pyrrole-ring shielded proton chemical shifts of H ₁₇ and H ₁₉	3
1.3. The marineosins are reminiscent of prodigiosin alkaloids	4
1.4. Two stable isomers of prodigiosin alkaloids in solution	5
1.5. Structure of obatoclax (GX15-070) (1.27).....	9
1.6. General structure of the tambjamine alkaloids	9
1.7. Diagnostic nOe correlations in spiroaminal 1.76	23
1.8. Diagnostic nOe correlations in model system 1.78 reminiscent of marineosin A (1.1).....	25
1.9. Diagnostic correlations in model system 1.113	30
2.1. Diagram of GPCR activation	45
2.2. Monomeric structure of the mGluRs	46
2.3. Receptor conformations of the mGluR dimer.....	47
2.4. Representative CRCs of increasing PAM and NAM concentrations	49
2.5. The first selective mGluR ₅ NAMs, SIB-1757 (2.1) and SIB-1893 (2.2).....	51
2.6. mGluR ₅ tool compounds MPEP (2.3) and MTEP (2.4).....	51
2.7. mGluR ₅ NAMs currently in clinical trials	52
2.8. Fenobam (2.8), an anxiolytic mGluR ₅ allosteric antagonist.....	52
2.9. M-5PEP (2.9) and Br-5MPEPy (2.10), mGluR ₅ allosteric partial antagonists.....	53
2.10. mGluR ₅ NAM tool compound 2.11 (VU0431316).....	54
2.11. mGluR ₅ NAM HTS hit and early analogs	55

2.12.	mGluR ₅ NAM tool compound VU0409106 (2.15).....	55
2.13.	Fold shift data for 2.11 (VU0431316)	66
2.14.	Compound 2.11 (VU0431316) liver S9 fraction incubation	68
2.15.	Compounds 2.15 (VU0409106) and 2.11 (VU0431316) binding studies	70
2.16.	Dose dependent inhibition of marble burying with 2.11 (VU0431316).....	71

LIST OF SCHEMES

Scheme	Page
1.1. Broger and co-workers synthesis of MBC (1.13).....	7
1.2. Enantioselective synthesis of metacycloprodigiosin (1.25).....	8
1.3. Enantioselective synthesis of prodigiosin R1 (1.26).....	9
1.4. Fenical's proposed biosynthesis of marineosins A (1.1) and B (1.2).....	12
1.5. Attempted inverse-electron demand hetero-Diels-Alder reaction of 1.30 to afford 1.31	13
1.6. Snider's alternative biosynthesis of the marineosins.....	15
1.7. Snider's spiroiminal model system.....	16
1.8. Snider's synthesis of the spiroiminal core of marineosins A (1.1) and B (1.2).....	17
1.9. Snider's functionalized model system 1.56	19
1.10. Snider's attempted synthesis of marineosin A (1.1).....	19
1.11. Huang's stereoselective synthesis of aza-spiropyran 1.64	21
1.12. Synthesis of key maleimide 1.68	21
1.13. Synthesis of key Grignard reagent 1.73	22
1.14. Synthesis of spiroaminal moiety of marineosin A (1.1).....	23
1.15. Attempts to install the A-ring pyrrole moiety.....	24
1.16. Late stage installation of the A-ring pyrrole.....	25
1.17. Synthesis of model system 1.87 reminiscent of marineosin B (1.2). (a) Preparation of (<i>S</i>)-maleimide fragment (1.83). (b) Preparation of (<i>S</i>)- spiroiminal (1.87).....	26
1.18. Optimization of late-stage pyrrole installation.....	27
1.19. Envisioned completion of marineosin A (1.1) based on developed model system 1.78	27

1.20.	Route to macrocyclic pyrrole 1.109 via critical intermediate 1.102	29
1.21.	Synthesis of the spiroaminal lactam moiety of marineosin A (1.1).....	30
2.1.	Representative example of heteroaryl substitution of the phenyl core via Route I.....	56
2.2.	Representative example of heteroaryl substitution of the phenyl core via Route II	56
2.3.	Preparation of substituted heteroarylamine carboxamides (2.35).....	58
2.4.	Aldehyde oxidase metabolism of 2.11 (VU0431316)	68

ABBREVIATIONS

7TM	seven-transmembrane
$[\alpha]$	specific rotation
Å	angstrom
AcOH	acetic acid
Ag ₂ O	silver(I) oxide
Bcl-2	B-cell lymphoma 2
BF ₃ ·OEt ₂	boron trifluoride diethyl etherate
BHB	brain homogenate binding
Bn	benzyl
BnBr	benzyl bromide
Boc	<i>tert</i> -butyloxycarbonyl
bs	broad singlet
°C	degrees Celsius
c	concentration
cAMP	cyclic adenosine monophosphate
CAN	ceric ammonium nitrate
cat.	catalytic
CDCl ₃	deuterated chloroform
CHCl ₃	chloroform
CH ₂ Cl ₂	dichloromethane
CNS	central nervous system

(COCl) ₂	oxalyl chloride
COSY	correlation spectroscopy
CRC	concentration response curve
CRD	cysteine-rich domain
Cs ₂ CO ₃	cesium carbonate
CuBr	copper(I) bromide
CuI	copper(I) iodide
δ	chemical shift in ppm
d	doublet
dd	doublet of doublets
ddd	doublet of doublet of doublets
dddd	doublet of doublet of doublet of doublets
DDQ	2,3-dichloro-5,6-dicyano-1,4-benzoquinone
DEPT	distortionless enhancement by polarization transfer
DIBAL-H	diisobutylaluminium hydride
DIPEA	<i>N,N</i> -diisopropylethylamine
DMAP	4-dimethylaminopyridine
DME	dimethoxyethane
DMF	dimethylformamide
DMSO	dimethyl sulfoxide
DMSO- <i>d</i> ₆	deuterated dimethyl sulfoxide
dq	doublet of quartets
dr	diastereomeric ratio

dt	doublet of triplets
<i>E</i>	<i>entgegen</i> (opposite)
EC ₈₀	concentration that leads to 80% maximal response
ED ₅₀	median effective dose
EDC	1-ethyl-3-(3-dimethylaminopropyl)carbodiimide
eq	equivalent
equiv	equivalent
ESI	electrospray ionization
ES-MS	electrospray mass spectrometry
Et	ethyl
Et ₂ O	diethyl ether
Et ₃ N	triethylamine
EtOAc	ethyl acetate
FXS	fragile X syndrome
g	gram(s)
GDP	guanosine 5'- diphosphate
GERD	gastroesophageal reflux disease
Glu Max	maximum glutamate response
GPCR	G-protein-coupled receptor
GTP	guanosine 5'-triphosphate
h	hour(s)
H ₂ O	water
HBr	hydrogen bromide

HCl	hydrogen chloride
HEK293	human embryonic kidney 293 cell line
HMBC	heteronuclear multiple-bond correlation spectroscopy
HOBt	hydroxybenzotriazole
HPLC	high-performance liquid chromatography
HRFABMS	high resolution fast-atom bombardment mass spectroscopy
HRMS	high-resolution mass spectrometry
HSQC	heteronuclear single-quantum correlation spectroscopy
HTS	high-throughput screen
Hz	hertz
IC ₅₀	half maximal inhibitory concentration
ImH	imidazole
<i>in situ</i>	in the reaction mixture
<i>in vacuo</i>	in a partial or full vacuum
IP	intraperitoneal
IR	infrared spectroscopy
<i>J</i>	coupling constant
K ₂ CO ₃	potassium carbonate
kg	kilogram(s)
LiBH ₄	lithium borohydride
LTD	long-term depression
μL	microliter(s)
μM	micromolar

μw	microwave
m	multiplet
M	mass or molar concentration
Me	methyl
Me_3OBF_4	trimethyloxonium tetrafluoroborate
MeCN	acetonitrile
MeI	iodomethane
MeOH	methanol
mg	milligram(s)
mGluR	metabotropic glutamate receptor
MgSO_4	magnesium sulfate
MHz	megahertz
min	minute(s)
mL	milliliter(s)
mmol	millimole(s)
MPEP	2-Methyl-6-(phenylethynyl)pyridine
mPEPy	3-methoxy-5-(pyridin-2-ylethynyl)pyridine
MS	molecular sieve
MTEP	3-((2-Methyl-4-thiazolyl)ethynyl)pyridine
n	number of independently performed experiments
Na_2CO_3	sodium carbonate
Na_2SO_4	sodium sulfate
NaClO_2	sodium chlorite

NaH	sodium hydride
NaHCO ₃	sodium bicarbonate
NaH ₂ PO ₄	monosodium phosphate
NAM	negative allosteric modulator
NaOCl	sodium hypochlorite
NaOMe	sodium methoxide
NaO <i>t</i> -Bu	sodium <i>tert</i> -butoxide
NCI	National Cancer Institute
NH ₄ Cl	ammonium chloride
NH ₄ OAc	ammonium acetate
NMDA	<i>N</i> -methyl- <i>D</i> -aspartate
NMO	<i>N</i> -methylnmorpholine <i>N</i> -oxide
NMP	<i>N</i> -methyl-2-pyrrolidone
NMR	nuclear magnetic resonance
nOe	nuclear Overhauser effect
NOESY	nuclear Overhauser effect spectroscopy
NT	neurotransmitter
O ₃	ozone
PAM	positive allosteric modulator
PD-LID	Parkinson's disease levodopa induced dyskinesia
Pd/C	palladium on carbon
Pd(OAc) ₂	palladium(II) acetate
Pd(PPh ₃) ₄	tetrakis(triphenylphosphine)palladium(0)

Pd ₂ (dba) ₃	tris(dibenzylideneacetone)dipalladium(0)
PG	protecting group
pH	measure of hydrogen ion concentration
Ph	phenyl
Ph ₃ P	triphenylphosphine
PhMe	toluene
PhNTf ₂	<i>N</i> -phenyl-bis(trifluoromethanesulfonimide)
pIC ₅₀	-log IC ₅₀
Piv	pivaloyl
PK	pharmacokinetic
PMB	<i>para</i> -methoxybenzyl
POCl ₃	phosphorus oxychloride
ppm	parts per million
Pr	propyl
<i>p</i> -TsOH	<i>p</i> -toluenesulfonic acid
pyr	pyridine
q	quartet
<i>R</i>	<i>Rectus</i> (right)
RCM	ring-closing metathesis
rDNA	ribosomal deoxyribonucleic acid
Red-Al	sodium bis(2-methoxyethoxy)aluminumhydride
rt	room temperature
s	singlet

<i>S</i>	<i>Sinister</i> (left)
SAR	structure-activity relationship
SEM	2-(trimethylsilyl)ethoxymethyl
SiEt ₃	triethylsilyl
SMe ₂	dimethyl sulfide
S _N AR	nucleophilic aromatic substitution
SO ₃	sulfur trioxide
t	triplet
<i>t</i> Bu	<i>tert</i> -butyl
TBAF	tetra- <i>n</i> -butylammonium fluoride
TBAI	tetrabutylammonium iodide
TBDPS	<i>tert</i> -butyldiphenylsilyl
TBHP	<i>tert</i> -butyl hydroperoxide
temp	temperature
TES	triethylsilyl
Tf ₂ O	triflic anhydride
TFA	trifluoroacetic acid
THF	tetrahydrofuran
THP	tetrahydropyran
TiCl ₄	titanium tetrachloride
TIPS	triisopropylsilyl
TLC	thin layer chromatography
TMSOTf	trimethylsilyl trifluoromethanesulfonate

TOCSY	total correlation spectroscopy
TOF	time of flight
TPAP	tetrapropylammonium perruthenate
Ts	tosyl
UV	ultraviolet
VFD	Venus flytrap domain
VO(acac) ₂	vanadyl acetylacetonate
Z	<i>zusammen</i> (together)

Chapter 1

SYNTHESIS AND OPTIMIZATION OF A MODEL SYSTEM REPRESENTING THE NATURAL PRODUCT MARINEOSIN A

1.1. Introduction

In 2008, Fenical and co-workers isolated marineosin A along with a less abundant isomer, marineosin B, from a marine sediment-derived actinomycete.¹ Although both compounds exhibited cytotoxicity, marineosin A proved more potent. The intriguing biological activity and novel chemical structure warranted completion of the total synthesis of this compound, which remains a challenging goal. The initial proposed biosynthesis failed in the laboratory, and, despite significant interest from the synthetic community, limited syntheses en route to marineosin A have been reported.²⁻⁴ The following describes the successful synthesis of model systems, designed to be a portion of the natural products. They were created as tools to develop chemistry and test the viability of proposed synthetic routes toward marineosin A. Moreover, the model systems were designed as possible minimal pharmacophores, which would greatly simplify structure-activity relationship (SAR) studies around the biologically active natural products.

1.1.1. Marineosins A and B

In 2008, Fenical and co-workers described the isolation, structural determination, and biological evaluation of two novel spiroimino alkaloids, marineosins A and B (**1.1** and **1.2**, Figure 1.1).¹ The marineosins were isolated off the shore of La Jolla, California,

from marine-derived actinomycete strain CNQ-617 (identified by 16S rDNA sequence data analysis).¹ Many actinomycetes are harmless, some are pathogens, and others have become an important source for secondary metabolites, including sources of antibiotics. Interestingly, the marineosins are thought to be a new species in the genus *Streptomyces*, which has been shown to have adapted to marine life and has produced a number of antibiotics.¹

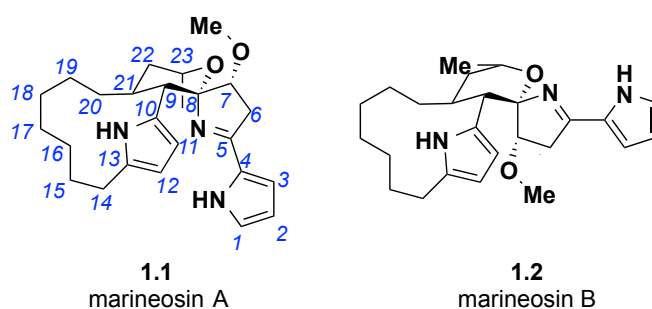


Figure 1.1. Structures of marineosins A (**1.1**) and B (**1.2**).

The natural products were analyzed by optical rotation, UV spectroscopy, high- and low-resolution ESI, HRFABMS, IR spectroscopy, ¹H and ¹³C NMR spectroscopy (including DEPT), and 2D NMR spectroscopy (including COSY, NOESY, HMBC, TOCSY, and HSQC-TOCSY).¹ **1.1** and **1.2** proved to be intriguing synthetic targets containing a novel spiroiminal center, two pyrrole moieties, and a 12-membered macrocyclic ring. The compounds are diastereomers with an epimeric relationship assigned at the C₈ spiroiminal and adjacent C₇ stereocenter. Of note, NOESY correlations and ¹H NMR vicinal coupling constants indicated that the tetrahydropyran (THP) ring in marineosin A (**1.1**) is in the chair conformation (Figure 1.2) while similar

analysis of marineosin B (**1.2**) confirmed this compound to be in a boat or twist boat conformation. This phenomenon is most likely due to the stabilizing anomeric effect expected in **1.1** that may not be present in **1.2** because of the inverted aminal nitrogen.¹

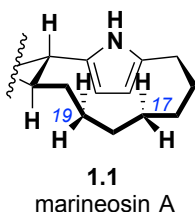


Figure 1.2. Large-ring conformation of **1.1** suggested by the pyrrole-ring shielded proton chemical shifts of H₁₇ and H₁₉.¹ (Adapted from Fenical 2008).

Antifungal activities against *Candida albicans* were extremely weak, but both **1.1** and **1.2** inhibited the human colon carcinoma HCT-116 cell line at IC₅₀'s of 0.5 μ M and 46 μ M, respectively. Marineosin A (**1.1**), the major isolated isomer, also proved to be broadly cytotoxic with considerable selectivity against melanoma and leukemia cell lines in the National Cancer Institute (NCI) 60 cell line panel.¹

The macrocycle of the marineosins resembles the cycloalkyl side chains of the prodigiosin alkaloids, secondary metabolites known for their bright red pigments and vast range of biological activities. The tricyclic core is also reminiscent of the bacterial prodigiosins.⁵ These structural similarities indicate that the marineosins could be derived from a prodigiosin-like biosynthesis pathway.¹

1.1.2. Prodigiosin Alkaloids

The marineosins closely resemble the prodigiosin alkaloids (Figure 1.3), which are produced by various marine bacteria. The prodigiosins exhibit a myriad of biological

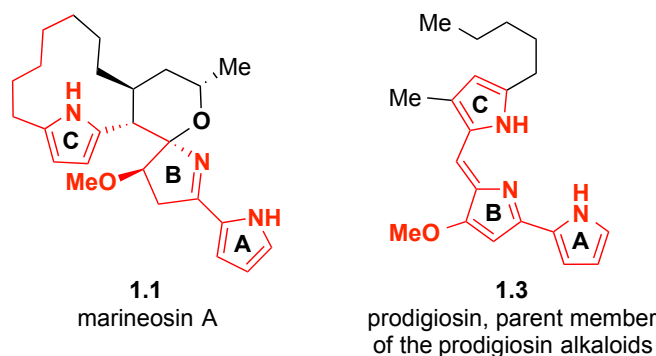


Figure 1.3. The marineosins are reminiscent of the prodigiosin alkaloids.

activities including immunosuppression, antimalarial, antimicrobial, and anticancer effects with nominal toxicity on normal cells.⁵ The prodigiosins possess extended conjugation through a pyrrolylpyrromethene skeleton, causing a deep red color, with either an alkyl chain or macrocyclic ring as the major substituent.

Notably, the conformation of the prodigiosin core in solution is strongly dependent on the pH of the solvent. Two stable isomers exist (**1.4** and **1.5**, Figure 1.4) based on the degree of protonation of the basic nitrogen. This process is due to an *E/Z* isomerization of the exocyclic double bond of the azafulvene and induces intramolecular hydrogen bonding at either the **B**-ring methoxy group or **B**-ring nitrogen, respectively.^{5,6} It is unlikely that both isomers show the same affinity to their still unidentified cellular target(s). Determining the pharmacology of prodigiosin derivatives with a defined configuration, i.e., marineosin A (**1.1**), could, therefore, be a valuable investigation towards a biochemical tool.

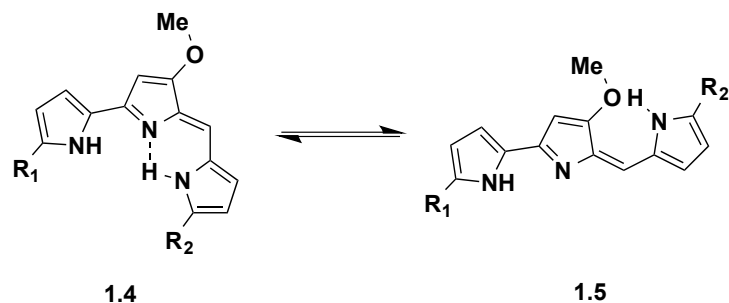


Figure 1.4. Two stable isomers of prodigiosin alkaloids in solution.⁶

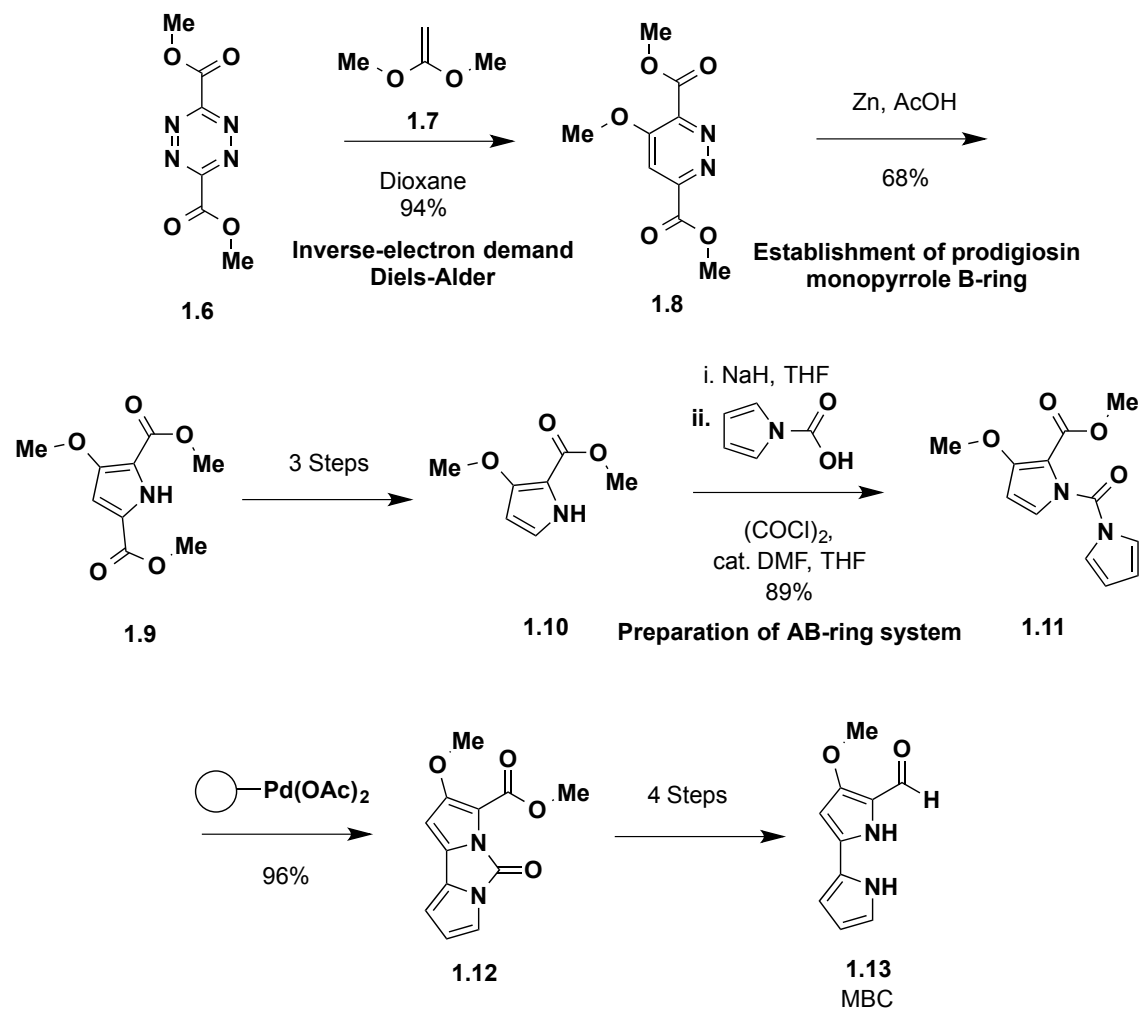
Prodigiosin natural products are produced through a number of biosynthetic pathways. A multitude of synthetic endeavors and SAR studies have focused on these compounds, and syntheses in the last 50 years have contributed greatly to heterocyclic chemistry.⁶⁻⁸ In particular, Boger and co-workers prepared the core of the prodigiosin precursor bipyrrole aldehyde 4-methoxy-2,2'-bipyrrole-5-carbaldehyde (MBC) (**1.13**, Scheme 1.1) utilizing an inverse-electron demand Diels-Alder reaction.^{9,10} 1,2,4,5-tetrazine (**1.6**) and 1,1-dimethoxy ethane (**1.7**) were reacted in dioxane to give pyridazine **1.8** in 94% yield. The prodigiosin B-ring (**1.9**) was established by reacting **1.8** with zinc dust and acetic acid. Subsequent hydrolysis, iodine-mediated iodination, and hydrogenolysis provided pyrrole **1.10**, which was further reacted with 1*H*-pyrrole-1-carboxylic acid to give urea **1.11**. Next, oxidative coupling with stoichiometric polymer-supported palladium acetate provided **1.12**. Finally, hydrolysis and reduction afforded MBC (**1.13**).

Thomson and Clift were the first to demonstrate enantioselective syntheses of two of the tripyrrole alkaloids, metacycloprodigiosin (**1.25**, Scheme 1.2) and prodigiosin R1 (**1.26**, Scheme 1.3).¹¹ Metacycloprodigiosin was prepared by a regio- and stereoselective 1,4-conjugate addition of ethylmagnesium bromide (EtMgBr) to enone **1.14**. The enolate

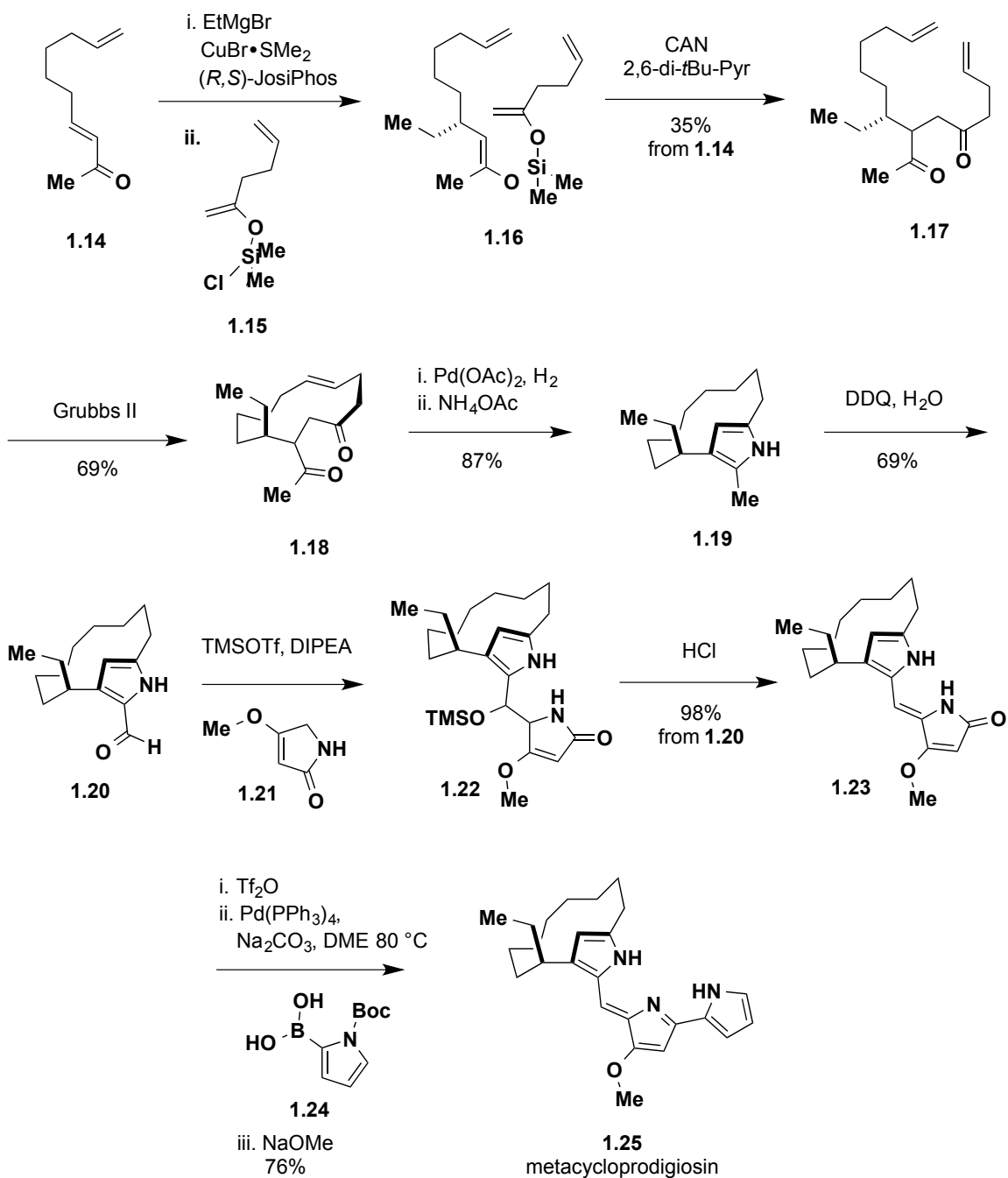
was then trapped with chlorosilane **1.15**. Oxidative bond formation, ring-closing metathesis (RCM), hydrogenation, and Paal-Knorr condensation provided chiral macrocyclic pyrrole **1.19**. Aldehyde **1.20** was prepared by methyl oxidation with 2,3-dichloro-5,6-dicyano-1,4-benzoquinone (DDQ), and aldol condensation afforded bipyrrrole **1.22**. Triflation, Suzuki coupling, and *tert*-butyloxycarbonyl (Boc) deprotection yielded metacycloprodigiosin (**1.25**) in 13% overall yield. This same strategy was used to synthesize prodigiosin R1 (**1.26**) in 7% overall yield.

While most SAR studies have focused on derivations of the **C**-ring,^{12,13} D'Alessio *et al.* found a nitrogen-containing **A**-ring and a **B**-ring alkoxy group to be important for immunosuppressive and cytotoxic activity, properties most likely due to different mechanisms of action.^{5,14} Furthermore, Melvin and co-workers found that **A**-ring replacements with substituted indoles and unnatural alkyl pyrrole substituents exhibited antiproliferative effects and suggest that the prodigiosins could be used as monotherapy or synergistically in combination with existing drugs.¹⁵ Obatoclax (GX15-070) (**1.27**, Figure 1.5), a Bcl-2 inhibitor, is an example of a prodigiosin analog currently in phase II clinical trials for the treatment of cancer.^{16,17}

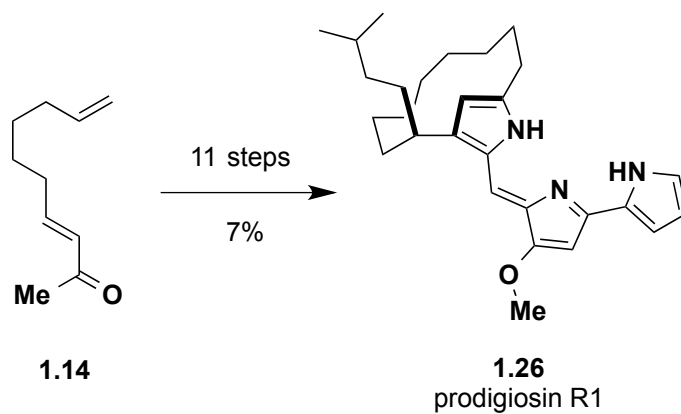
The tambjamine alkaloids (Figure 1.6) are the most closely related group of natural products to the prodigiosins. They differ structurally by an enamine moiety but exhibit cytotoxic activity similar to that of the prodigiosins.⁵



Scheme 1.1. Broger and co-workers synthesis of MBC (**1.13**).^{9,10}
 (Adapted from Boger 1988, 1987).



Scheme 1.2. Enantioselective synthesis of metacycloprodigosin (**1.25**).¹¹



Scheme 1.3. Enantioselective synthesis of prodigiosin R1 (**1.26**).¹¹

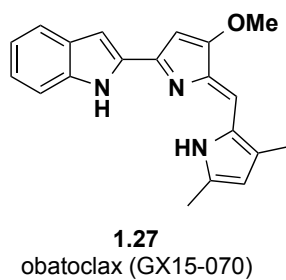


Figure 1.5. Structure of obatoclax (GX15-070) (**1.27**).

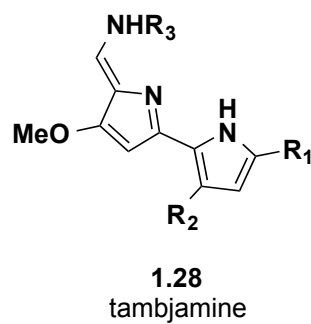


Figure 1.6. General structure of the tambjamine alkaloids.

1.2. Significance

Cancer is a heterogeneous disease that can rapidly mutate and become resistant to therapy; therefore, cancer drug discovery is difficult and complex. The development of probe molecules that can be used to validate “druggable” cancer targets is a critical part of the cancer drug discovery process.

Although many large pharmaceutical companies have marginalized natural product divisions in the last 20–30 years, the increasing failure rate of the modern drug discovery process, namely high-throughput screens (HTSs) of synthetic libraries, continues to advocate for a role for natural products.¹⁸ Historically, drugs were often derived from natural products, and they are once again gaining substantial attention, especially in the area of oncology. According to the NCI, over half of the drugs approved to treat cancer come from a natural product or natural product precursor, and two recently approved drugs, eribulin and trabectedin, have come from marine organisms.¹⁹

Marineosin A (**1.1**), a marine derived natural product, is biologically interesting in that it was shown to inhibit the growth of HCT-116 cells at an IC_{50} of 0.5 μ M. This compound also exhibited broad cytotoxicity with considerable selectivity against melanoma and leukemia cell lines. Therefore, this natural product could serve as a lead structure in the search for new tool compounds and/or drugs.¹

1.2.1. Towards the Total Synthesis of Marineosin A

Due to the unprecedented spiroimino core, these new members of the prodiginine family of natural products are also intriguing synthetic targets. Our synthetic endeavor towards **1.1** is a proposed sequence of 29 reactions that begins from a chiral pool starting

material and calls for late-stage pyrrole installation. Progress towards the natural product has resulted in an advanced synthetic intermediate containing the 12-membered macrocyclic pyrrole core.³ The proposed route for the completion of **1.1** is based on methodology developed en route to a functionalized model system and final reaction conditions determined from the smaller model system described herein.^{3,20}

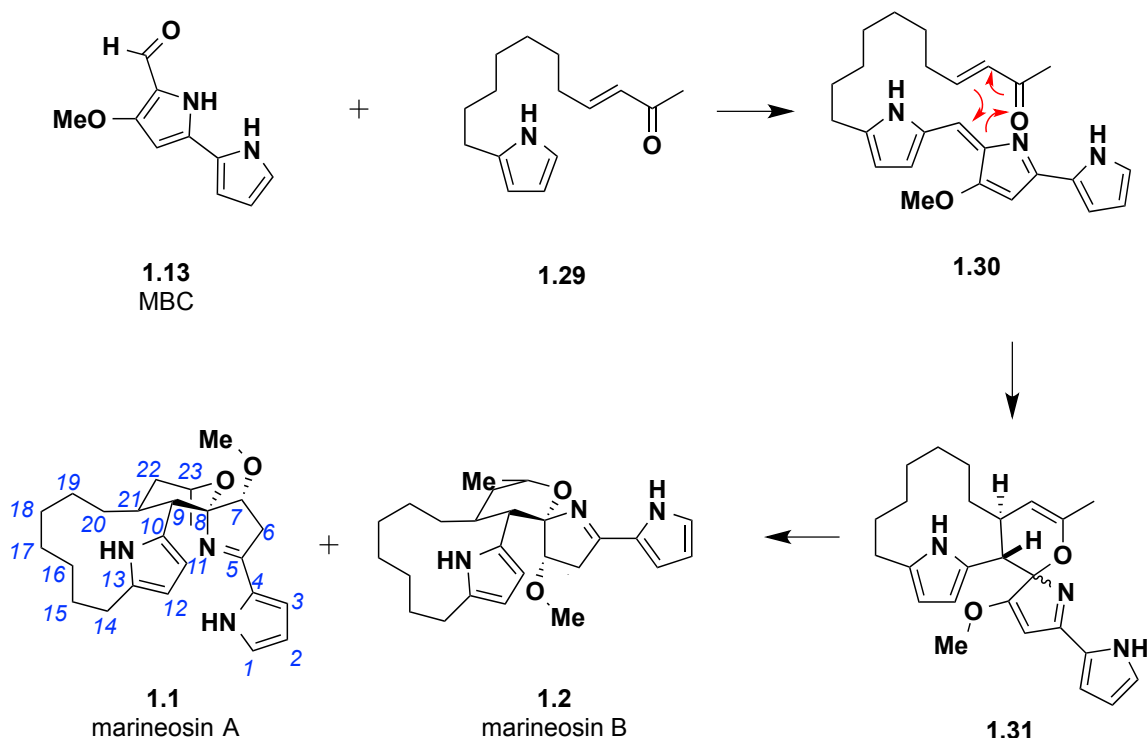
1.2.2. Determining the Minimal Pharmacophore of Marineosin A and Optimizing Structure-Activity Relationships

While the synthesis of the natural product is complex, a simplified molecule maintaining the cytotoxicity seen in the marineosins would greatly enhance throughput in the development of SAR and biological assays, studies critical to the development of **1.1** as a tool compound. The model system provides a means of studying the SAR of unnatural analogs to determine the functional groups necessary for activity as well as those that are amenable to transformation. Theoretically, derivations of the most potent compounds can then be used to develop a functionally selective and cell-permeable chemical probe with low nanomolar potency.

1.3. Literature Review

1.3.1. Evaluation of Fenical's Biosynthetic Proposal

Fenical proposed a biosynthetic route (Scheme 1.4) to the marineosins from undecylprodigiosin that proceeded through an intramolecular inverse-electron demand hetero-Diels-Alder, a reaction known to impart stereoselectivity and stereospecificity to highly substituted cyclic cores.^{1,8} Attempts within the Lindsley group to achieve a

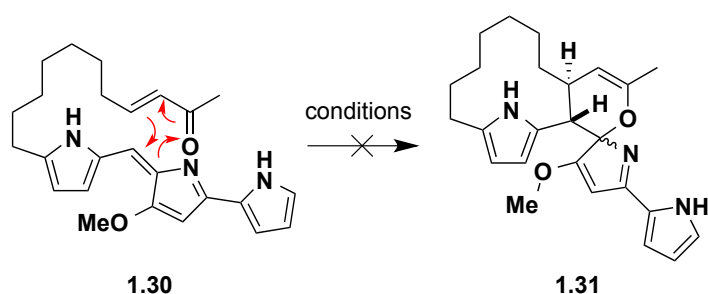


Scheme 1.4. Fenical's proposed biosynthesis of marineosins A (**1.1**) and B (**1.2**).¹
(Adapted from Fenical 2008).

biomimetic synthesis of the marineosin core based on this hypothetical cycloaddition failed despite examining a broad range of reaction conditions.²

In 2010, Aldrich *et al.* reported the evaluation of Fenical's proposed biosynthesis beginning with the condensation of the known primary precursor to the prodigiosin alkaloids, MBC (**1.13**), with a novel 2-keto-undec-3-enylpyrrole (**1.29**) to give enone **1.30**.² This enone could hypothetically undergo an intramolecular, inverse-electron demand hetero-Diels-Alder cyclization from above or below the enone plane to give the THP ring and spiroiminol (**1.31**) in one step. Subsequent reduction would give marineosins A (**1.1**) and B (**1.2**).

Compound **1.13** was easily prepared through literature precedents in the syntheses of the tambjamines (**1.28**) and obatoclax (**1.27**). Although enone **1.30** (depicted as a single isomer for clarity as a Diels-Alder substrate) was produced in sufficient quantities, the proposed Diels-Alder reaction was deemed unsuccessful after exploring hundreds of reaction conditions (varying solvents, temperatures, microwave conditions, photochemical procedures, and Lewis acid catalysts) (Scheme 1.5). Employing molecular modeling, analysis of the 10,000 lowest energy conformers failed to identify a favorable Diels-Alder transition state. Due to flexibility of the long alkyl linker, intramolecular hydrogen bonds, and the key atoms remaining separated by at least 5 Å, it was concluded that **1.30** is energetically unfavorable towards the proposed mechanism. In addition, intermolecular Diels-Alder trials were also unsuccessful, proving the C₈-C₉ olefin an insufficient dienophile. This is likely due to the removal of electron density by extended conjugation in the poly-pyrrole π -system. Therefore, a Diels-Alder cycloaddition approach is not a viable route to **1.1** and **1.2** in the laboratory.



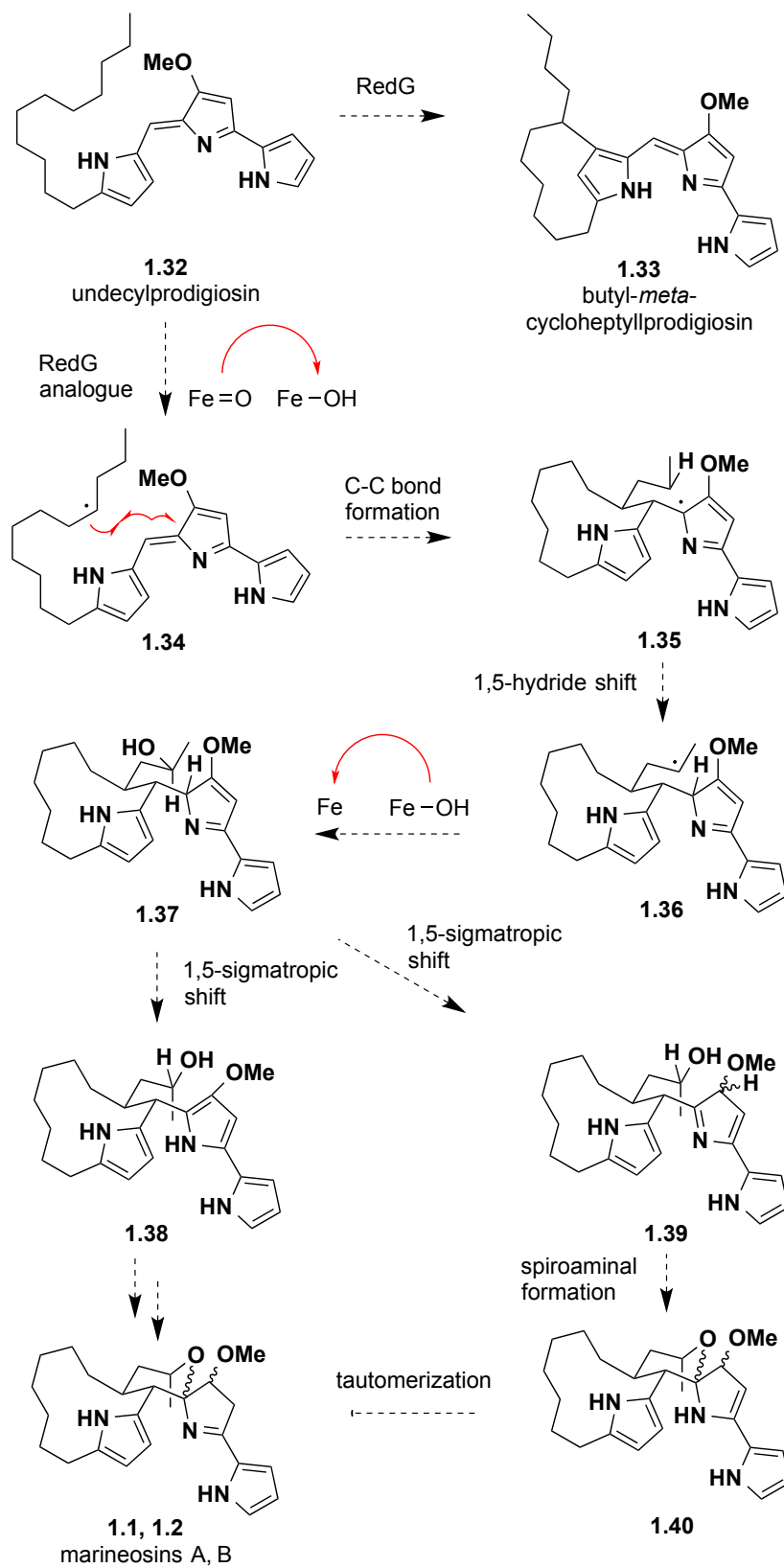
Scheme 1.5. Attempted inverse-electron demand hetero-Diels-Alder reaction of **1.30** to afford **1.31**.²

While there have been many successful Diels-Alder cycloadditions en route to complex natural products, confirmation of the existence of “Diels-Alderase,” enzymes that catalyze Diels-Alder reactions in nature, continues to be elusive.²¹ Even though an enzyme that performs this reaction has not been identified, we cannot rule out that nature could generate the correct electronics and conformation required to catalyze the reaction. An alternative synthetic strategy that does not proceed through a tripyrrole prodigiosin alkaloid intermediate is being pursued in the Lindsley lab since validation of the biomimetic approach was unsuccessful.

1.3.2. Snider’s Alternative Biosynthetic Proposal and Spiroiminal Synthesis

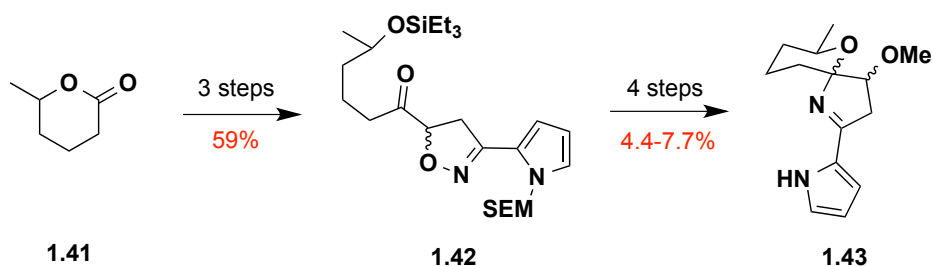
In 2010, Snider and co-workers proposed an alternative biosynthesis to the marineosins (Scheme 1.6).²² Snider’s group was skeptical of Fenical’s suggested biosynthesis because of the required six-electron oxidation of undecylprodigiosin (**1.32**) to form **1.30** followed by a four-electron reduction of **1.31** to give the marineosins. They instead proposed a single two-electron oxidation of **1.32** by a RedG homolog, RedG being an enzyme in the *red* gene cluster known to catalyze the production of prodigiosins.^{22,23}

The gene cluster from which the marineosins were isolated, *Streptomyces* CNQ-617, was designated a MAR3 clade has been sequenced by Reynolds and Salem.^{1,24} Enzymes MarG and MarA were determined to be involved in the biosynthesis of the marineosins. In Snider’s proposal, the RedG homolog oxidizes **1.32** to form either a radical or cation, which in turn undergoes an intramolecular Friedel-Crafts reaction to form **1.33**. A related enzyme could form radical **1.34** by oxidizing the adjacent carbon.



Scheme 1.6. Snider's alternative biosynthesis of the marineosins.²²

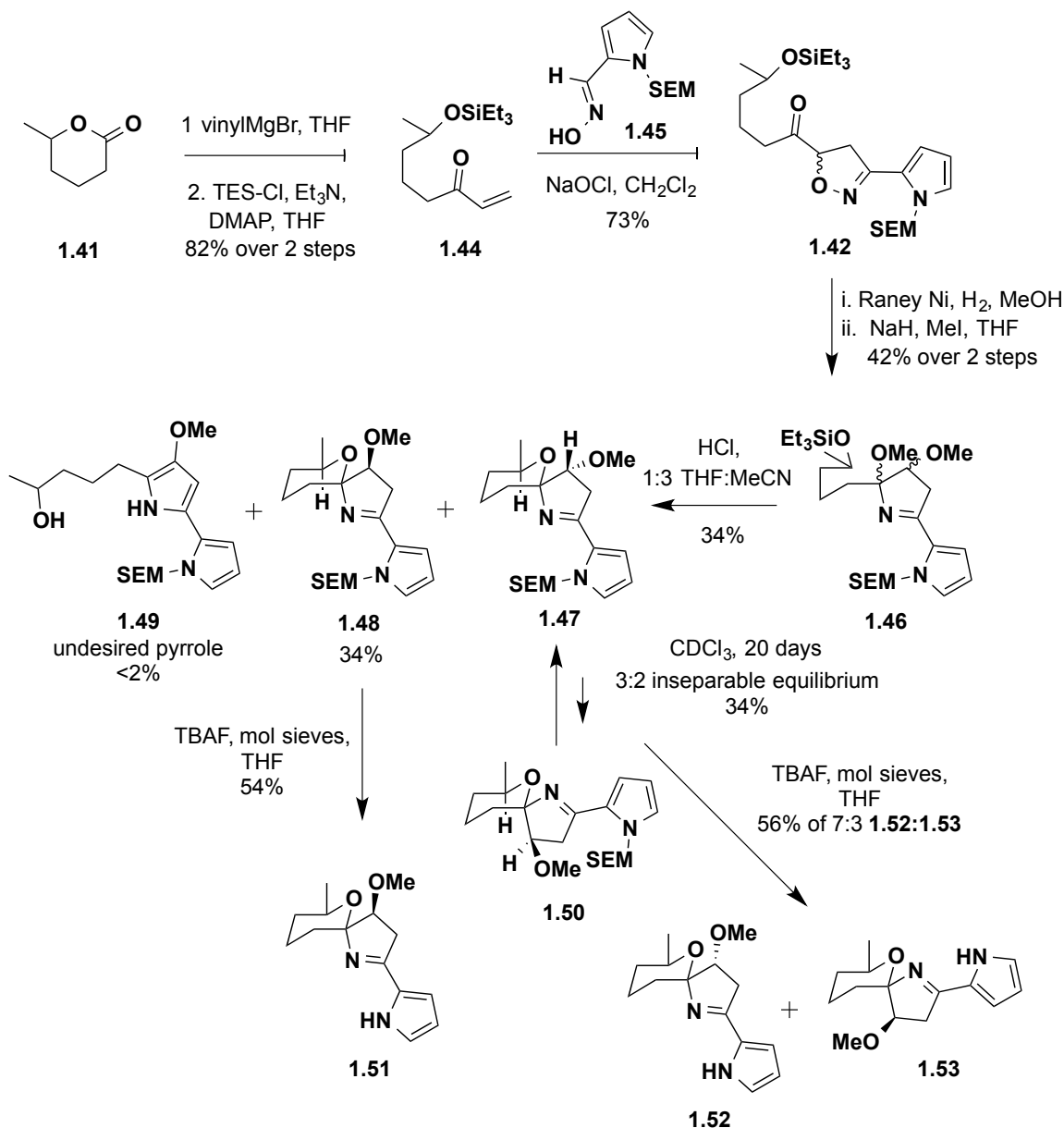
This radical could then add to the exocyclic olefin to produce macrocyclic radical **1.35**, which transforms to macrocycle **1.36** with a simple, 1,5-hydride shift. Because the radical in **1.36** is adjacent to the enzyme active site responsible for generating radical **1.34**, this compound could be oxidized to macrocyclic alcohol **1.37**, which could then proceed through a 1,5-sigmatropic hydride shift to form either 1*H*-pyrrole **1.38** or 3*H*-pyrrole **1.39**. While formation of both **1.38** and **1.39** are theoretically possible, it is unlikely that **1.38** would cyclize to form the marineosins due to the required loss of pyrrole aromaticity, which would be energetically unfavorable. More likely, **1.39** would rapidly cyclize to form spiroaminal **1.40**, and the enamine would tautomerize to the imine, giving the natural products. In this mechanism, only a single enzyme, likely a nonheme iron-dependent dioxygenase, would be necessary to convert **1.32** to **1.1** and **1.2**. Snider and co-workers went on to prepare a model of the spiroiminal moiety (**1.43**, Scheme 1.7) of **1.1** and **1.2** based on this proposal.²²



Scheme 1.7. Snider's spiroiminal model system.²² (Adapted from Snider 2010).

Snider's approach to model **1.43** included early incorporation of the A-ring pyrrole and was based on routes in which the dihydropyrrole ring of the spiroiminal is formed before the THP. They found the A-ring pyrrole to be unstable and subject to methylation

and initially developed a route to phenyl-substituted spiroiminals from enone **1.44** (Scheme 1.8). Ultimately, their final model synthesis required protection of the pyrrole substituent.



Scheme 1.8. Snider's synthesis of the spiroiminal core of marineosins A (**1.1**) and B (**1.2**).²² (Adapted from Snider 2010).

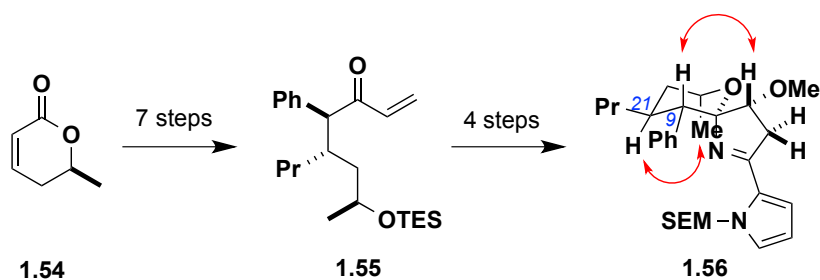
Beginning with lactone **1.41**, they prepared a model of the marineosins lacking only the macrocyclic ring. Vinylmagnesium bromide opened the lactone to the known hydroxyl ketone (85% yield), which was quenched with triethylsilyl chloride (TES-Cl) to form enone **1.44** in 96% yield. This enone was then reacted with oxime **1.45** in aqueous sodium hypochlorite to provide isoxazoline **1.42**. Hydrogenolysis of isoxazoline **1.42** with Raney nickel followed by methylation with iodomethane (MeI) gave iminal **1.46**. Exposure of iminal **1.46** to hydrochloric acid (HCl) provided various amounts of all of the possible marineosin diastereomers. Removal of the TES protecting groups from the diastereomers provided the deprotected analogs (**1.51–1.53**), which were obtained after 14–20 days of equilibration.²²

The seven-step route, which included long equilibration times and inseparable equilibration mixtures, led to spiroiminals with the same relative stereochemistry as the marineosins. Comparison of these models, which contain an equatorial methyl group, with the marineosins suggests that the trans-fused macrocyclic ring in the natural products forces the methyl group into an axial conformation. Snider comments that steric interactions between the methoxy group and the A-ring pyrrole largely prevent the formation of the other two, less stable, isomers at the spiroiminal center (C₈).²²

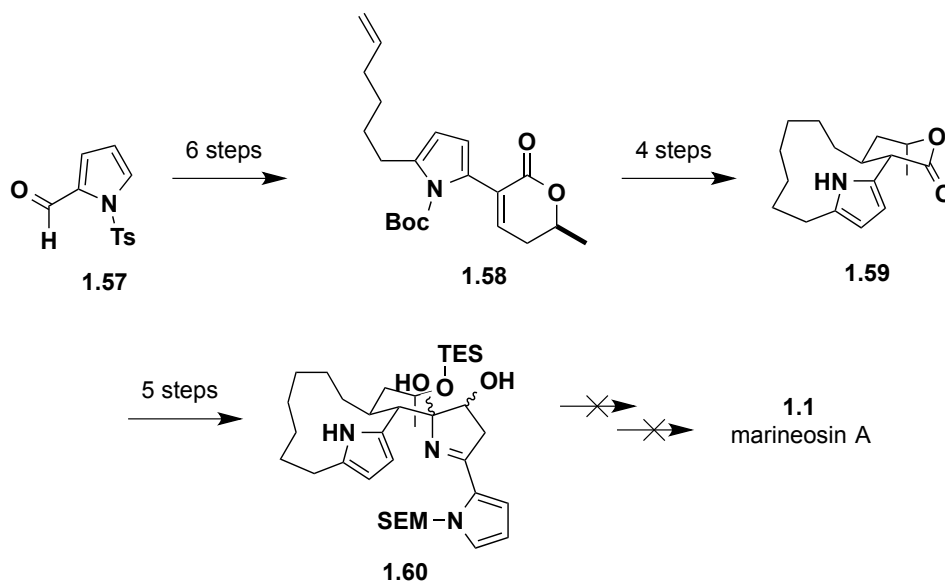
1.3.3. Snider's Functionalized Model System and Progress Towards Marineosin A

Earlier this year, Snider's group published a more functionalized model system in order to obtain a spiroiminal with the correct conformation as **1.1**.²⁵ The 11-step synthesis installs a C₉ phenyl and a C₂₁ propyl group into their previous model system, forcing the pyran into the marineosin A conformation (**1.56**, Scheme 1.9). In the same paper, they

describe a 10–step stereospecific synthesis of macrocyclic pyrrole lactone **1.59** followed by a 5–step transformation to a hemi-iminal intermediate (**1.60**, Scheme 1.10). This intermediate proved to be extremely acid sensitive and decomposed upon both methylation and spiroiminal formation, steps necessary to form **1.1**. TES protection of macrocyclic pyrrole **1.59** failed to form the hemi-iminal, and deprotection of this compound also proved unsuccessful.²⁵



Scheme 1.9. Snider's functionalized model system **1.56**.²⁵ (Adapted from Snider 2013).

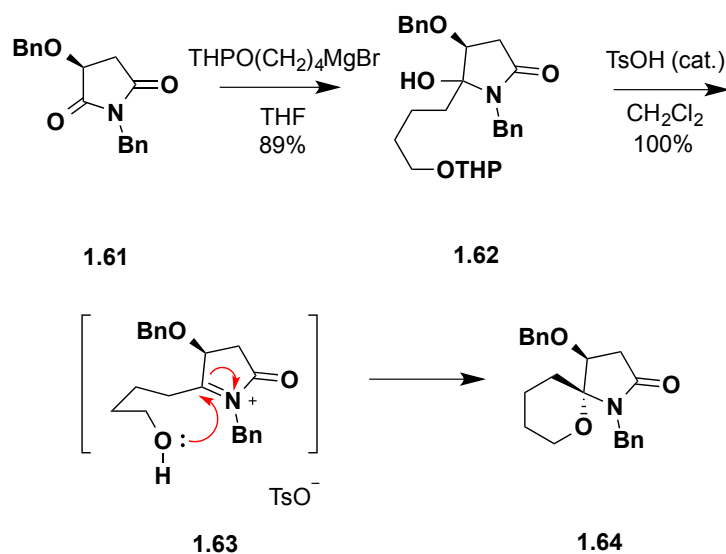


Scheme 1.10. Snider's attempted synthesis of marineosin A (**1.1**).²⁵ (Adapted from Snider 2013).

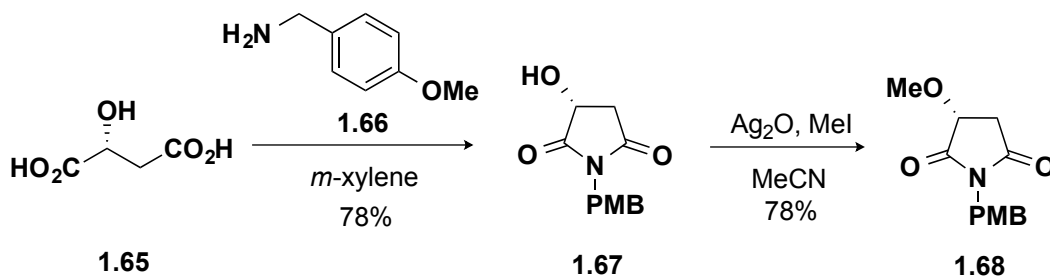
1.4. Synthesis and Optimization of Model System

Snider's model system proved to be a significant development towards the synthesis of the marineosins; however, our group envisioned a synthesis avoiding early pyrrole installation.²² Previous synthesis attempts within the Lindsley group had, like Snider, found the A-ring pyrrole to be unstable and prone to reactivity issues, leaving advanced intermediates and strategies ultimately abandoned. Therefore, a route avoiding early pyrrole incorporation could prove valuable towards the total synthesis of **1.1** and **1.2**. We developed a six step enantioselective route to two spiroiminal model systems reminiscent of **1.1** and **1.2** with late stage pyrrole installment via nucleophilic displacement of an iminium triflate salt.²⁰

The maleimide-based methodology is based on Huang and co-workers concise and selective synthesis of aza-spiropyran **1.64** (Scheme 1.11) in which Grignard addition to a chiral hydroxy-maleimide followed by acid-catalyzed intramolecular N-acyliminium cyclization forms the spiroaminal core.²⁶ We prepared maleimide **1.67** (Scheme 1.12) from a known procedure, refluxing (*R*)-hydroxysuccinic acid (**1.65**) with *p*-methoxybenzyl amine (**1.66**) in *m*-xylene for 24 hours.²⁷ Purification by recrystallization from benzene provided **1.67** in 78% yield. The free hydroxyl group was subsequently alkylated with MeI and silver(I) oxide in acetonitrile at reflux for one hour. Purification by flash chromatography provided **1.68** (78% yield), the relevant maleimide for a model system of **1.1**.

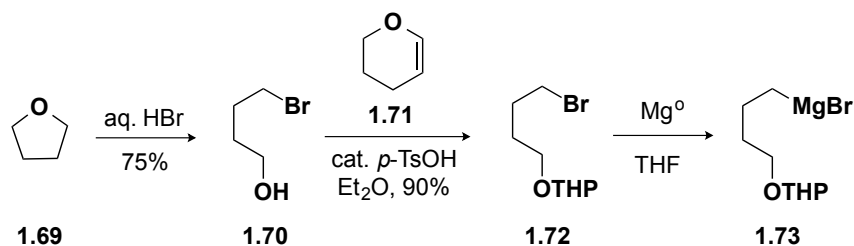


Scheme 1.11. Huang's stereoselective synthesis of aza-spiropyran **1.64**.²⁶



Scheme 1.12. Synthesis of key maleimide **1.68**.²⁰

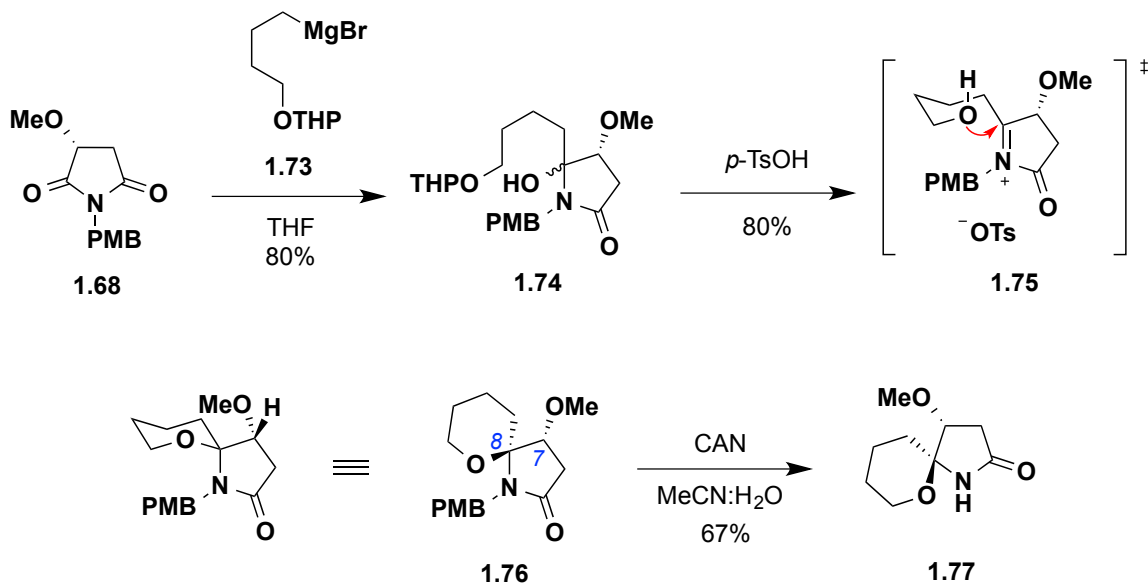
Grignard reagent **1.73** (Scheme 1.13) was readily obtained by adding aqueous hydrogen bromide to refluxing tetrahydrofuran (THF) to obtain alcohol **1.70** (75% yield) followed by THP protection with 3,4-dihydro-2*H*-pyran (**1.71**) and *p*-toluenesulfonic acid (*p*-TsOH) in diethyl ether (**1.72**, 90% yield).²⁰ Grignard conversion proceeded via a Grieco method in which bromide **1.72** was added to magnesium powder suspended in THF. The reaction mixture was heated periodically until it sustained reflux.²⁸



Scheme 1.13. Synthesis of key Grignard reagent **1.73**.²⁰

With the two key fragments, **1.68** and **1.73**, in hand, we were equipped to form the spiroaminal (Scheme 1.14). The solution of Grignard **1.73** was added dropwise to ether **1.68** in THF at -20 °C. This reaction mixture was kept between -10 and -15 °C and was quenched with water after 2.5 hours. Purification by flash chromatography afforded tertiary alcohol **1.74** as an epimeric mixture in a combined yield of 80%. Addition of *p*-TsOH cleaved the THP ether to form iminium salt **1.75**, which was cyclized to form spiroaminal **1.76** (80% yield) as a single diastereomer, a conversion directed by the C₇ (*R*)-methoxy substituent. Removal of the *para*-methoxybenzyl (PMB) protecting group by ceric ammonium nitrate (CAN) generated lactam **1.77** in 67% yield.²⁰

The stereochemistry of **1.76**, with *anti* O₇, O₈ geometry, was determined by NOESY and literature precedents (Figure 1.7).²⁹ While the stereochemistry of the model system at C₇ is the same as **1.1**, the absolute stereochemistry at C₈ is opposite that of the natural product. Compound **1.76**, however, still proved useful as a tool to study conditions for final A-ring pyrrole installation.



Scheme 1.14. Synthesis of spiroaminal moiety of marineosin A (**1.1**).²⁰

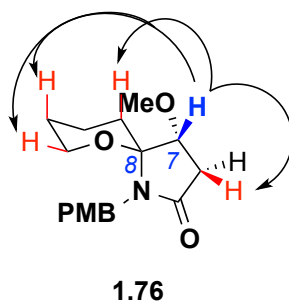
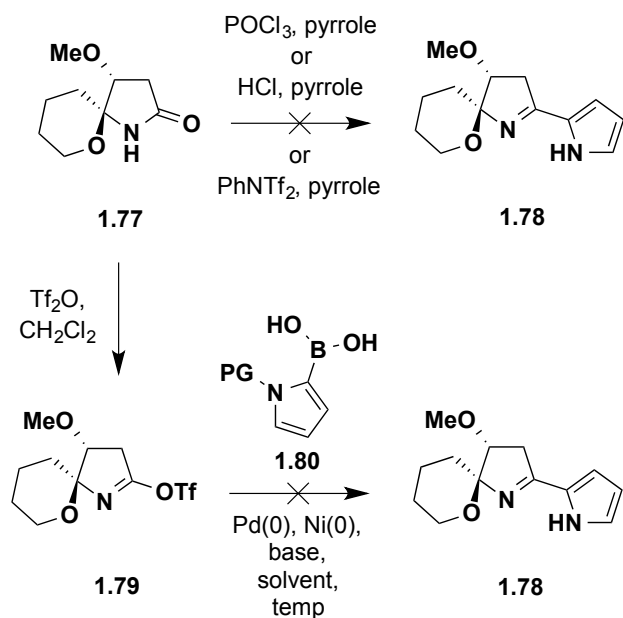


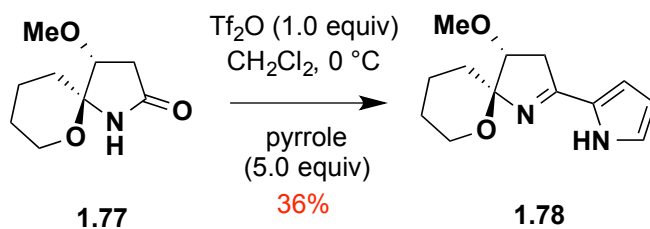
Figure 1.7. Diagnostic nOe correlations in spiroaminal **1.76**.²⁰

We planned to install the pyrrole through classical Vilsmeier-type chemistry using phosphorus oxychloride (POCl_3) and pyrrole, but these attempts proved unsuccessful.²⁹ Transforming the lactam to the triflate followed by a Suzuki coupling with *N*-protected, 2-pyrrole boronic acid also failed to provide the desired product despite examining a range of reaction conditions (Scheme 1.15).²⁰



Scheme 1.15. Attempts to install the A-ring pyrrole moiety.²⁰

In 2000, Baraznenok *et al.* had shown that addition of triflic anhydride to indolin-2-one followed immediately by the addition of a functionalized indole afforded the *bis*-indole product.³⁰ Based on this precedent, we treated lactam **1.77** with 2.0 equivalents of triflic anhydride (Tf₂O) to generate the iminium triflate salt. Addition of 5.0 equivalents of pyrrole in dichloromethane at 0 °C provided only a trace amount (<5% yield) of model system **1.78**. After assessment of the reaction conditions, we found that using only 1.0 equivalent of triflic anhydride provided the desired model system (**1.78**) of **1.1** in 36% yield (~9% yield overall) (Scheme 1.16). A two-dimensional NOESY experiment confirmed the stereochemistry of **1.78** (Figure 1.8). We did not see any equilibration to the *syn* O₇, O₈ isomer even after two weeks in deuterated chloroform.^{22,29} This lack of epimerization is likely due to favorable stabilization of the oxocarbenium ion and lack of a disruptive diaxial interaction.



Scheme 1.16. Late stage installation of the A-ring pyrrole.²⁰

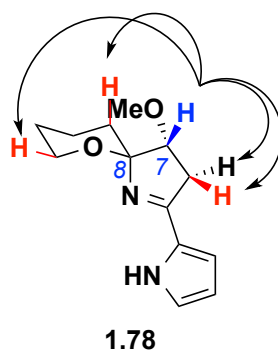
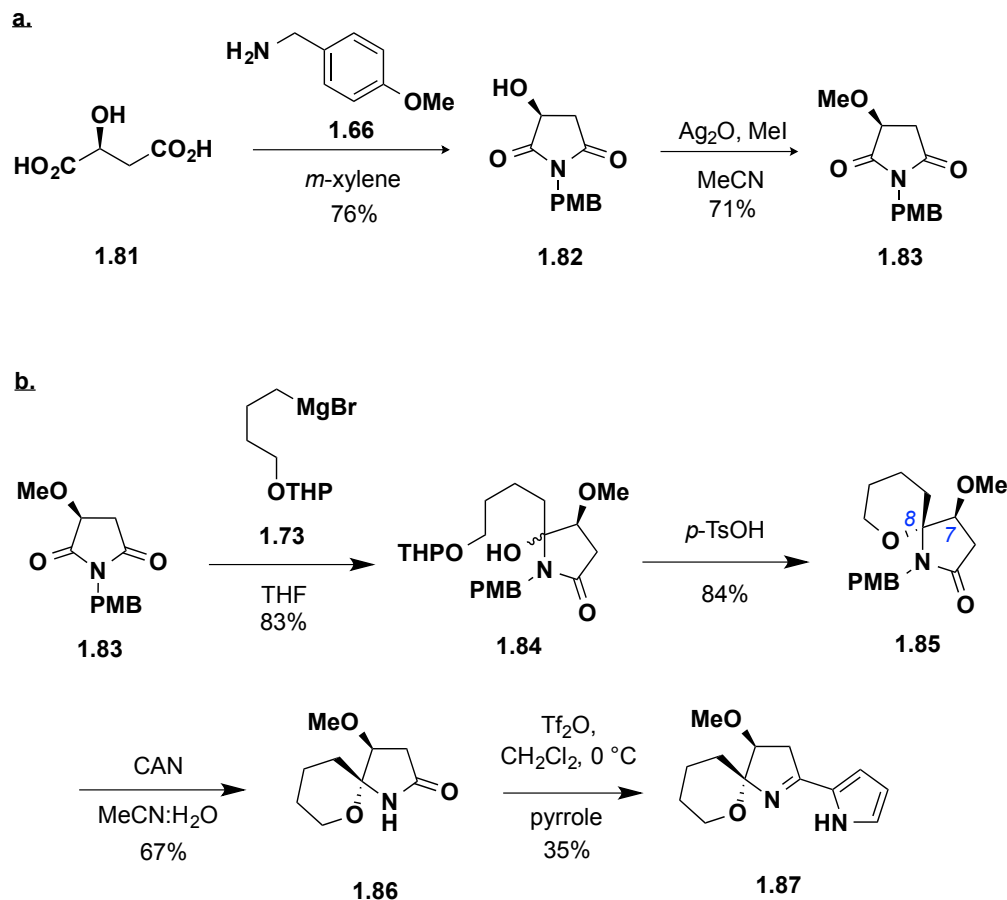


Figure 1.8. Diagnostic nOe correlations in model system **1.78** reminiscent of marineosin A (**1.1**).²⁰

Repetition of the reaction sequence starting with the (*S*)-hydroxy succinic acid afforded model system **1.87**, confirmed by NOESY and reminiscent of **1.2**, in ~9% overall yield (Scheme 1.17). Although the stereocenters of these models are configurationally opposite to **1.1** and **1.2**, we predict that additional substituents on the pyran ring will provide the *syn* isomers based on increased steric demands.²⁰

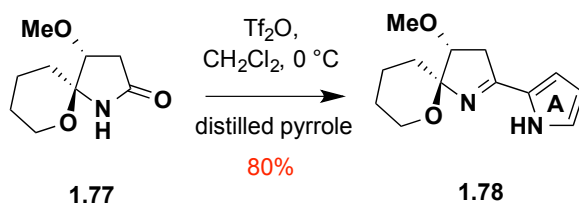
Model systems **1.78** and **1.87** were evaluated in our HCT-116 human colon carcinoma cytotoxicity assay in order to ascertain if they represented minimum pharmacophores of **1.1** and **1.2**, respectively. Interestingly, both compounds were inactive, suggesting a larger construct and/or stereochemical conformation is necessary



Scheme 1.17. Synthesis of model system **1.87** reminiscent of marineosin B (**1.2**). (a) Preparation of (*S*)-maleimide fragment (**1.83**). (b) Preparation of (*S*)-spiroiminal (**1.87**).

for biological activity.²⁰ These compounds also proved to be inactive in a large kinase panel screen.

Shortly after our publication of the previously described spiroiminal systems, Shi and co-workers demonstrated a similar Vilsmeier-Haack type transformation with triflic anhydride and *distilled* pyrrole.^{20,31} We decided to test these reaction conditions on our own substrate and were able to improve the yield for our pyrrole installation from 36% yield to 80% yield (Scheme 1.18). Further attempts using pyrrole as the solvent resulted in no reaction.



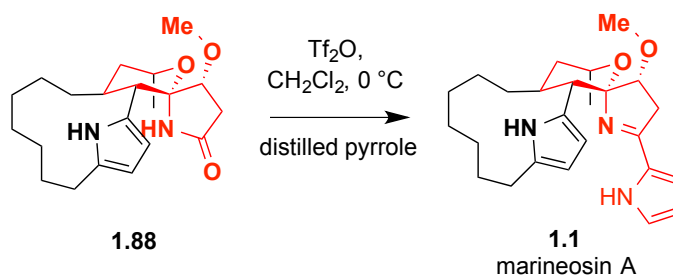
Scheme 1.18. Optimization of late-stage pyrrole installation.

1.5. Conclusions

In conclusion, we have developed an enantioselective synthesis of two spiroiminal model systems reminiscent of marineosins A (**1.1**) and B (**1.2**) starting from chiral molecules. The chemistry developed for late stage pyrrole installation occurs in a single pot reaction in which the triflate is formed *in situ* and intercepted by the pyrrole nucleophile. Optimization of this reaction resulted in a yield increase from 36% yield to 80% yield. The application of this chemistry will be applied to the total synthesis of **1.1** (Scheme 1.19), of which the macrocyclic pyrrole (**1.109**, Scheme 1.20) and another, more advanced, functionalized spiroaminal model system have been developed.³

1.6. Future Directions

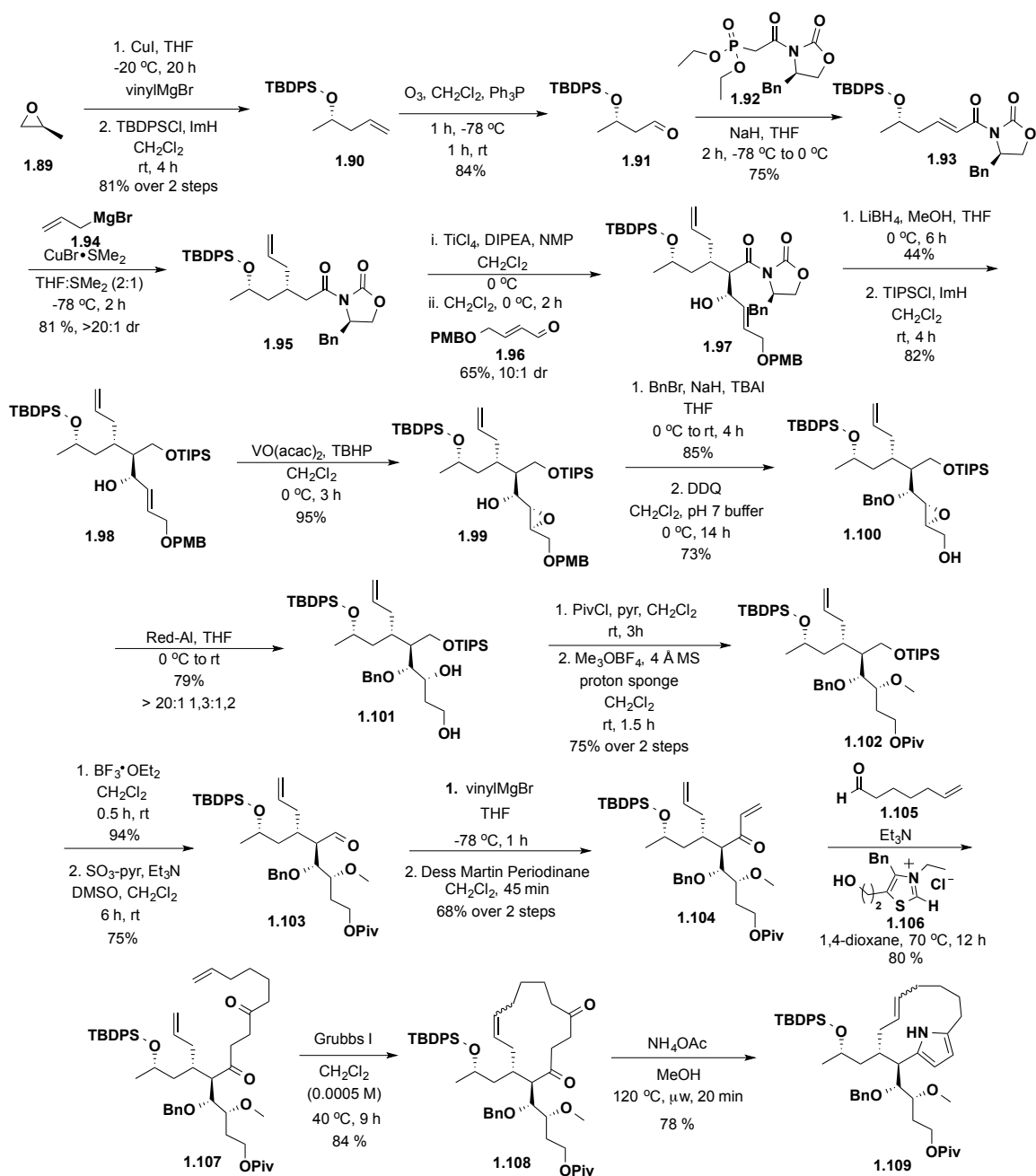
The total synthetic route is a diastereoselective sequence of 29 reactions starting from a chiral starting material (Scheme 1.20). Twenty intermediates have been fully characterized and confirmed. The first reaction is a copper assisted epoxide opening of (*S*)-propylene oxide (**1.89**) by vinyl magnesium bromide. A Michael Addition, subsequent aldol condensation, and methylation are key reactions in the formation of poly-functionalized **1.102**, a critical intermediate. Pivotal reactions from **1.102** towards



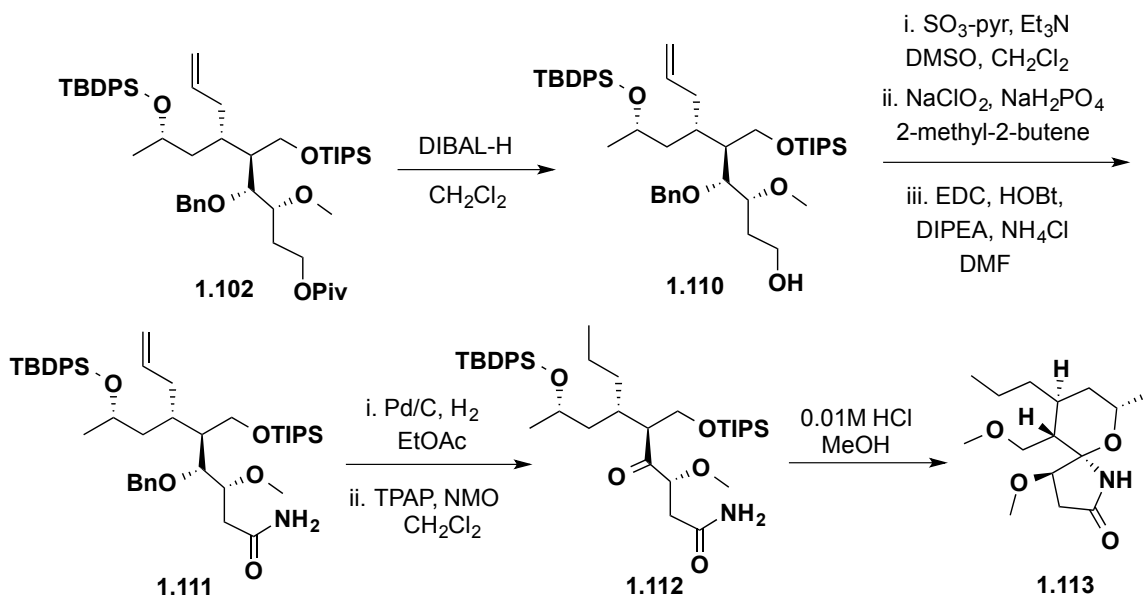
Scheme 1.19. Envisioned completion of marineosin A (**1.1**) based on developed model system **1.78**.²⁰ (Adapted from Lindsley 2013).

the natural product include a carbon-carbon bond forming Stetter reaction, a macrocyclic ring closing metathesis, and a Paal-Knorr pyrrole synthesis, which provides the most advanced intermediate (**1.109**).

We are confident in the proposed final steps including the acid-mediated cyclization to the spiroaminal based on the synthesis of functionalized model system **1.113** (Scheme 1.21) formed from common intermediate **1.102**. The pivaloyl group of **1.102** was removed with diisobutylaluminium hydride (DIBAL-H). Oxidation under Parikh-Doering conditions provided the ensuing aldehyde, which was further oxidized under Pinnick conditions.^{32,33} The resulting carboxylic acid was converted to the primary amide (**1.111**) using standard coupling conditions with ammonium chloride. Hydrogenolysis of the benzyl ether and contemporaneous hydrogenation of the olefin provided the secondary alcohol, which was immediately oxidized to the ketone (**1.112**) under Ley conditions.³⁴ Acid mediated cyclization and global deprotection with 0.01 M hydrochloric acid (HCl) provided spiroaminal **1.113**, which was confirmed to have the same absolute stereochemistry as marineosin A (**1.1**) (Figure 1.9).³ At this point in the synthesis, treatment with phosphorous oxychloride and pyrrole were used to provide the spiroiminal A-ring pyrrole.²⁹ While there was formation of the desired product, the



Scheme 1.20. Route to macrocyclic pyrrole **1.109** via critical intermediate **1.102**.³
(Adapted from Lindsley 2013).



Scheme 1.21. Synthesis of the spiroaminal lactam moiety of marineosin A (**1.1**).³

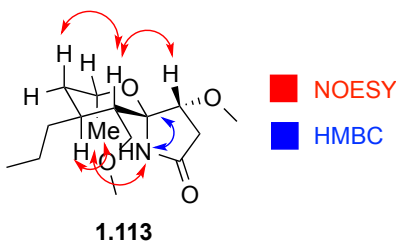


Figure 1.9. Diagnostic correlations in model system **1.113**.³

considerable polarity did not allow for separation from the pyrrole solvent and the instability did not allow for reverse-phase chromatography, thus indicating the need for different reaction conditions.⁸

Despite having found successful reaction conditions for our model systems, it is possible that these same conditions may not be effective for synthesizing **1.1**. One potential difficulty is the stability of macrocyclic pyrrole **1.109**. Although the exact

stability of this compound is unknown, degradation ensued after four days on the bench, where it was exposed to air and light. Storing this compound at 0 °C under argon may prevent degradation from occurring. However, pyrrole protection may be necessary to progress the substrate through successive reactions.

Successful completion of the total synthesis of these complex compounds remains a challenging goal. However, once the synthesis of the more potent marineosin A (**1.1**) is accomplished, a thorough biological screening will be completed. Furthermore, in order for **1.1** and/or its derivatives to be useful tool compounds, the target(s) of these compounds must also be elucidated. Therefore, this work has the potential to elucidate a new target for cancer drug design. In the event that the marineosin A (**1.1**) target is not a new target, useful correlations made between these molecules and current cancer research will still be obtained. Additionally, completion of this research will add to the current knowledge of the prodigiosins and has the potential to produce compounds that are antimalarial, immunosuppressive, and/or antibacterial, as have been found with the prodigiosin compounds.

1.7. Experimental Section

1.7.1. Methods and Materials

All reagents and solvents were commercial grade and purified prior to use when necessary. Analytical TLC was performed on Sorbent Technologies HL 0.25 mm silica gel plates with UV indicator. Visualization was accomplished by irradiation under a 254 nm UV lamp and/or the use of an iodine chamber. Chromatography on silica gel was

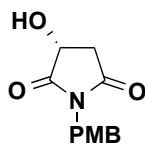
performed using Silica Gel 60 (230-400 mesh) from Sorbent Technologies.

^1H and ^{13}C NMR spectra were recorded on a Bruker DRX-400 (400 and 100 MHz, respectively) NMR instrument. Chemical shifts are reported in ppm from the solvent resonance as an internal standard. Data are reported as follows: chemical shift, multiplicity, coupling constant (Hz), and number of protons.

Optical rotations were measured on a JASCO P-2000 digital polarimeter at room temperature. Concentration (c) in g/100 mL and solvent are given in parentheses.

A Micromass Q-ToF API-US mass spectrometer was used to acquire HRMS data. The value Δ is the error in the measurement (in ppm) given by the equation $\Delta = [(M_E - M_T) / M_T] \times 10^6$, where M_E is the experimental mass and M_T is the theoretical mass. The HRMS results were obtained with ES as the ion source and leucine enkephalin as the reference.

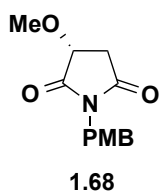
1.7.2. Experimental Procedures



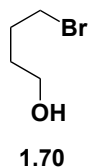
1.67

(R)-3-hydroxy-1-(4-methoxybenzyl)pyrrolidine-2,5-dione (1.67). To a solution of (*R*)-2-hydroxysuccinic acid (3.2 g, 24.0 mmol) in 50% aqueous methanol (5 mL) was slowly added (4-methoxyphenyl)methanamine (3.14 mL, 24.0 mmol). Methanol was removed under reduced pressure. The reaction mixture was partitioned with *m*-xylene (64 mL) and heated to 190 °C. Water was azeotropically removed with a Dean-Stark trap. After 24

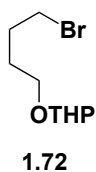
hours, the solvent was removed under reduced pressure. The residue was partitioned with ethanol (25 mL) and concentrated. Recrystallization from benzene provided 4.4 g (78%) of maleimide **1.67**. ^1H NMR (CDCl_3 , 400 MHz) δ 2.66 (dd, $J = 4.8, 18.2$ Hz, 1H), 2.93 (bs, 1H), 3.05 (dd, $J = 8.5, 18.2$ Hz, 1H), 3.78 (s, 3H), 4.56-4.65 (m, 3H), 6.83 (d, $J = 8.7$ Hz, 2H), 7.32 (d, $J = 8.7$ Hz, 2H). ^{13}C NMR (CDCl_3 , 100 MHz) δ 37.1, 41.8, 55.2, 66.8, 113.9, 127.4, 130.3, 159.3, 174.0, 178.3. HRMS (TOF, ES $^+$): $\text{C}_{12}\text{H}_{13}\text{NO}_4\text{Na}$ [$\text{M}+\text{Na}$] $^+$ calcd 258.0742, found 258.0741. $[\alpha]_{\text{D}}^{22} = +43.1$ (c 1, MeOH).



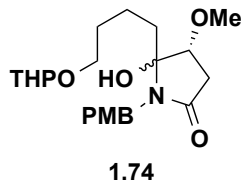
(R)-3-methoxy-1-(4-methoxybenzyl)pyrrolidine-2,5-dione (1.68). To a solution of maleimide **1.67** (4.15 g, 20.3 mmol) in acetonitrile (40 mL) at rt was added silver(I) oxide (4.69 g, 20.3 mmol) and MeI (3.6 mL, 57.9 mmol). The reaction mixture was refluxed for 1 h. After cooling to rt the reaction mixture was filtered and concentrated. The residue was purified on silica gel (20:80 EtOAc:hexanes) to provide 3.92 g (78%) of ether **1.68**. ^1H NMR (CDCl_3 , 400 MHz) δ 2.60 (dd, $J = 4.2, 18.2$ Hz, 1H), 2.98 (dd, $J = 8.2, 18.2$ Hz, 1H), 3.60 (s, 3H), 3.78 (s, 3H), 4.18 (dd, $J = 4.2, 8.2$ Hz, 1H), 4.59 (d, $J = 2.4$ Hz, 2H), 6.83 (d, $J = 8.7$ Hz, 2H), 7.32 (d, $J = 8.7$ Hz, 2H). ^{13}C NMR (CDCl_3 , 100 MHz) δ 35.5, 41.3, 54.9, 58.4, 74.5, 113.7, 127.5, 123.0, 159.0, 173.6, 175.1. HRMS (TOF, ES $^+$): $\text{C}_{13}\text{H}_{15}\text{NO}_4\text{Na}$ [$\text{M}+\text{Na}$] $^+$ calcd 272.0899, found 272.0900. $[\alpha]_{\text{D}}^{22} = +45.7$ (c 1, MeOH).



4-bromobutan-1-ol (1.70). To neat, refluxing THF (67.5 mL, 832 mmol) was added 48% aqueous hydrobromic acid (31 mL, 274 mmol) dropwise. The reaction mixture was held at reflux for 2 hours. After cooling to rt, the reaction was neutralized with saturated NaHCO₃, extracted with diethyl ether, dried over sodium sulfate, and concentrated to provide 31.4 g (75%) of alcohol **1.70**. NMR spectra matched that of commercial-grade material.

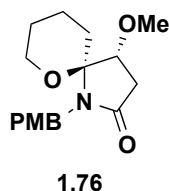


2-(4-bromobutoxy)tetrahydro-2H-pyran (1.72). To a stirred solution of alcohol **1.70** (1.95 g, 12.7 mmol) in diethyl ether (12 mL) at 0 °C was added *p*-TsOH (5 mg, 0.02 mmol) followed by dropwise addition of 3,4-dihydro-2H-pyran (1.5 mL, 16.6 mmol). The reaction mixture was allowed to reach rt. After 1 h, the reaction mixture was washed with saturated NaHCO₃ (2 x 10 mL) and brine. The organic layer was dried over K₂CO₃, filtered, and concentrated to provide 2.70 g (90%) of pyran **1.72**. NMR spectra matched that of a literature report.²⁸

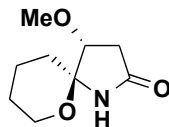


(4R)-5-hydroxy-4-methoxy-1-(4-methoxybenzyl)-5-(4-((tetrahydro-2H-pyran-2-yl)oxy)butyl)pyrrolidin-2-one (1.74). A flame-dried flask was charged with magnesium powder (447 mg, 18.4 mmol) and placed under an inert argon atmosphere. The magnesium was suspended in anhydrous THF (21 mL). To this mixture was added pyran **1.72** (1.4 mL, 7.5 mmol). After warming to 50 °C, pyran **1.72** (2.0 mL, 10.7 mmol) was added dropwise. The reaction mixture was heated periodically until it sustained reflux. A separate flame-dried flask was charged with ether **1.68** (1.5 g, 6.0 mmol) and THF (30 mL). After cooling to -20 °C, the solution of Grignard **1.73** was added dropwise via syringe. The reaction mixture was kept between -10 °C and -15 °C. After 2.5 h, water (5 mL) was added and the reaction was allowed to reach rt. The product was extracted with diethyl ether (3 x 20 mL). The combined organics were washed with brine, dried over Na₂SO₄, and concentrated. The residue was purified on silica gel (30:70 EtOAc:hexanes) to provide 6.61 g (80%) of tertiary alcohol **1.74**. ¹H NMR (CDCl₃, 400 MHz) δ 1.48-1.59 (m, 5H), 1.61-1.75 (m, 2H), 1.77-1.90 (m, 1H), 2.12-2.24 (m, 2H), 2.57 (d, *J* = 17.9 Hz, 1H), 2.71 (dddd, *J* = 1.9, 7.2, 17.8 Hz, 1H), 3.27 (s, 3H), 3.29-3.34 (m, 1H), 3.45-3.50 (m, 1H), 3.63-3.71 (m, 1H), 3.77 (s, 3H), 3.80-3.85 (m, 1H), 4.49-4.52 (m, 1H), 4.55-4.66 (m, 3H), 4.85 (q, *J* = 6.8 Hz, 1H), 6.81 (d, *J* = 8.6 Hz, 2H), 7.13 (d, *J* = 8.6 Hz, 2H). ¹³C NMR (CDCl₃, 100 MHz) δ 19.6, 19.8, 23.4, 23.5, 25.4 (2C), 30.1, 30.2, 30.7, 30.8, 36.0 (2C), 42.9 (2C), 55.1, 55.2, 62.3, 62.6, 66.5, 66.7, 72.0 (2C), 98.9, 99.0, 107.0, 107.1, 113.9 (2C), 127.9, 128.3, 128.4, 139.2, 139.3, 158.8 (2C), 173.0, 173.1. HRMS

(TOF ES+): C₂₂H₃₃NO₆Na [M+Na]⁺ calcd 430.2206, found 430.2210. [α]²²_D = -15.0 (c 0.6, CHCl₃). HRMS (TOF, ES+): C₁₃H₁₅NO₄Na [M+Na]⁺ calcd 272.0899, found 272.0900.

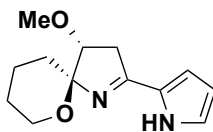


(4R,5S)-4-methoxy-1-(4-methoxybenzyl)-6-oxa-1-azaspiro[4.5]decan-2-one (1.76). To a stirred solution of tertiary alcohol **1.74** (390 mg, 1.0 mmol) in CH₂Cl₂ (6 mL) at 0 °C was added *p*-TsOH monohydrate (41 mg, 0.2 mmol). After 30 minutes the solvent was removed. The residue was purified on silica gel (30:70 EtOAc:hexanes) to provide 244 mg (80%) of spiroaminal **1.76**. ¹H NMR (CDCl₃, 400 MHz) δ 1.39-1.51 (m, 4H), 1.63-1.70 (m, 1H), 1.85-1.92 (m, 1H), 2.47 (d, *J* = 17.4 Hz, 1H), 2.65 (dd, *J* = 5.5, 17.4 Hz, 1H), 3.32 (s, 3H), 3.61 (m, 1H), 3.73 (s, 3H), 3.84 (dd, *J* = 2.4, 11.2 Hz, 1H), 3.95 (d, *J* = 5.5 Hz, 1H), 4.11 (d, *J* = 16.0 Hz, 1H), 4.70 (d, *J* = 16.0 Hz, 1H), 6.78 (d, *J* = 8.7 Hz, 2H), 7.14 (d, *J* = 8.7 Hz, 2H). ¹³C NMR (CDCl₃, 100 MHz) δ 20.0, 24.6, 27.9, 34.3, 41.8, 55.0, 56.6, 64.7, 74.9, 94.9, 113.5, 127.9, 130.5, 158.2, 174.5. HRMS (TOF, ES+): C₁₇H₂₄NO₄ [M+H]⁺ calcd 306.1705, found 306.1702. [α]²²_D = -50.6 (c 1, CHCl₃).



1.77

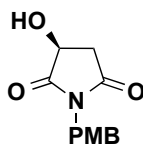
(4R,5S)-4-methoxy-6-oxa-1-azaspiro[4.5]decan-2-one (1.77). To a stirred solution of spiroaminal **1.76** (258 mg, 0.85 mmol) in acetonitrile (27 mL) and water (3.5 mL) was added CAN (1.4 g, 2.5 mmol). After 1.5 h, a second portion of CAN (467 mg, 0.8 mmol) was added. After 1 h, the acetonitrile was removed under reduced pressure. The product was extracted with CH₂Cl₂ (4 x 15 mL). The combined organic layers were washed with brine, dried over Na₂SO₄, and concentrated. The residue was purified on silica gel (30:70 EtOAc/hexanes) to provide 105 mg (67%) of amide **1.77**. ¹H NMR (CDCl₃, 400 MHz) δ 1.54-1.63 (m, 2H), 1.63-1.73 (m, 1H), 1.73-1.83 (m, 3H), 2.29 (dd, *J* = 1.7, 17.2 Hz, 1H), 2.70 (dd, *J* = 5.6, 17.2 Hz, 1H), 3.34 (s, 3H), 3.66-3.72 (m, 3H), 8.64 (bs, 1H). ¹³C NMR (CDCl₃, 100 MHz) δ 19.4, 25.2, 29.3, 35.7, 57.3, 62.7, 82.4, 91.8, 177.3. HRMS (TOF, ES⁺): C₉H₁₆NO₃ [M+H]⁺ calcd 186.1130, found 186.1131. [α]_D²² = -97.1 (c 1.1, CHCl₃).



1.78

(4R,5S)-4-methoxy-2-(1H-pyrrol-2-yl)-6-oxa-1-azaspiro[4.5]dec-1-ene (1.78). A flame-dried flask was charged with amide **1.77** (64 mg, 0.3 mmol) and placed under an inert argon atmosphere. After cooling to 0° C, CH₂Cl₂ (4 mL) and trifluoromethanesulfonic anhydride (58.2 μL, 0.3 mmol) were added. After 2 minutes, pyrrole (119.8 μL, 1.7 mmol) was added. After 10 minutes, the reaction was quenched

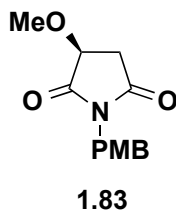
with saturated NaHCO₃ and allowed to reach rt. The product was extracted with CH₂Cl₂ (3 x 5 mL). The combined organics were dried over Na₂SO₄ and concentrated. The residue was purified on silica gel (30:70 EtOAc/hexanes) to provide 29 mg (36%) of pyrrole **1.78**. ¹H NMR (CDCl₃, 400 MHz) δ 1.54-1.78 (m, 5H), 1.86-1.99 (m, 2H), 2.78 (dd, *J* = 5.3, 16.5 Hz, 1H), 3.21 (dd, *J* = 6.8, 16.5 Hz, 1H), 3.44 (s, 3H), 3.72 (d, *J* = 10.8 Hz, 1H), 3.84 (t, *J* = 6.2 Hz, 1H), 4.15 (dt, *J* = 2.8, 11.1 Hz, 1H), 6.21 (t, *J* = 3.2 Hz, 1H), 6.57 (d, *J* = 3.5 Hz, 1H), 6.90 (s, 1H). ¹³C NMR (CDCl₃, 100 MHz) δ 19.6, 25.8, 29.2, 38.7, 58.2, 64.2, 85.3, 102.8, 110.7, 112.8, 121.1, 126.3, 164.6. HRMS (TOF, ES⁺): C₁₃H₁₉N₂O₂ [M+H]⁺ calcd 235.1447, found 235.1447. [α]_D²² = -65.2 (c 1.6, CHCl₃).



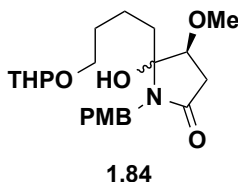
1.82

(S)-3-hydroxy-1-(4-methoxybenzyl)pyrrolidine-2,5-dione (1.82). To a solution of (*S*)-2-hydroxysuccinic acid (8.05 g, 60.0 mmol) in 50% aqueous methanol (12 mL) was slowly added (4-methoxyphenyl)methanamine (7.84 mL, 60.0 mmol). Methanol was removed under reduced pressure. The reaction mixture was partitioned with *m*-xylene (160 mL) and heated to 190 °C. Water was azeotropically removed with a Dean-Stark trap. After 24 hours, the solvent was removed under reduced pressure. The residue was partitioned with ethanol (50 mL) and concentrated. Recrystallization from benzene provided 10.99 g (78%) of maleimide **1.82**. ¹H NMR (CDCl₃, 400 MHz) δ 2.66 (dd, *J* = 4.8, 18.2 Hz, 1H), 2.93 (bs, 1H), 3.05 (dd, *J* = 8.5, 18.2 Hz, 1H), 3.78 (s, 3H), 4.56-4.65 (m, 3H), 6.83 (d, *J* = 8.7 Hz, 2H), 7.32 (d, *J* = 8.7 Hz, 2H). ¹³C NMR (CDCl₃, 100 MHz)

δ 37.1, 41.8, 55.2, 66.8, 113.9, 127.4, 130.3, 159.3, 174.0, 178.3. HRMS (TOF, ES⁺): C₁₂H₁₃NO₄Na [M+Na]⁺ calcd 258.0742, found 258.0741. $[\alpha]_D^{22} = 44.5$ (c 1, MeOH).

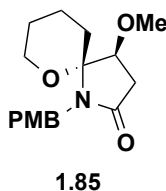


(S)-3-methoxy-1-(4-methoxybenzyl)pyrrolidine-2,5-dione (1.83). To a solution of maleimide **1.82** (8.00 g, 34.0 mmol) in acetonitrile (70 mL) at rt was added silver(I) oxide (7.88 g, 34.0 mmol) and iodomethane (6.1 mL, 97.2 mmol). The reaction mixture was refluxed for 1 h. After cooling to rt the reaction mixture was filtered and concentrated. The residue was purified on silica gel (20:80 EtOAc:hexanes) to provide 6.61 g (78%) of ether **1.83**. ¹H NMR (CDCl₃, 400 MHz) δ 2.60 (dd, $J = 4.2, 18.2$ Hz, 1H), 2.98 (dd, $J = 8.2, 18.2$ Hz, 1H), 3.60 (s, 3H), 3.78 (s, 3H), 4.18 (dd, $J = 4.2, 8.2$ Hz, 1H), 4.59 (d, $J = 2.4$ Hz, 2H), 6.83 (d, $J = 8.7$ Hz, 2H), 7.32 (d, $J = 8.7$ Hz, 2H). ¹³C NMR (CDCl₃, 100 MHz) δ 35.5, 41.3, 54.9, 58.4, 74.5, 113.7, 127.5, 123.0, 159.0, 173.6, 175.1. HRMS (TOF, ES⁺): C₁₃H₁₅NO₄Na [M+Na]⁺ calcd 272.0899, found 272.0900. $[\alpha]_D^{22} = -55.6$ (c 1, MeOH).



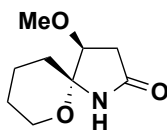
(4S)-5-hydroxy-4-methoxy-1-(4-methoxybenzyl)-5-((tetrahydro-2H-pyran-2-yl)oxy)butylpyrrolidin-2-one (1.84). A flame-dried flask was charged with magnesium

powder (1.51 g, 60.8 mmol) and placed under an inert argon atmosphere. The magnesium was suspended in anhydrous THF (70 mL). To this mixture was added pyran **1.72** (3.8 mL, 20.3 mmol). After warming to 50 °C, pyran **1.72** (7.6 mL, 40.5 mmol) was added dropwise. The reaction mixture was heated periodically until it sustained reflux. A separate flame-dried flask was charged with ether **1.83** (5.05 g, 20.3 mmol) and THF (100 mL). After cooling to -20 °C, the solution of Grignard **1.73** was added dropwise via syringe. The reaction mixture was kept between -10 °C and -15 °C. After 2.5 h, water (10 mL) was added and the reaction was allowed to reach rt. The product was extracted with diethyl ether (3 x 20 mL). The combined organics were washed with brine, dried over Na₂SO₄, and concentrated. Tertiary alcohol **1.84** was used in the next reaction without any further purification.



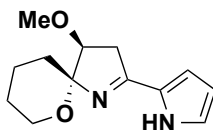
(4*S*,5*R*)-4-methoxy-1-(4-methoxybenzyl)-6-oxa-1-azaspiro[4.5]decan-2-one (1.85). To a stirred solution of tertiary alcohol **1.84** (6.82 g, 16.8 mmol) in CH₂Cl₂ (100 mL) at 0 °C was added *p*-TsOH monohydrate (796 mg, 4.19 mmol). After 30 minutes the solvent was removed. The residue was purified on silica gel (30:70 EtOAc:hexanes) to provide 4.28 g (84%) of spiroaminal **1.85**. ¹H NMR (CDCl₃, 400 MHz) δ 1.39-1.51 (m, 4H), 1.63-1.70 (m, 1H), 1.85-1.92 (m, 1H), 2.47 (d, *J* = 17.4 Hz, 1H), 2.65 (dd, *J* = 5.5, 17.4 Hz, 1H), 3.32 (s, 3H), 3.61 (m, 1H), 3.73 (s, 3H), 3.84 (dd, *J* = 2.4, 11.2 Hz, 1H), 3.95 (d, *J* = 5.5 Hz, 1H), 4.11 (d, *J* = 16.0 Hz, 1H), 4.70 (d, *J* = 16.0 Hz, 1H), 6.78 (d, *J* = 8.7 Hz, 2H),

7.14 (d, $J = 8.7$ Hz, 2H). ^{13}C NMR (CDCl_3 , 100 MHz) δ 20.0, 24.6, 27.9, 34.3, 41.8, 55.0, 56.6, 64.7, 74.9, 94.9, 113.5, 127.9, 130.5, 158.2, 174.5. HRMS (TOF, ES⁺): $\text{C}_{17}\text{H}_{24}\text{NO}_4$ $[\text{M}+\text{H}]^+$ calcd 306.1705, found 306.1702. $[\alpha]_{\text{D}}^{22} = +74.3$ (c 1, CHCl_3).



1.86

(4*S*,5*R*)-4-methoxy-6-oxa-1-azaspiro[4.5]decan-2-one (1.86). To a stirred solution of spiroaminal **1.85** (2.23 g, 7.33 mmol) in acetonitrile (200 mL) and water (30.0 mL) was added CAN (12.0 g, 22.0 mmol). After 1.5 h, a second portion of CAN (4.02 g, 7.33 mmol) was added. After 1 h, the acetonitrile was removed under reduced pressure. The product was extracted with CH_2Cl_2 (4 x 20 mL). The combined organic layers were washed with brine, dried over Na_2SO_4 , and concentrated. The residue was purified on silica gel (30:70 EtOAc/hexanes) to provide 911 mg (67%) of amide **1.86**. ^1H NMR (CDCl_3 , 400 MHz) δ 1.54-1.63 (m, 2H), 1.63-1.73 (m, 1H), 1.73-1.83 (m, 3H), 2.29 (dd, $J = 1.7, 17.2$ Hz, 1H), 2.70 (dd, $J = 5.6, 17.2$ Hz, 1H), 3.34 (s, 3H), 3.66-3.72 (m, 3H), 8.64 (bs, 1H). ^{13}C NMR (CDCl_3 , 100 MHz) δ 19.4, 25.2, 29.3, 35.7, 57.3, 62.7, 82.4, 91.8, 177.3. HRMS (TOF, ES⁺): $\text{C}_9\text{H}_{16}\text{NO}_3$ $[\text{M}+\text{H}]^+$ calcd 186.1130, found 186.1131. $[\alpha]_{\text{D}}^{22} = +58.9$ (c 1, CHCl_3).



1.87

(4*S*,5*R*)-4-methoxy-2-(1*H*-pyrrol-2-yl)-6-oxa-1-azaspiro[4.5]dec-1-ene (1.87). A flame-dried flask was charged with amide **1.86** (18.5 mg, 0.1 mmol) and placed under an inert argon atmosphere. After cooling to 0 °C, CH₂Cl₂ (1 mL) and trifluoromethanesulfonic anhydride (17.0 μL, 0.1 mmol) were added. After 2 minutes, pyrrole (33.0 μL, 0.5 mmol) was added. After 10 minutes, the reaction was quenched with saturated NaHCO₃ and allowed to reach rt. The product was extracted with CH₂Cl₂ (3 x 5 mL). The combined organics were dried over Na₂SO₄ and concentrated. The residue was purified on silica gel (30:70 EtOAc/hexanes) to provide 8.2 mg (35%) of pyrrole **1.87**. ¹H NMR (CDCl₃, 400 MHz) δ 1.54-1.78 (m, 5H), 1.86-1.99 (m, 2H), 2.78 (dd, *J* = 5.3, 16.5 Hz, 1H), 3.21 (dd, *J* = 6.8, 16.5 Hz, 1H), 3.44 (s, 3H), 3.72 (d, *J* = 10.8 Hz, 1H), 3.84 (t, *J* = 6.2 Hz, 1H), 4.15 (dt, *J* = 2.8, 11.1 Hz, 1H), 6.21 (t, *J* = 3.2 Hz, 1H), 6.57 (d, *J* = 3.5 Hz, 1H), 6.90 (s, 1H). ¹³C NMR (CDCl₃, 100 MHz) δ 19.6, 25.8, 29.2, 38.7, 58.2, 64.2, 85.3, 102.8, 110.7, 112.8, 121.1, 126.3, 164.6. HRMS (TOF, ES⁺): C₁₃H₁₉N₂O₂ [M+H]⁺ calcd 235.1447, found 235.1447. [α]_D²² = +43.1 (c 1.7, CHCl₃).

Chapter 2

DISCOVERY OF VU0431316, A NEGATIVE ALLOSTERIC MODULATOR OF THE METABOTROPIC GLUTAMATE RECEPTOR 5

2.1. Introduction

Metabotropic glutamate receptor 5 (mGluR₅) is involved in a variety of psychiatric and neurologic disorders, and mGluR₅ therapeutics have the potential to dramatically improve the treatments available for these disorders. Because conventional orthosteric modulators of mGluR₅ can lack satisfactory aqueous solubility, demonstrate poor oral bioavailability, and/or exhibit unfavorable effects, there is a need for selective allosteric modulators of mGluR₅ that overcome these deficiencies. While MPEP and MTEP have proven to be valuable negative allosteric modulator (NAM) tool compounds, both of these compounds have characteristics that prevent them from becoming full therapeutic molecules. Thus, there has been an interest in the development of mGluR₅ NAMs within chemotypes that do not contain a disubstituted alkyne motif. The following describes the successful discovery of tool compound VU0431316 from an aryl ether series of mGluR₅ NAMs.

2.1.1. Metabotropic Glutamate Receptors

Metabotropic glutamate receptors (mGluRs) are part of family C (also known as family 3) of the G-protein-coupled receptor (GPCR) superfamily.³⁵ GPCRs are membrane-bound proteins characterized by seven-transmembrane (7TM) helices that transmit extracellular signals through the receptor to internally associated G-proteins.

When activated by an extracellular ligand, GPCRs undergo a conformational change that activates an associated G-protein, composed of a heterotrimeric complex of α , β , and γ subunits. The activated G-protein exchanges GDP for GTP at the α subunit. This exchange triggers the α subunit as well as the combined β,γ subunit to disassociate from the receptor and activate signal transduction pathways (Figure 2.1).³⁵ Not surprisingly, GPCRs, the largest class of cell-surface receptors, have been implicated in a number of disorders and are the therapeutic target of nearly half of the pharmaceuticals on the market today.³⁶

GPCRs can be activated by a number of ligands including light, peptides, and neurotransmitters (NTs); however, mGluRs are exclusively activated by L-glutamate, the most abundant excitatory NT in the mammalian central nervous system (CNS).^{35,37,38} Metabotropic glutamate receptors exist as dimers and are distinguished from the other families of GPCRs by their large, extracellular domain, known as the Venus flytrap domain (VFD) (Figure 2.2). Extracellular signals are transduced, most likely via a disulfide bridge, from the VFD to a cysteine-rich domain (CRD), which connects the VFD to the 7TM domain. Eight subtypes of mGluRs have been identified, many having splice variants with differing C-terminal tails. The eight subtypes are further classified into groups (Table 2.1) based on sequence homology, G-protein coupling, and ligand selectivity.³⁵

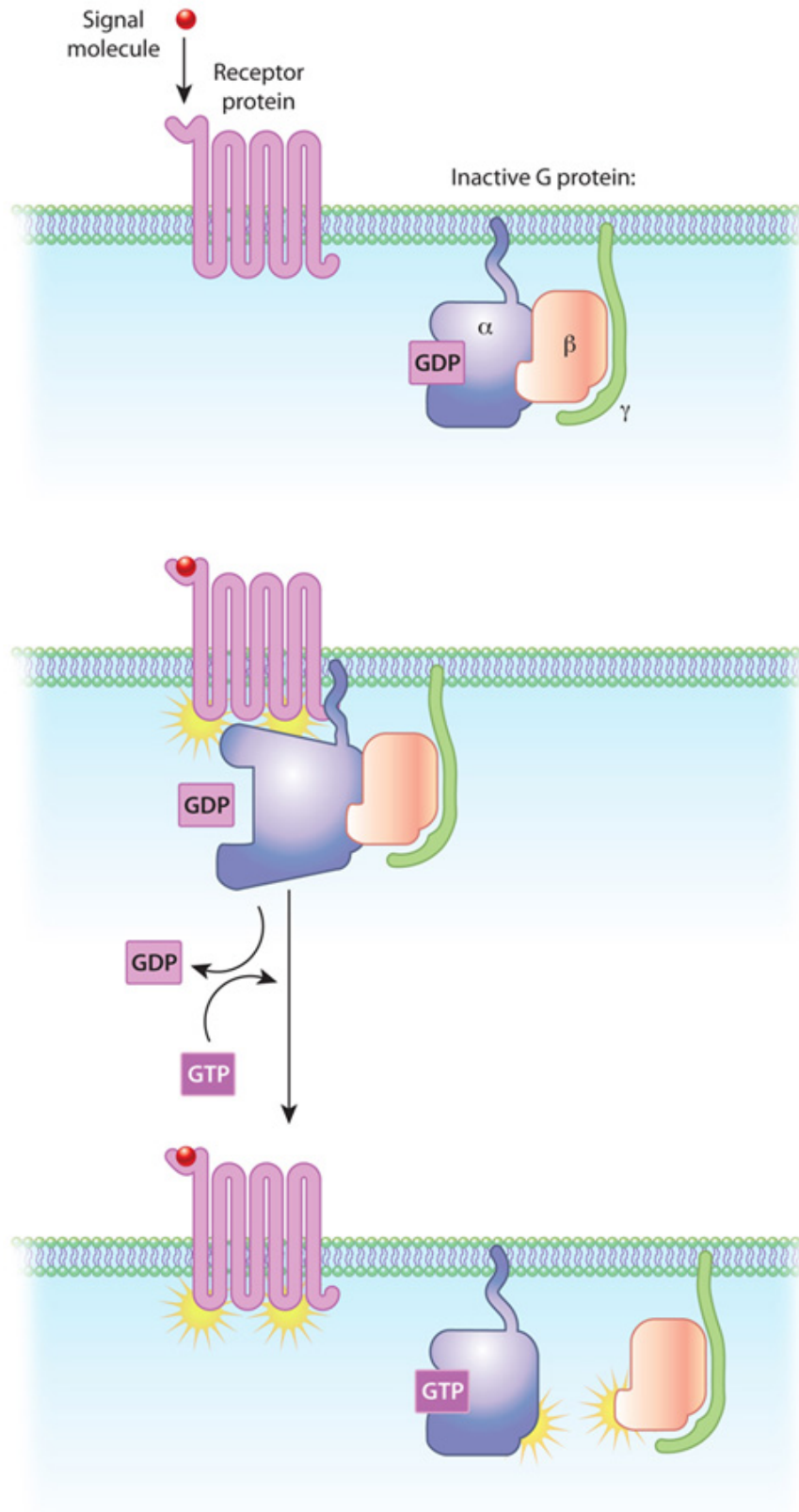


Figure 2.1. Diagram of GPCR activation.³⁹

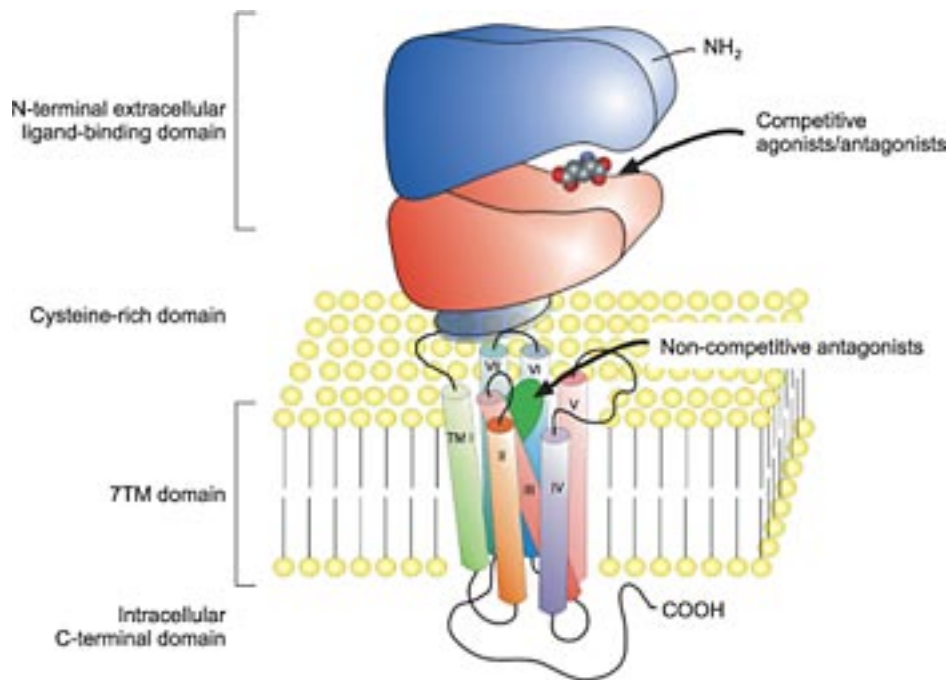
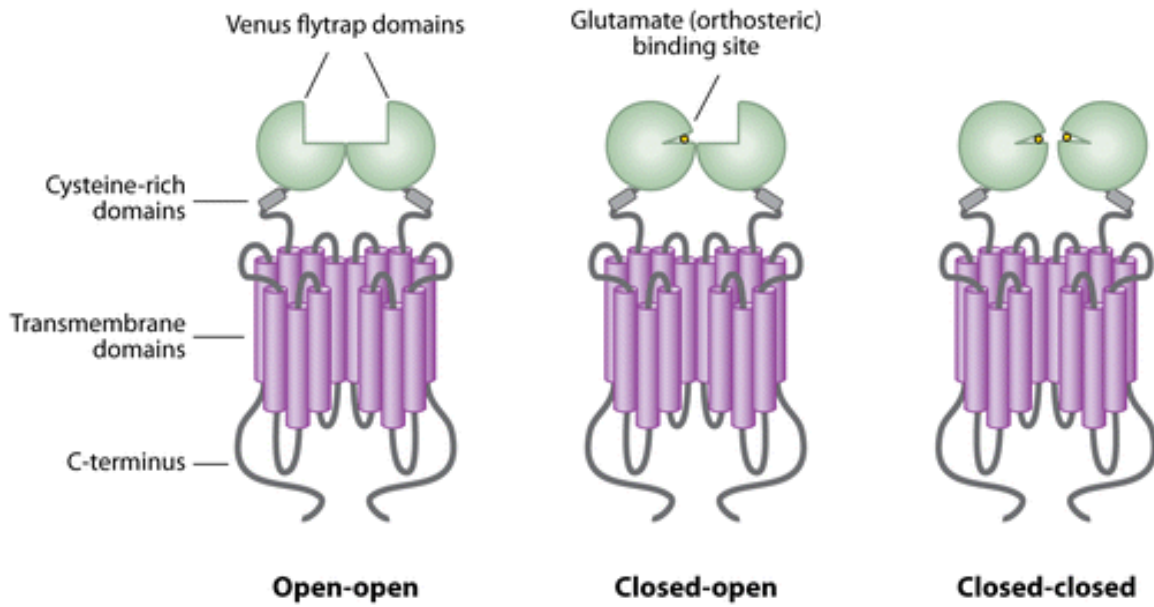


Figure 2.2. Monomeric structure of the mGluRs.⁴⁰

Table 2.1. mGluR Group classifications

Group	mGluR Subtypes
I	1, 5
II	2, 3
III	4, 6, 7, 8

The VFD, located at the N-terminal, contains the glutamate-binding site. Two VFDs are thought to dimerize back to back. Glutamate binding at one or both of these domains causes conformational changes that can activate the receptor, leading to three main states of an mGluR: open-open (inactive), closed-open (active), and closed-closed (active) (Figure 2.3). While it remains controversial as to whether or not binding of



AR Niswender CM, Conn PJ. 2010.
 Annu. Rev. Pharmacol. Toxicol. 50:295–322

Figure 2.3. Receptor conformations of the mGluR dimer.³⁵

glutamate to only one dimer activates the entire complex, it is clear that antagonists stabilize the open-open (inactive) state. This indicates that the relative orientation of the VFDs is important for activation. The VFDs also bind the divalent cations magnesium and calcium at the orthosteric site, which can also activate or potentiate the receptor.³⁵

In general, activating the different groups of mGluRs leads to independent intracellular pathways; however, it is now recognized that mGluRs from all groups can modulate additional signaling pathways depending on cell type or neuronal population.³⁵ Group I receptors favor coupling to $G_{\alpha q}$, stimulating phospholipase C and increasing intracellular calcium and inositol phosphate levels. These receptors are mostly located postsynaptically, and their activation leads to cell depolarization and increasing neuronal excitability. Groups II and III, located presynaptically, predominately couple to $G_{\alpha i}$,

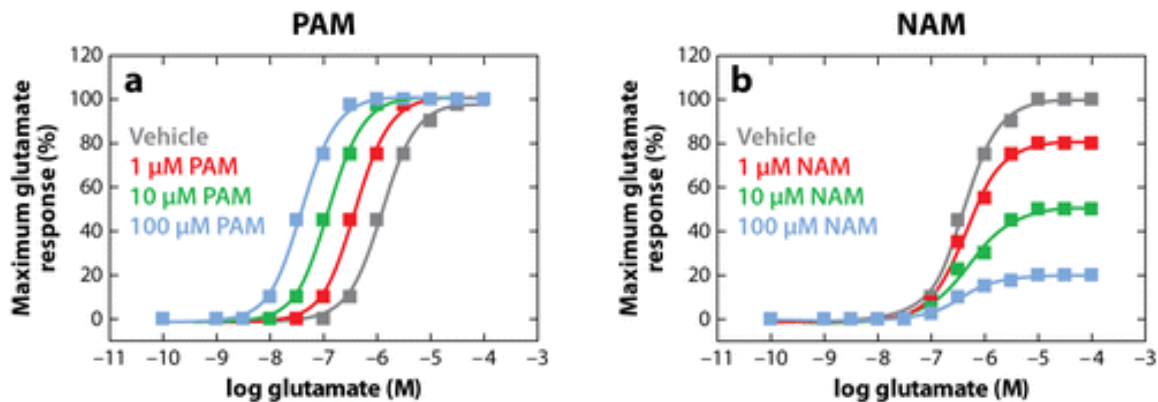
leading to a decrease in cAMP and typically have an inhibitory effect on NT release at various types of synapses.^{35,38}

2.1.2. Allosteric Modulators

The orthosteric binding site is highly conserved across all mGluRs, making it difficult to develop selective orthosteric ligands.⁴¹ Additionally, many orthosteric ligands, designed as glutamate analogs, lack the physical properties required to engender favorable drug-like features such as oral bioavailability and/or CNS penetration.³⁸ An alternative method of modulating these targets that avoids these issues has been achieved through the development of allosteric ligands. Such allosteric ligands bind at a topographically distinct binding site located in the 7TM domain; therefore, these compounds are non-competitive with the endogenous glutamate (see Figure 2.2). The higher sequence divergence in the 7TM region across receptor subtypes provides the prospect of greater selectivity. Furthermore, selective cooperativity may favor a certain subtype over all others. Allosteric modulators also have the advantage of providing a “ceiling” on the magnitude of their effect, meaning that large doses are less likely than their orthosteric counterparts to produce target-based toxic effects.³⁶

The allosteric modulator approach has proved effective in many instances, garnering much attention from the medicinal chemistry community.^{38,41} One of the more developed areas of allosteric modulation has been the design of small molecule negative allosteric modulators (NAMs).⁴¹ These compounds do not directly inactivate the receptors, but rather decrease the affinity for an orthosteric agonist at the VFD. Thus, NAMs are appropriate agents for inhibiting the physiological activation of mGluRs.³⁸

Positive allosteric modulators (PAMs), on the other hand, work to increase the affinity of the receptor, potentiating the response to orthosteric agonists.³⁵ Allosteric modulators have appropriately been described as dimmer switches that allow receptors to be tuned up or down, offering control over the desired intensity of the physiological response. Figure 2.4 is a schematic representation of (a) PAM and (b) NAM activity in an in vitro calcium mobilization assay. Increasing PAM concentrations progressively shift the concentration response curve (CRC) to the left with increasing potency, while increasing NAM concentrations progressively shift the *magnitude* of glutamate concentration response with little change in potency, demonstrating their non-competitive nature.³⁵



 Niswender CM, Conn PJ. 2010. Annu. Rev. Pharmacol. Toxicol. 50:295–322

Figure 2.4. Representative CRCs of increasing PAM and NAM concentrations.³⁵

2.2. Significance

Genetic deletions of the mGluRs in knockout mice have revealed potential roles for each of them in cell function in various disease states.³⁵ Specifically, studies of synaptic plasticity in the *Fmr1* knockout mouse have identified a connection between

mGluR₅ signaling and fragile-X syndrome (FXS), a leading cause of autism and the most common inherited form of mental retardation. The genetic defect in FXS is in the gene encoding the fragile X mental retardation protein, a protein that promotes long-term depression (LTD). Mouse models of FXS show that group I-dependent LTD is excessive, suggesting that antagonism of mGluRs 1 or 5 could represent a novel mechanism of treatment.³⁵

Metabotropic glutamate receptor 5 has also been extensively studied for the treatment of anxiety. The glutamate receptor increases excitability by modulating various ion channels and potentiating *N*-methyl-*D*-aspartate (NMDA) receptor currents. Antagonism could dampen these glutamatergic activities that are thought to underlie anxiety disorders.³⁶ In addition, well-studied mGluR₅ NAMs indicate that the Group I receptor is involved in other disorders such as drug addiction, gastroesophageal reflux disease (GERD), and Parkinson's disease levodopa induced dyskinesia (PD-LID).³⁸ Overall, because of the ubiquitous distribution of glutamatergic synapses, mGluR therapeutics have the potential to dramatically improve the treatments available for a wide variety of psychiatric and neurologic disorders.^{35,42}

2.3. Literature Review

In 1999, Varney *et al.* described the first selective mGluR₅ NAMs, SIB-1757 and SIB-1893 (**2.1** and **2.2**, Figure 2.5).⁴³ Allosteric proved to be the key to finding highly selective inhibitors, exhibiting selectivity not previously seen with any mGluR subtype orthosteric ligand. Subsequent structural analogs led to the development of the disubstituted alkynes MPEP and MTEP (**2.3** and **2.4**, Figure 2.6), the most well studied

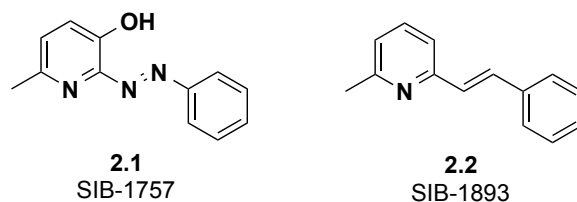


Figure 2.5. The first selective mGluR₅ NAMs, SIB-1757 (**2.1**) and SIB-1893 (**2.2**).

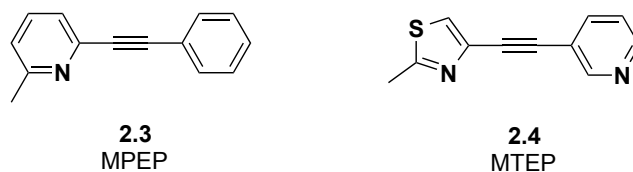


Figure 2.6. mGluR₅ tool compounds MPEP (**2.3**) and MTEP (**2.4**).

mGluR₅ NAMs to date. Both **2.3** and **2.4** have proven efficacious in numerous animal models including those related to drug addiction, anxiety, GERD, FXS, and PD-LID.^{38,41} Since the discovery of these tool compounds, many selective mGluR₅ NAMs have been developed based on the disubstituted alkyne scaffold. In fact, most of the compounds progressing to clinical trials have come from this class of compounds, including three with confirmed ongoing clinical activity: RG7090 (RO4917523), mavoglurant (AFQ056), and dipraglurant (ADX48621) (**2.5**, **2.6**, and **2.7**, Figure 2.7).⁴¹ Additionally, radioligands and PET tracers for the MPEP allosteric site have been developed to aid in the development of clinical compounds.³⁶

Clinical validation for mGluR₅ NAMs came in 2005 with the development of the allosteric antagonist fenobam (**2.8**, Figure 2.8). Fenobam was efficacious in a preclinical model of anxiety and further demonstrated clinical efficacy as an anxiolytic.³⁶

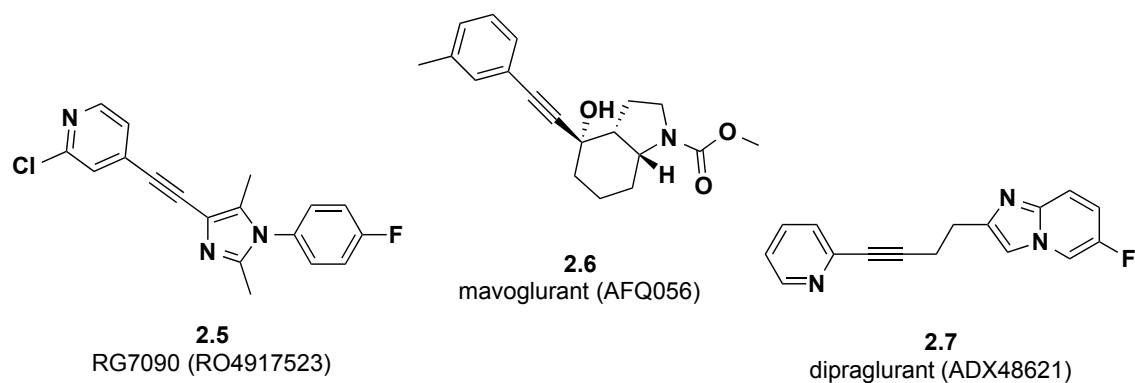


Figure 2.7. mGluR₅ NAMs currently in clinical trials.⁴¹

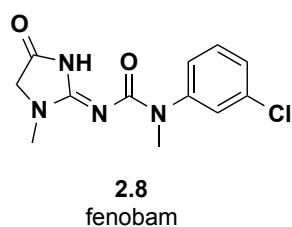


Figure 2.8. Fenobam (**2.8**), an anxiolytic mGluR₅ allosteric antagonist.

Potential concerns for the use of mGluR₅ NAMs include target-related adverse effects such as cognition impairment or psychotomimetic effects. A possible solution to these problems was discovered in 2005 in mGluR₅ allosteric partial antagonists. These molecules fully occupy the MPEP site, but, due to limited negative cooperativity, only partially block agonist responses resulting in partial inhibition of the receptor. M-5MPEP and Br-5MPEPy (**2.9** and **2.10**, Figure 2.9) were shown to maximally inhibit mGluR₅ by 50% at full occupation, demonstrating a reduction in response along with some level of activity maintenance.³⁶

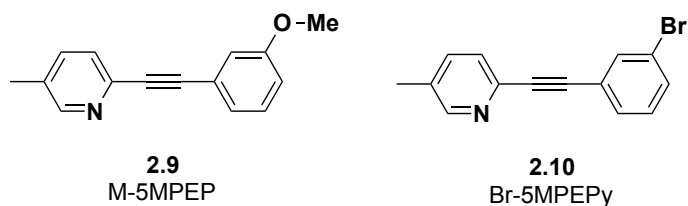


Figure 2.9. M-5PEP (**2.9**) and Br-5MPEPy (**2.10**), mGluR₅ allosteric partial antagonists.

2.4. Discovery of VU0431316

While MPEP and MTEP have proven to be valuable tool compounds, both of these compounds have characteristics that prevent them from becoming full therapeutic molecules. Namely, MPEP has been shown to directly inhibit NMDA receptor activity at high concentrations. Moreover, it is also considered to be an mGluR₄ PAM. MTEP, on the other hand, does not exhibit any selectivity issues but is a potent inhibitor of cytochrome P450 A12, which could potentially lead to adverse drug interactions. MTEP is also efficiently cleared when administered intravenously to rhesus monkeys.³⁸

Further, because conventional orthosteric modulators of mGluR₅ can lack satisfactory aqueous solubility, demonstrate poor oral bioavailability, and/or exhibit unfavorable effects, there is a need for selective negative allosteric modulators of mGluR₅ that overcome these deficiencies.³⁸ We, therefore, have been interested in developing mGluR₅ NAMs within chemotypes that do not contain a disubstituted alkyne motif.⁴¹ Herein describes the discovery of tool compound VU0431316 (**2.11**, Figure 2.10) from an aryl ether series of mGluR₅ NAMs.

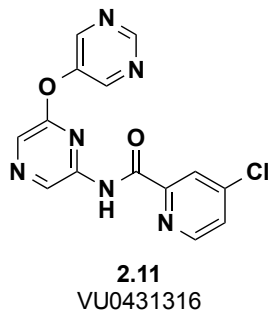
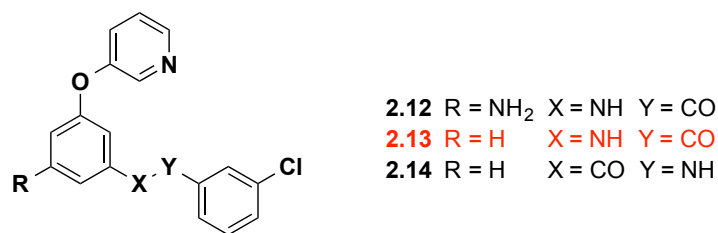


Figure 2.10. mGluR₅ NAM tool compound **2.11** (VU0431316).

2.4.1. Development of Structure-Activity Relationships

We began our search for novel chemotypes of mGluR₅ NAMs by developing hits identified from a functional cell-based HTS of 160,000 compounds. This is the same assay utilized as our primary assay for lead optimization and works by measuring the ability of a compound to block the mobilization of calcium induced by an EC₈₀ concentration of glutamate in HEK293A cells expressing rat mGluR₅. Aryl ether benzamide **2.12** was among the confirmed hits demonstrating good potency and was subjected to initial structural modifications (Figure 2.11).⁴¹ Removal of the primary amine provided **2.13**, which proved to be four-fold more potent than **2.12**. Alternating the orientation of the amide bond afforded compound **2.14**. While **2.14** was more than 20-fold less potent than **2.13**, it was ultimately optimized to tool compound VU0409106 as recently described by Felts *et al.* (**2.15**, Figure 2.12).⁴¹ We envisioned that further optimization of **2.13** would also lead to interesting analogs, and this effort is described below.



2.12 mGluR₅ IC₅₀ = 284 nM **2.13** mGluR₅ IC₅₀ = 81 nM **2.14** mGluR₅ IC₅₀ = 1960 nM

Figure 2.11. mGluR₅ NAM HTS hit and early analogs.⁴¹

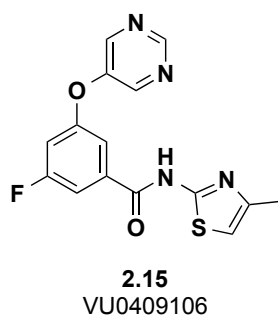
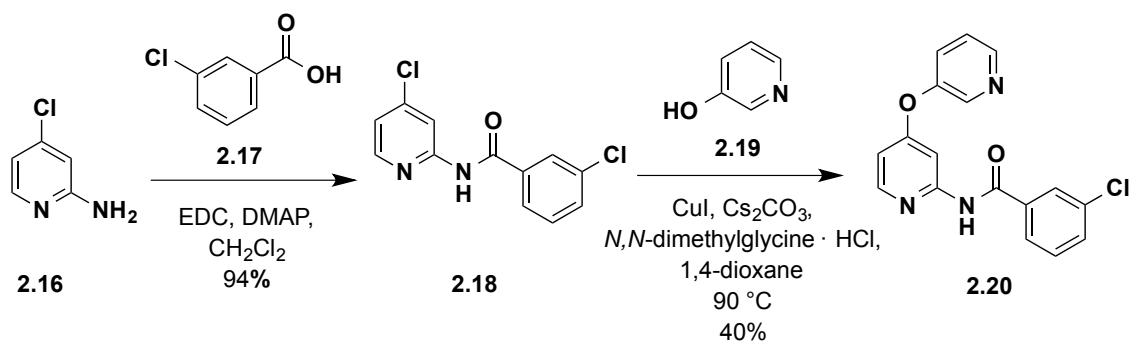
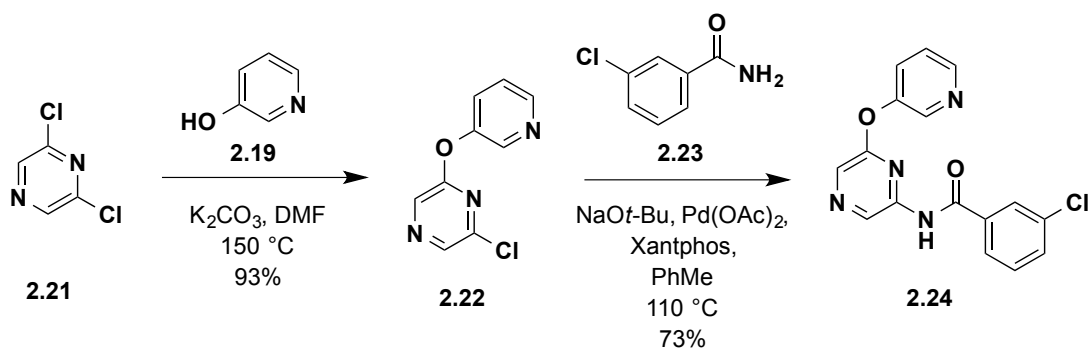


Figure 2.12. mGluR₅ NAM tool compound VU0409106 (**2.15**).

The first SAR endeavor from **2.13** was heteroaryl substitution of the phenyl core. These analogs were created through one of two different routes.³⁸ In Route I, e.g. Scheme 2.1, coupling of a commercially available haloheteroarylamine (**2.16**) with a carboxylic acid (**2.17**) or acid chloride afforded the amide intermediate (**2.18**). Nucleophilic aromatic substitution (S_NAR) with 3-hydroxypyridine (**2.19**) under basic conditions provided the biaryl ether analog (**2.20**). In Route II, e.g. Scheme 2.2, formation of the ether occurred first via S_NAR substitution of a dihalo-heteroaryl compound (**2.21**) with 3-hydroxypyridine (**2.19**). The ether (**2.22**) was then subjected to a palladium catalyzed coupling with a primary amide (**2.23**) to give the desired analog (**2.24**).



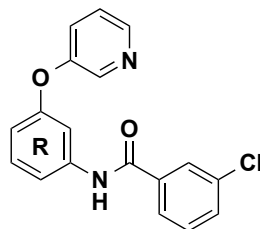
Scheme 2.1. Representative example of heteroaryl substitution of the phenyl core via Route I.



Scheme 2.2. Representative example of heteroaryl substitution of the phenyl core via Route II.

Table 2.2 shows the heteroaryl substitution library. Potency data in the primary assay is presented here as both pIC_{50} and IC_{50} values for convenient evaluation of SAR. Approximately half of the chemotype modifications exhibited a great decrease in potency. Interestingly, derivatives **2.25** and **2.27** were five-fold less potent than **2.13**, however, the combination of these substitutions yielded pyrazine **2.24** with ample activity. We anticipated that optimization of **2.24** might restore lost potency, thus we continued SAR exploration from this analog. A large change in potency was observed

Table 2.2. Heteroaryl core SAR



Cmpd	R	mGluR ₅ pIC ₅₀ (± SEM) ^a	mGluR ₅ IC ₅₀ (nM)	% Glu Max (± SEM) ^{a,b}
2.25		6.39 ± 0.07	403	1.11 ± 0.40
2.24		6.89 ± 0.04	129	0.99 ± 0.33
2.26		5.43 ± 0.26	3699	-4.99 ± 4.65
2.27		6.44 ± 0.19	359	1.99 ± 0.74
2.20		6.00 ± 0.21	994	1.79 ± 0.70
2.28		<5.0 ^c	>10,000	44.08 ± 7.74
2.29		5.53 ± 0.23	2928	1.13 ± 0.54

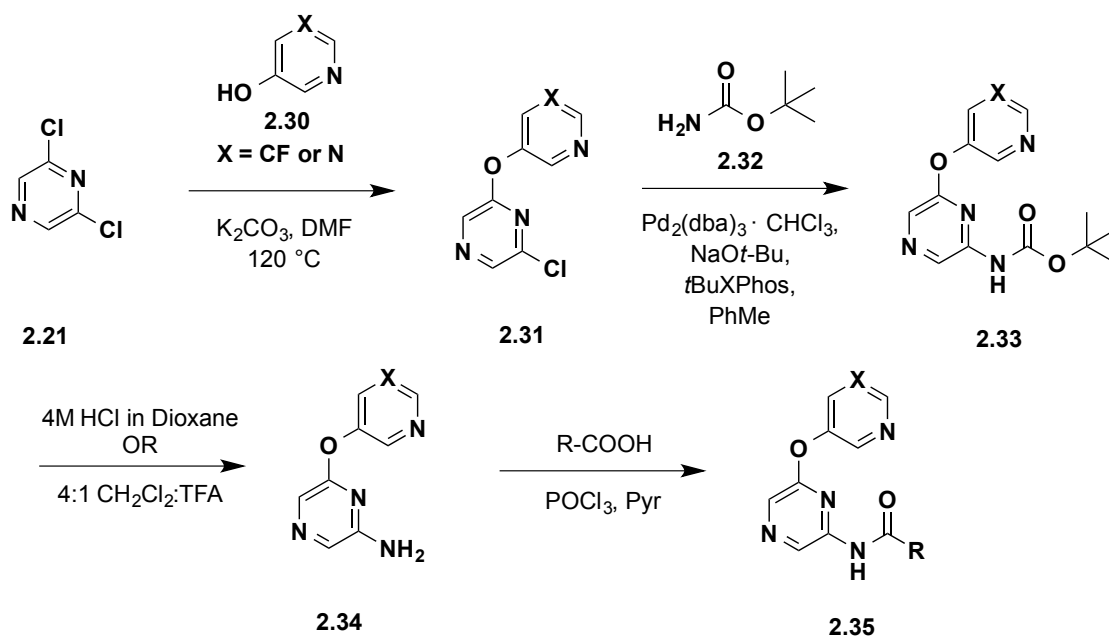
^a Calcium mobilization mGluR₅ assay; values are average of n ≥ 3

^b Amplitude of response in the presence of 30 μM test compound as a percentage of maximal response (100 μM glutamate); average of n ≥ 3

^c CRC does not plateau

with the minor structural modification from pyrazine **2.24** to pyrimidine **2.28**. This type of observation, nonetheless, can often be the case in allosteric modulator chemotypes.⁴¹

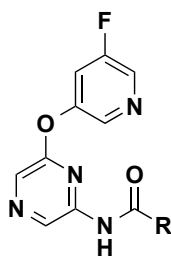
Next, with the optimized pyrazine core in hand, we evaluated modifications of the northern pyridine ether using “head groups” known to increase potency in similar mGluR₅ NAMs of this chemotype. Preparation of these analogs followed the general methods outlined in Scheme 2.3. S_NAR substitution of one of the chlorine atoms in 2,6-dichloropyrazine (**2.21**) with either 5-fluoropyridin-3-ol or pyrimidin-5-ol (**2.30**) under basic conditions provided ether intermediate **2.31**. Palladium catalyzed coupling of **2.31** with *tert*-butyl carbamate (**2.32**) afforded carbamate **2.33**. The amine was liberated by treatment with acid and was then coupled to a carboxylic acid via Kraus and co-workers 2005 procedure to yield substituted heteroarylamine carboxamide analogs (**2.35**).⁴⁴



Scheme 2.3. Preparation of substituted heteroarylamine carboxamides (**2.35**).

Table 2.3 shows the library of compounds tested with the fluoropyridine ether motif. Most of these substitutions were not tolerated, including those with five-membered ring heteroaryls. Analog **2.43**, prepared with 3-chlorobenzoic acid as in the lead compound, exhibited enhanced potency with the fluoropyridine head group. Compound **2.47**, prepared with 3-methylbenzoic acid, was also moderately potent. Preparations with the corresponding picolinic acids afforded analog **2.36** and **2.37**, respectively. While the potency of **2.37** decreased compared to the benzoic acid analog, **2.36** exhibited a slight increase in potency from **2.43**.

Table 2.3. Northern fluoropyridine SAR



Cmpd	R	mGluR ₅ pIC ₅₀ (± SEM) ^a	mGluR ₅ IC ₅₀ (nM)	% Glu Max (± SEM) ^{a,b}
2.36		6.95 ± 0.29	111	1.95 ± 0.26
2.37		6.51 ± 0.15	311	1.70 ± 0.39
2.38		5.20 ± 0.11	6370	7.77 ± 2.80
2.39		5.46 ± 0.15	3453	0.06 ± 2.37

Table 2.3. continued

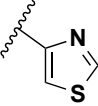
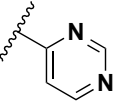
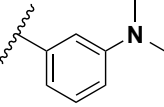
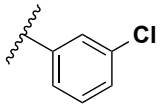
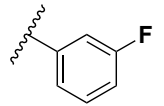
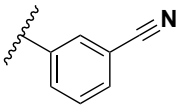
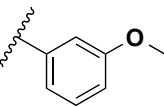
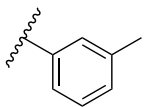
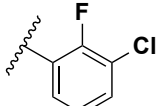
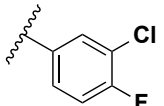
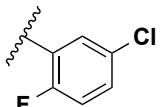
Cmpd	R	mGluR ₅ pIC ₅₀ (± SEM) ^a	mGluR ₅ IC ₅₀ (nM)	% Glu Max (± SEM) ^{a,b}
2.40		5.07 ± 0.05	8425	22.27 ± 11.40
2.41		<4.5	>30,000	-
2.42		<5.0 ^c	>10,000	52.16 ± 10.51
2.43		6.93 ± 0.10	118	1.96 ± 0.32
2.44		5.42 ± 0.09	3824	-0.37 ± 1.69
2.45		6.18 ± 0.16	662	1.20 ± 0.29
2.46		5.36 ± 0.17	4397	-5.63 ± 5.06
2.47		6.70 ± 0.18	199	2.08 ± 0.35
2.48		<4.5	>30,000	-
2.49		5.34 ± 0.15	4585	-2.80 ± 6.19
2.50		6.05 ± 0.13	894	1.01 ± 0.75

Table 2.3. continued

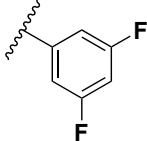
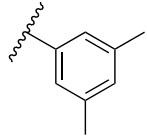
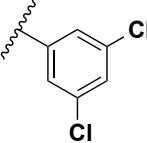
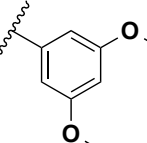
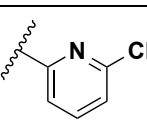
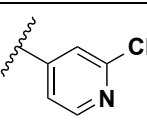
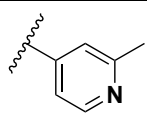
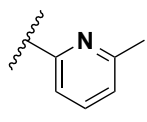
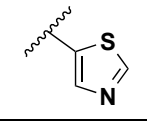
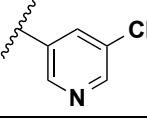
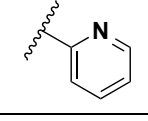
Cmpd	R	mGluR ₅ pIC ₅₀ (± SEM) ^a	mGluR ₅ IC ₅₀ (nM)	% Glu Max (± SEM) ^{a,b}
2.51		<4.5	>30,000	-
2.52		5.18 ± 0.18	6596	6.63 ± 2.02
2.53		<4.5	>30,000	-
2.54		<4.5	>30,000	-
2.55		<4.5	>30,000	-
2.56		<4.5	>30,000	-
2.57		<4.5	>30,000	-
2.58		<4.5	>30,000	-
2.59		<4.5	>30,000	-
2.60		5.23 ± 0.13	5933	1.59 ± 1.95
2.61		<5.0 ^c	>10,000	39.71 ± 15.28

Table 2.3. continued

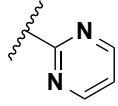
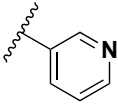
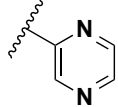
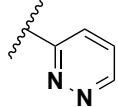
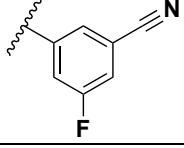
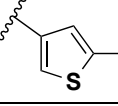
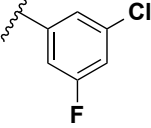
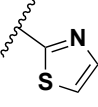
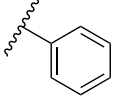
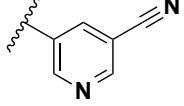
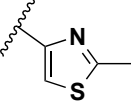
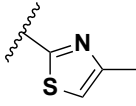
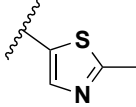
Cmpd	R	mGluR ₅ pIC ₅₀ (± SEM) ^a	mGluR ₅ IC ₅₀ (nM)	% Glu Max (± SEM) ^{a,b}
2.62		<4.5	>30,000	-
2.63		<4.5	>30,000	-
2.64		<4.5	>30,000	-
2.65		<4.5	>30,000	-
2.66		<4.5	>30,000	-
2.67		6.00 ± 0.04	990	1.10 ± 0.75
2.68		<5.0 ^c	>10,000	47.94 ± 9.54
2.69		<5.0 ^c	>10,000	39.75 ± 9.28
2.70		5.06 ± 0.09	8646	-9.42 ± 2.26
2.71		<5.0 ^c	>10,000	35.99 ± 8.34
2.72		5.33 ± 0.17	4642	18.85 ± 6.13

Table 2.3. continued

Cmpd	R	mGluR ₅ pIC ₅₀ (± SEM) ^a	mGluR ₅ IC ₅₀ (nM)	% Glu Max (± SEM) ^{a,b}
2.73		<5.0 ^c	>10,000	20.22 ± 10.44
2.74		<4.5	>30,000	-

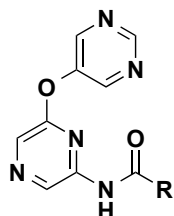
^a Calcium mobilization mGluR₅ assay; values are average of n ≥ 3

^b Amplitude of response in the presence of 30 μM test compound as a percentage of maximal response (100 μM glutamate); average of n ≥ 3

^c CRC does not plateau

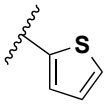
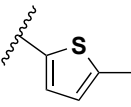
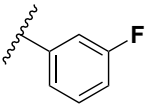
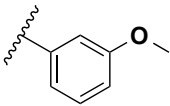
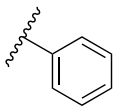
Further exploration with a pyrimidine head group (Table 2.4) gave similar results. Many analogs were inactive in our primary assay, and the active compounds were those with substitutions at the 3-position with or without the picolinic nitrogen. Again, analog **2.11** (VU0431316), with the 3-chloropicolinic acid, proved to be the most potent compound, exhibiting an IC₅₀ of 62 nM. This compound was further characterized and studied in a variety of in vitro and in vivo assays, ultimately becoming tool compound VU0431316. Figure 2.13 shows the relevant fold-shift data for this compound via the calcium mobilization assay previously described. A detailed description of this assay can be found in the literature.⁴⁵

Table 2.4. Northern pyrimidine SAR



Cmpd	R	mGluR ₅ pIC ₅₀ (± SEM) ^a	mGluR ₅ IC ₅₀ (nM)	% Glu Max (± SEM) ^{a,b}
2.11 (VU0431316)		7.20 ± 0.06	62	1.58 ± 0.10
2.75		6.94 ± 0.10	116	1.24 ± 0.04
2.76		6.15 ± 0.17	709	1.48 ± 0.22
2.77		<4.5	>30,000	-
2.78		6.67 ± 0.16	212	1.52 ± 0.50
2.79		6.72 ± 0.22	193	2.10 ± 0.79
2.80		7.00 ± 0.29	100	2.26 ± 0.56
2.81		<5.0 ^c	>10,000	15.24 ± 8.21
2.82		<5.0 ^c	>10,000	35.34 ± 6.43

Table 2.4. continued

Cmpd	R	mGluR₅ pIC₅₀ (± SEM)^a	mGluR₅ IC₅₀ (nM)	% Glu Max (± SEM)^{a,b}
2.83		<5.0 ^c	>10,000	20.50
2.84		<4.5	>30,000	-
2.85		5.29 ± 0.17	5138	1.48 ± 2.73
2.86		5.39 ± 0.15	4111	-4.32 ± 2.68
2.87		<5.0 ^c	>10,000	11.99 ± 11.06

^a Calcium mobilization mGluR₅ assay; values are average of n ≥ 3

^b Amplitude of response in the presence of 30 μM test compound as a percentage of maximal response (100 μM glutamate); average of n ≥ 3

^c CRC does not plateau

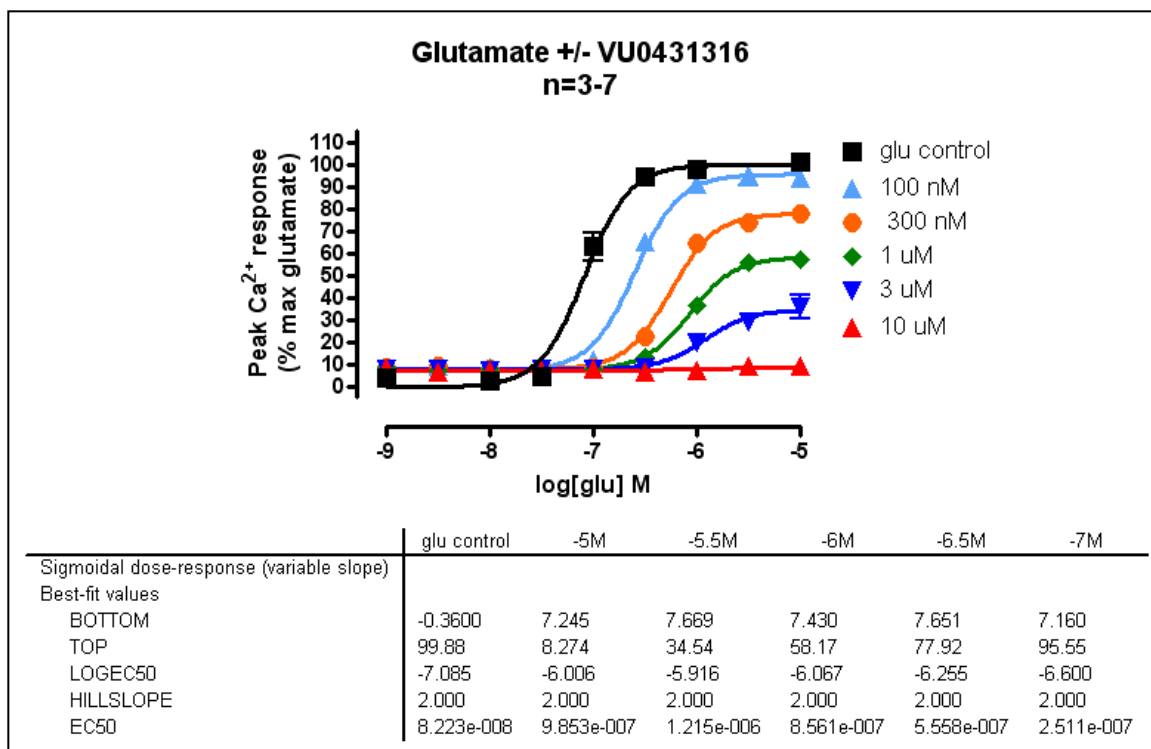


Figure 2.13. Fold shift data for **2.11** (VU0431316).

2.4.2. Drug Metabolism and Pharmacokinetics

Measuring intrinsic clearance in rodent and human liver microsomes is an important assay in which to assess cytochrome P450 metabolism. Table 2.5 shows **2.11**'s (VU0431316's) CYP profile, with the only concern being CYP1A2. Protein binding (Table 2.6) estimates how much free drug there is available to interact with the receptor. Using methods developed by Kalvass and Maurer, nonspecific binding to rodent brain homogenates (BHB) with **2.11** (VU0431316) showed good free fraction, which was expected with the low lipophilic compound ($c\text{Log}P = 0.84$; calculated using ADRIANA. Code (www.molecular-networks.com)).⁴⁶

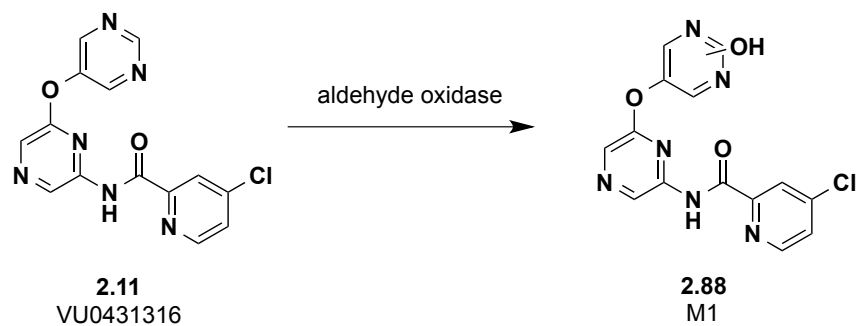
Table 2.5. CYP450 inhibition

CYP	IC ₅₀ (μM)
3A4	≥ 30
2D6	>30
2C9	>30
1A2	0.64
2C19	>30

Table 2.6. Protein binding

Protein Binding	% Bound
Human PPB	91.0
Mouse BHB	94.6

Previous in house studies with the northern pyrimidine ethers have indicated a major role of nonP450-mediated metabolism. In 2012, Morrison *et al.* published on the aldehyde oxidase metabolism of **2.15** (VU0409106), fully elucidating and characterizing this metabolic pathway.⁴⁷ Scheme 2.4 and Figure 2.14 show that **2.11** (VU0431316) is subject to aldehyde oxidase metabolism to metabolite M1.



Scheme 2.4. Aldehyde oxidase metabolism of **2.11** (VU0431316).

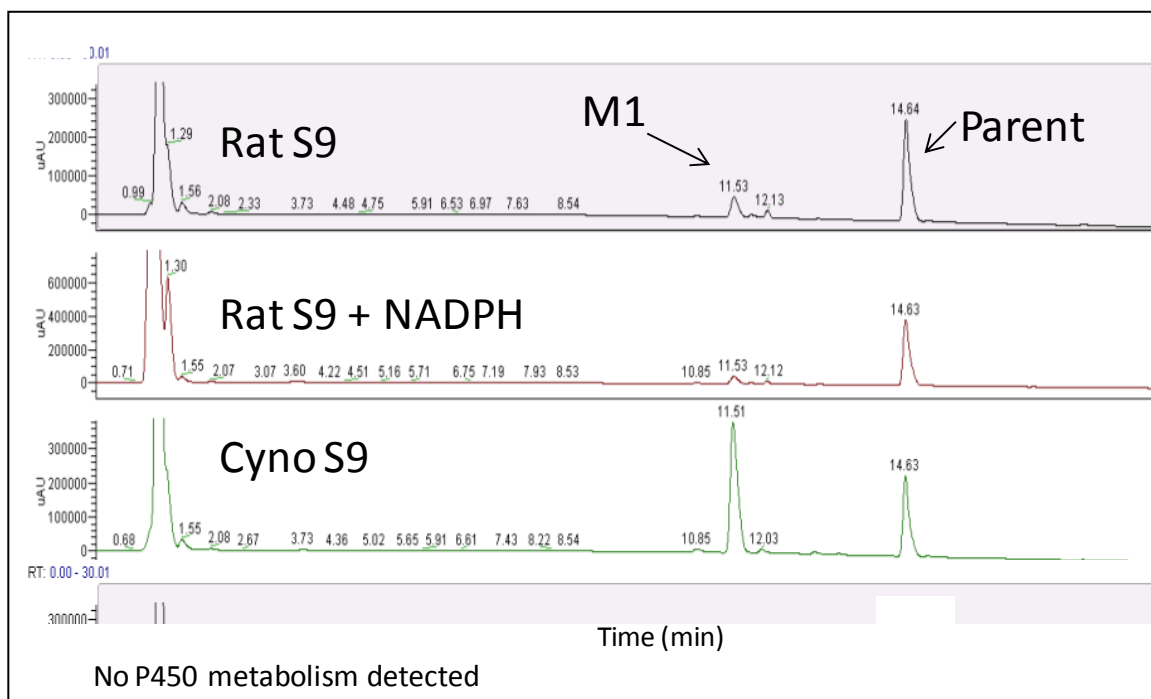


Figure 2.14. Compound **2.11** (VU0431316) liver S9 fraction incubation.

2.4.3. Behavioral Pharmacology

Because of its promising potency, *in vitro* data, and rat pharmacokinetic (PK) profile (data not shown), compound **2.11** (VU0431316) was deemed appropriate to test in an acute behavioral study in mice. Prior to this study, it was imperative to better understand the molecular pharmacology of **2.11** (VU0431316). Competition binding experiments with [³H]3-methoxy-5-(pyridin-2-ylethynyl)pyridine ([³H]mPEPy), a close structural analog of MPEP (**2.3**), were completed by determining the inhibition of this compound with **2.11** (VU0431316). This study confirmed that **2.11** (VU0431316) inhibits [³H]mPEPy and, therefore, binds at the known mGluR₅ allosteric site (mGluR₅ K_i = 37 nM) (Figure 2.15, data for **2.15** (VU0409106) also shown).

Mice are known to bury both harmless and noxious objects, and it was suggested that the burying of glass marbles could be a useful behavioral test for anxiolytic activity.^{48,49} In 1986, Broekkamp *et al.* demonstrated that dosing mice with a variety of anxiolytic compounds differentially inhibited marble burying.⁴⁹ Njung'e and Handley later proposed that marble burying may actually be a correlation test of anxiety; that is, modeling a different behavior that is affected by anxiolytic compounds.⁴⁸ More recent data indicates that mice might not be deliberately burying marbles but rather that the marbles fall through the displaced bedding.⁵⁰ Nevertheless, this behavioral assay studies the digging behavior of mice and is accepted as a convenient and rapid means to probe hippocampal function. MPEP (**2.3**) and fenobam (**2.8**) are effective in this model as is **2.15** (VU0409106).⁴¹

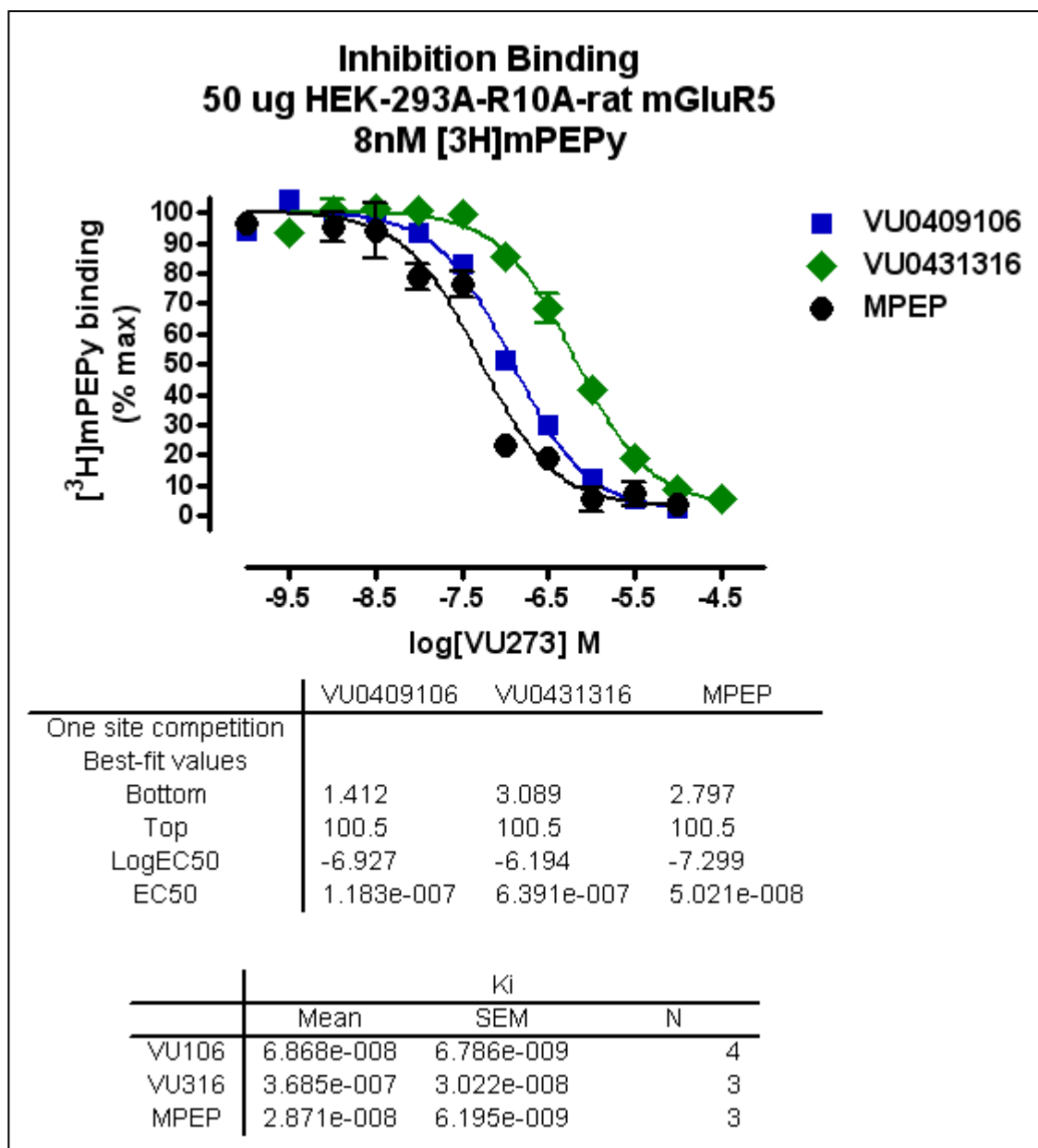


Figure 2.15. Compounds **2.15** (VU0409106) and **2.11** (VU0431316) binding studies.

The marble burying paradigm was performed with naïve mice. A dose response study using intraperitoneal (IP) dosing of **2.11** (VU0431316) was conducted using a 15-minute pretreatment. Dose-dependent inhibition was observed with no noticeable sedation within the dose range tested (Figure 2.16). The median effective dose (ED₅₀), for **2.11** (VU0431316) was determined to be 6.6 mg/kg. For a more detailed experimental procedure, see Lindsley 2011.⁵¹

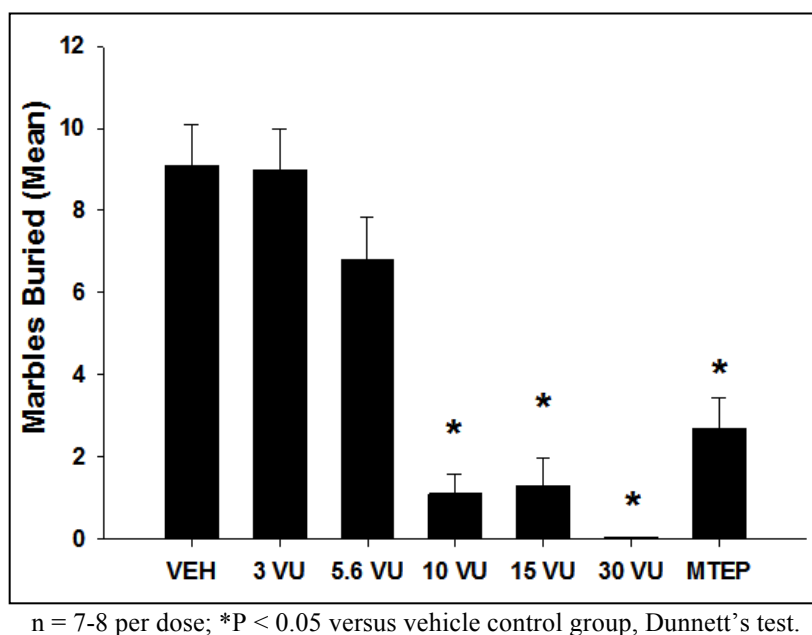


Figure 2.16. Dose dependent inhibition of marble burying with **2.11** (VU0431316).

2.5. Conclusions and Future Directions

In summary, substantial SAR was developed in a heteroarylamine carboxamide series of mGluR₅ NAMs leading to identification of tool compound **2.11** (VU0431316). This compound is a potent noncompetitive antagonist that binds at the known allosteric site of mGluR₅. Compound **2.11** (VU0431316) proved efficacious in a mouse marble

burying model of anxiety, an assay known to be sensitive to mGluR₅ NAMs. Forthcoming *in vivo* experiments with this compound include behavioral assays of other mGluR₅ diseases and monkey PK studies.

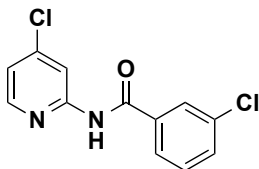
2.6. Experimental Section

2.6.1. Methods and Materials

All reagents and solvents were commercial grade and purified prior to use when necessary. Analytical TLC was performed on Sorbent Technologies HL 0.25 mm silica gel plates with UV indicator. Visualization was accomplished by irradiation under a 254 nm UV lamp and/or the use of an iodine chamber. Chromatography on silica gel was performed using Silica Gel 60 (230-400 mesh) from Sorbent Technologies.

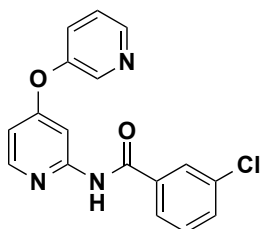
¹H NMR spectra were recorded on a Bruker DRX-400 (400 MHz) NMR instrument. Chemical shifts are reported in ppm from the solvent resonance as an internal standard. Data are reported as follows: chemical shift, multiplicity, coupling constant (Hz), and number of protons.

2.6.2. Selected Experimental Procedures



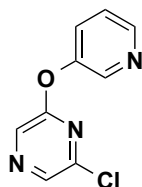
3-chloro-N-(4-chloropyridin-2-yl)benzamide (2.18). 2-amino-4-chloropyridine (90 mg, 0.70 mmol, 1.1 eq), 3-chlorobenzoic acid (0.1 mg, 0.6 mmol, 1 eq), 1-ethyl-3-(3-

dimethylaminopropyl) carbodiimide (135 mg, 0.704 mmol, 1.10 eq) and 4-dimethylaminopyridine (7.8 mg, 0.064 mmol, 0.10 eq) were dissolved in CH₂Cl₂ (5 mL) and stirred at rt overnight. Water was added and the layers separated. The organic layer was dried (MgSO₄), filtered and concentrated *in vacuo*. Purification by flash chromatography on silica gel afforded 160 mg (94%) of the title compound as a white solid: ¹H NMR (400 MHz, DMSO-*d*₆) δ 11.21 (s, 1H), 8.39 (d, *J* = 5.4 Hz, 1H), 8.27 (d, *J* = 1.6 Hz, 1H), 8.06 (t, *J* = 1.8 Hz, 1H), 7.96 (dt, *J* = 7.6, 1.2 Hz, 1H), 7.67 (ddd, *J* = 8.0, 2.1, 1.0 Hz, 1H), 7.54 (t, *J* = 7.9 Hz, 1H), 7.32 (dd, *J* = 5.4, 2.0 Hz, 1H); ES-MS [M+1]⁺:267.1.

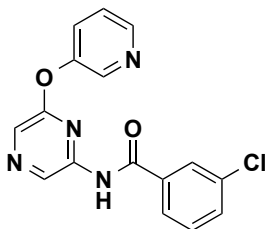


3-chloro-N-4-(pyridin-3-yloxy)pyridin-2-ylbenzamide (2.20). Compound **2.18** (50 mg, 0.19 mmol, 1.0 eq) 3-hydroxypyridine (26.7 mg, 0.281 mmol, 1.50 eq), CuI (3.7 mg, 0.019 mmol, 0.10 eq) Cs₂CO₃ (122 mg, 0.374 mmol, 2.00 eq) and *N,N*-dimethylglycine hydrochloride (7.8 mg, 0.056 mmol, 0.30 eq) were dissolved in 1,4-dioxane (1 mL) in a flame-dried sealed tube and heated overnight at 90 °C. The reaction was cooled to rt, plugged through celite and concentrated. Purification by flash chromatography on silica gel afforded 24 mg (40%) of the title compound as a pale yellow oil: chromatography on silica gel afforded 160 mg (94%) of the title compound as a white solid: ¹H NMR (400 MHz, DMSO-*d*₆) δ 11.06 (s, 1H), 8.55-8.53 (m, 2H), 8.31 (d, *J* = 5.7 Hz, 1H), 8.01 (m, 1H), 7.92 (d, *J* = 7.8 Hz, 1H), 7.79 (d, *J* = 2.3 Hz, 1H), 7.73 (ddd, *J* = 8.4, 2.6, 1.2 Hz,

1H), 7.64 (d, $J = 8.6$ Hz, 1H), 7.55 (dd, $J = 8.4, 4.7$ Hz, 1H), 7.51 (t, $J = 7.9$ Hz, 1H), 6.82 (dd, $J = 5.7, 2.4$ Hz, 1H); ES-MS $[M+1]^+$: 326.1.

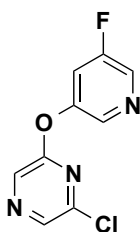


2-chloro-6-(pyridin-3-yloxy)pyrazine (2.22). 2,6-dichloropyrazine (1.0 g, 6.7 mmol, 1.0 eq), 3-hydroxypyridine (638 mg, 6.71 mmol, 1.00 eq) and K_2CO_3 (1.11 g, 8.03 mmol, 1.20 eq) were dissolved in DMF (10 mL) and heated in a microwave for 15 minutes at 150 °C. The reaction was cooled, diluted with EtOAc and washed with H_2O (3x). The organic layer was dried ($MgSO_4$), filtered, and concentrated *in vacuo*. Purification by flash chromatography on silica gel afforded 1.3 g (93%) of the title compound as a white solid: 1H NMR (400 MHz, $CDCl_3$) δ 8.59 (d, $J = 2.3$ Hz, 1H), 8.56 (d, $J = 4.4$ Hz, 1H), 8.41 (s, 1H), 8.37 (s, 1H), 7.71 (dq, $J = 8.4, 1.3$ Hz, 1H), 7.51 (dd, $J = 8.4, 4.9$ Hz, 1H); ES-MS $[M+1]^+$: 208.1.

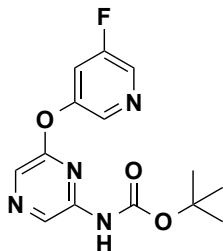


3-chloro-N-(6-(pyridin-3-yloxy)pyrazin-2-yl)benzamide (2.24). Compound **2.22** (944 mg, 4.55 mmol, 1.00 eq), 3-chlorobenzamide (1.06 g, 6.81 mmol, 1.50 eq), $NaOt-Bu$ (612 mg, 6.37 mmol, 1.40 eq), $Pd(OAc)_2$ (51 mg, 0.23 mmol, 0.050 eq) and Xantphos (263 mg, 0.455 mmol, 0.100 eq) were dissolved in toluene (9.4 mL) in a flame-dried

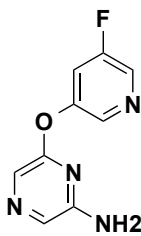
sealed tube and heated at 110 °C for 18h. The reaction was cooled to rt, diluted with CH₂Cl₂ and filtered through a plug of celite. Purification by flash chromatography on silica gel afforded 1.08 g (73%) of the title compound as a white solid: ¹H NMR (400 MHz, DMSO-*d*₆) δ 11.07 (s, 1H), 9.17 (s, 1H), 8.59 (d, *J* = 2.7 Hz, 1H), 8.46 (dd, *J* = 4.7, 1.2 Hz, 1H), 8.33 (s, 1H), 8.00 (t, *J* = 1.8 Hz, 1H), 7.89 (d, *J* = 7.8 Hz, 1H), 7.77 (ddd, *J* = 8.4, 2.8, 1.4 Hz, 1H), 7.67-7.64 (m, 1H), 7.54-7.48 (m, 2H); ES-MS [M+1]⁺: 327.1.



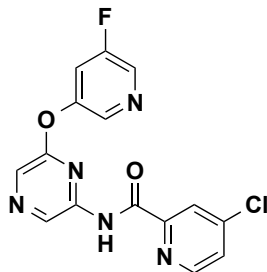
2-chloro-6-((5-fluoropyridin-3-yl)oxy)pyrazine (2.31a). A mixture of 2,6-dichloropyrazine (4.0 g, 27 mmol, 1.0 eq), 5-fluoropyridin-3-ol (3.0 g, 27 mmol, 1.0 eq), and potassium carbonate (5.6 g, 40 mmol, 1.5 eq) in DMF (80 mL) was microwaved at 120 °C for 10 minutes. The reaction was diluted with CH₂Cl₂ and washed with H₂O (3x) and brine (1x). The organic layer was dried (MgSO₄), filtered, and concentrated *in vacuo*. The crude product was diluted in toluene, concentrated onto silica gel, and washed with EtOAc. The filtrate was collected and concentrated *in vacuo*. Purification by flash chromatography on silica gel (25:75 EtOAc/hexanes) afforded 3.8 g (62%) of the title compound as a white solid. ¹H NMR (400 MHz, DMSO-*d*₆) δ 8.68 (s, 1H), 8.61 (s, 1H), 8.58 (d, *J* = 2.4 Hz, 1H), 8.52 (d, *J* = 1.1 Hz, 1H), 7.95 (dt, *J* = 9.8, 2.4 Hz, 1H); ES-MS [M+1]⁺: 226.1.



tert-butyl (6-((5-fluoropyridin-3-yl)oxy)pyrazin-2-yl)carbamate (2.33a). Compound **2.31a** (1.0 g, 4.0 mmol, 1.0 eq), *tert*-butyl carbamate (623 mg, 5.32 mmol, 1.20 eq), tris (dibenzylideneacetone) dipalladium-chloroform adduct (138 mg, 0.130 mmol, 0.0300 eq), sodium *tert*-butoxide (596 mg, 6.21 mmol, 1.40 eq), and 2-di-*tert*-butylphosphino-2',4',6'-triisopropylbiphenyl (199 mg, 0.400 mmol, 0.0900 eq) stirred in toluene (17 mL) at rt overnight. The mixture was filtered through celite and washed with 5% MeOH in CH₂Cl₂. The filtrate was collected and concentrated *in vacuo*. Purification by flash chromatography on silica gel (30:70 EtOAc/hexanes) afforded 870 mg (64%) of the title compound as a white solid.

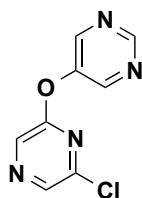


6-((5-fluoropyridin-3-yl)oxy)pyrazin-2-amine (2.34a). Compound **2.33a** (120 mg, 0.390 mmol, 1.00 eq) was stirred in 4M HCl in dioxane (1.90 mL) at rt overnight. The reaction mixture was concentrated *in vacuo* to give quantitative yield of the title compound as a pink HCl salt. ¹H NMR (400 MHz, DMSO-*d*₆) δ 8.46 (d, *J* = 2.4 Hz, 1H), 8.38 (s, 1H), 7.77 (dt, *J* = 10.1, 2.3 Hz, 1H), 7.65 (s, 1H), 7.56 (s, 1H), 7.16 (t, *J* = 51.0 Hz, 2H); ES-MS [M+1]⁺: 207.1.



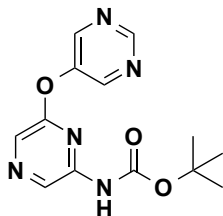
4-chloro-N-(6-((5-fluoropyridin-3-yl)oxy)pyrazin-2-yl)picolinamide (2.36).

Compound **2.34a** (1.0 eq) and 4-chloropicolinic acid (1.1 eq) were dissolved in pyridine (0.08 M reaction c) and cooled to -15 °C. Phosphorus oxychloride (1.1 eq) was added dropwise. The resulting reaction mixture was stirred at -15 °C for 30 minutes. The reaction was quenched with ice water, warmed to rt, and allowed to stir overnight. The reaction was diluted in CH₂Cl₂, and the layers were separated via phase separation. The organic layer was dried on air concentrator and purified by reverse-phase preparatory HPLC to afford the title compound. ¹H NMR (400 MHz, DMSO-*d*₆) δ 10.53 (s, 1H), 9.23 (s, 1H), 8.70 (d, *J* = 5.3 Hz, 1H), 8.56-8.55 (m, 2H), 8.45 (s, 1H), 8.19 (d, *J* = 1.9 Hz, 1H), 7.99 (dt, *J* = 10.0, 2.4 Hz, 1H), 7.88 (dd, *J* = 5.3, 2.1 Hz, 1H); ES-MS [M+1]⁺: 346.1.

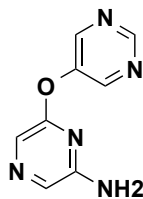


5-((6-chloropyrazin-2-yl)oxy)pyrimidine (2.31b). A mixture of 2,6-dichloropyrazine (500 mg, 3.36 mmol, 1.00 eq), pyrimidin-5-ol (320 mg, 3.36 mmol, 1.00 eq), and potassium carbonate (696 mg, 5.03 mmol, 1.50 eq) in DMF (10.0 mL) was microwaved at 120 °C for 10 minutes. The reaction was diluted with CH₂Cl₂ and washed with H₂O

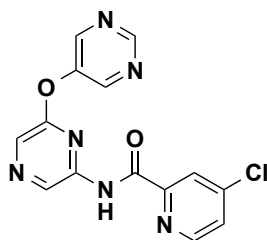
(3x) and brine (1x). The organic layer was dried (MgSO₄), filtered, and concentrated *in vacuo*. Purification by flash chromatography on silica gel (30:70 EtOAc/hexanes) afforded 220 mg (31%) of the title compound as an off-white solid. ¹H NMR (400 MHz, DMSO-*d*₆) δ 9.15 (s, 1H), 8.93 (s, 2H), 8.73 (s, 1H), 8.62 (s, 1H); ES-MS [M+1]⁺: 209.1.



***tert*-butyl (6-(pyrimidin-5-yloxy)pyrazin-2-yl)carbamate (2.33b).** Compound **2.31b** (400 mg, 1.92 mmol, 1.00 eq), *tert*-butyl carbamate (270 mg, 2.30 mmol, 1.20 eq), tris (dibenzylideneacetone) dipalladium-chloroform adduct (60 mg, 0.060 mmol, 0.030 eq), sodium *tert*-butoxide (258 mg, 2.68 mmol, 1.40 eq), and 2-di-*tert*-butylphosphino-2',4',6'-triisopropylbiphenyl (86 mg, 0.17 mmol, 0.090 eq) stirred in toluene (7.2 mL) at rt overnight. The mixture was filtered through celite and washed with 5% MeOH in CH₂Cl₂. The filtrate was collected and concentrated *in vacuo*. Purification by flash chromatography on silica gel (40:60 EtOAc/hexanes) afforded 240 mg (43%) of the title compound as a light yellow solid. ¹H NMR (400 MHz, DMSO-*d*₆) δ 10.14 (s, 1H), 9.09 (s, 1H), 8.91 (s, 2H), 8.82 (s, 1H), 8.25 (s, 1H), 1.45 (s, 9H); ES-MS [M+1]⁺: 290.1.



6-(pyrimidin-5-yloxy)pyrazin-2-amine (2.34b). Compound **2.33b** (480 mg, 1.66 mmol, 1.00 eq) was stirred in 4:1 CH₂Cl₂:TFA (2.00 mL) at rt overnight. The reaction mixture was concentrated *in vacuo* and diluted in EtOAc. The organic layer was washed with saturated NaHCO₃ (3x) and brine (1x), dried (MgSO₄), filtered and concentrated *in vacuo* to give 300 mg (96%) of the title compound as an orange solid. ¹H NMR (400 MHz, DMSO-*d*₆) δ 9.04 (s, 1H), 8.79 (s, 2H), 7.65 (s, 1H), 7.60 (s, 1H), 6.64 (s, 2H); ES-MS [M+1]⁺: 190.1.

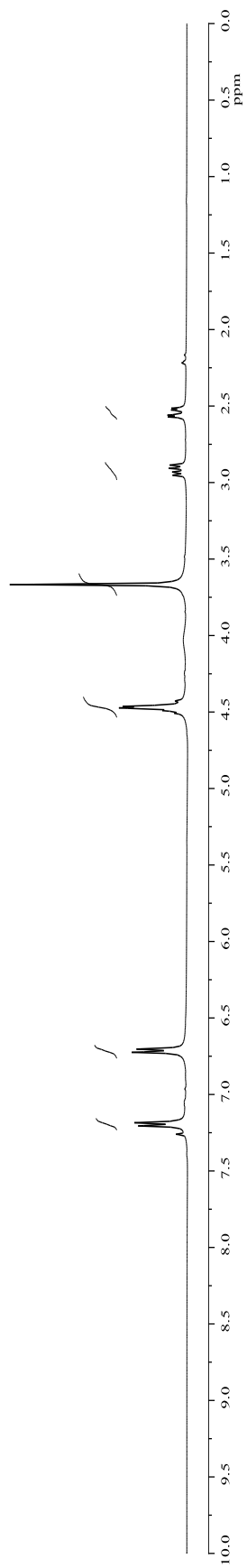
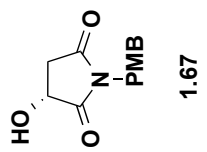


4-chloro-N-(6-(pyrimidin-5-yloxy)pyrazin-2-yl)picolinamide (2.11, VU0431316). Compound **2.34b** (1.0 eq) and 4-chloropicolinic acid (1.1 eq) were dissolved in pyridine (0.08 M reaction c) and cooled to -15 °C. Phosphorus oxychloride (1.1 eq) was added dropwise. The resulting reaction mixture was stirred at -15 °C for 30 minutes. The reaction was quenched with ice water, warmed to rt, and allowed to stir overnight. The reaction was diluted in CH₂Cl₂, and the layers were separated via phase separation. The organic layer was dried on air concentrator and purified by reverse-phase preparatory HPLC to afford the desired product. ¹H NMR (400 MHz, DMSO-*d*₆) δ 10.64 (s, 1H),

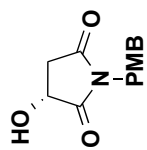
9.24 (s, 1H), 9.14 (s, 1H), 8.99 (s, 2H), 8.71 (d, $J = 5.3$ Hz, 1H), 8.50 (s, 1H), 8.19 (d, $J = 1.8$ Hz, 1H), 7.89 (dd, $J = 5.3, 2.0$ Hz, 1H); ES-MS $[M+1]^+$: 329.1.

Appendix A

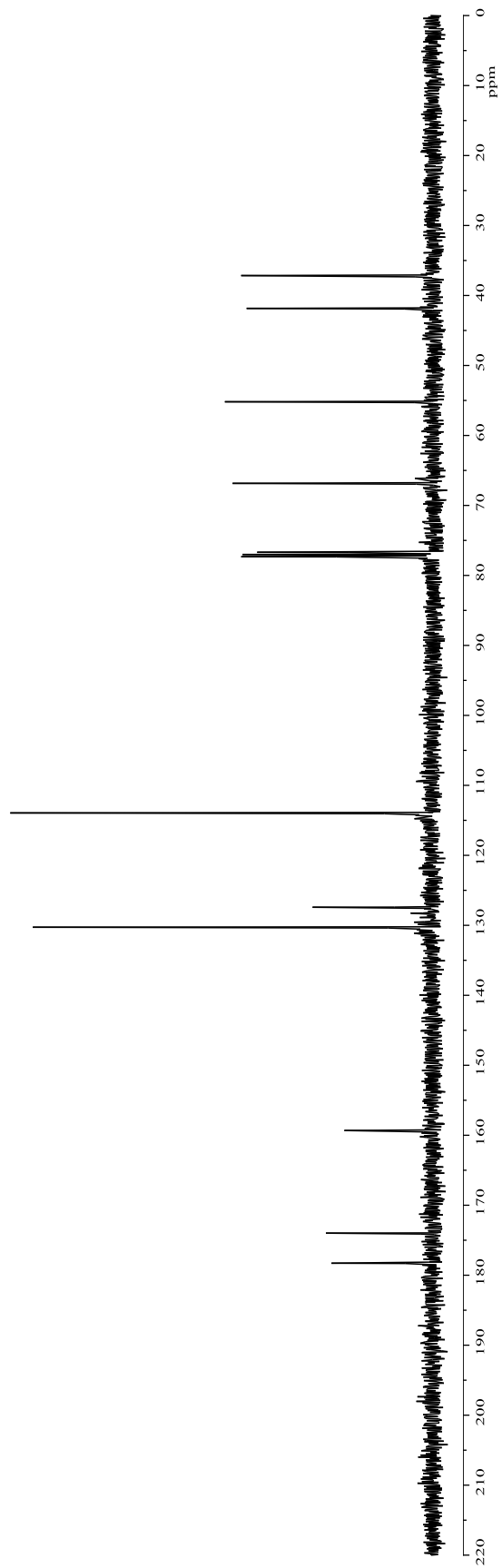
SPECTRA RELEVANT TO CHAPTER 1



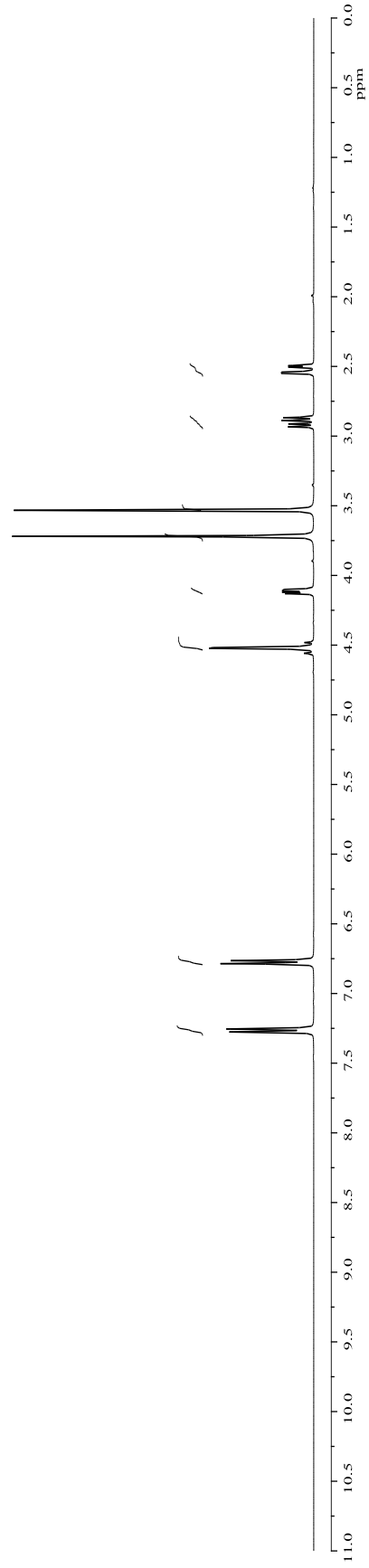
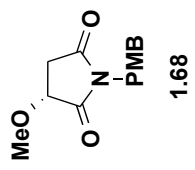
The 400 MHz ¹H NMR spectrum of compound 1.67 in CDCl₃.



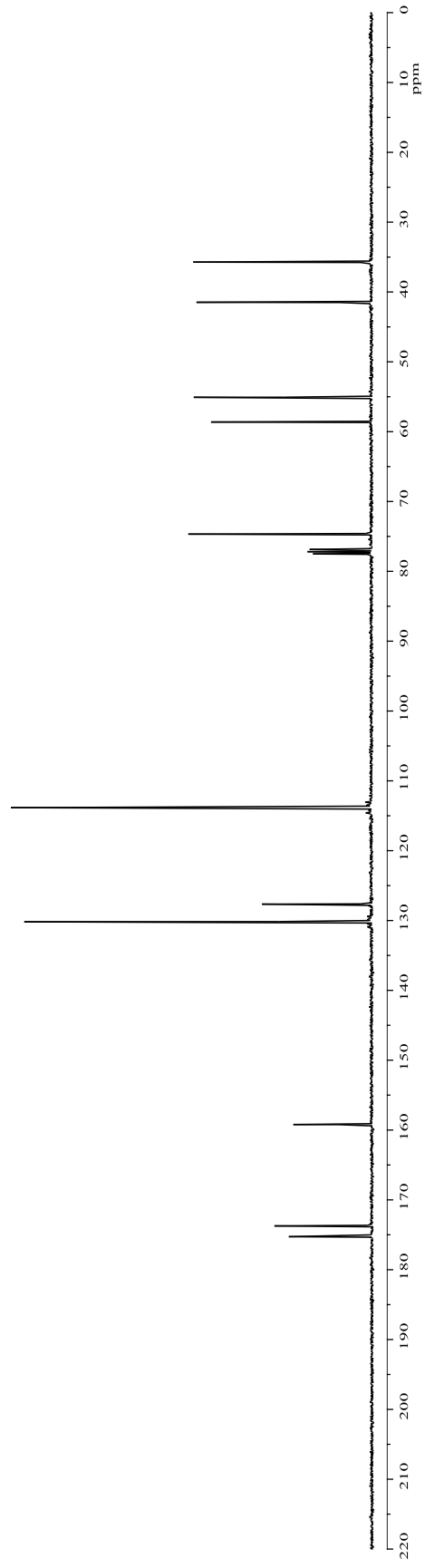
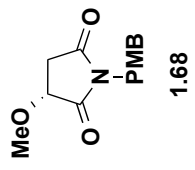
1.67



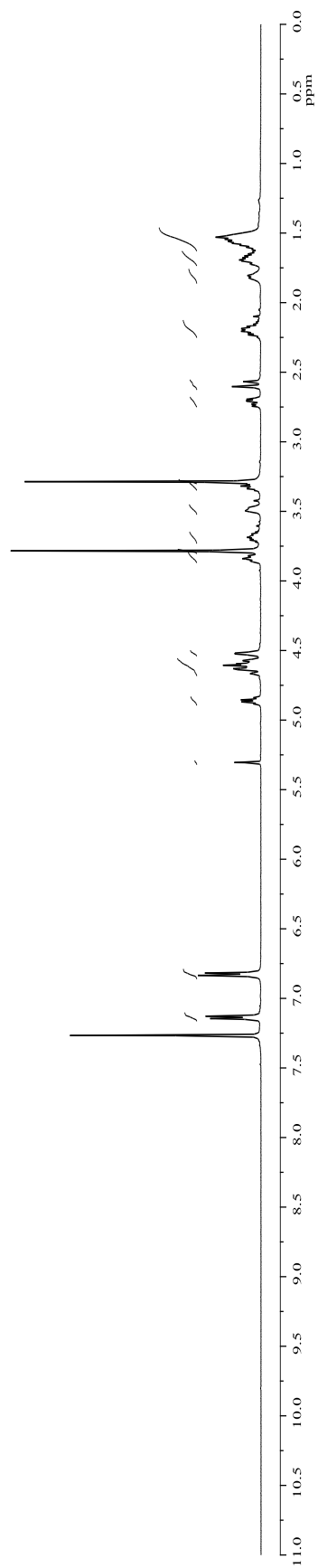
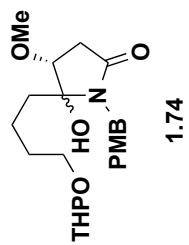
The 100 MHz ¹³C NMR spectrum of compound 1.67 in CDCl₃.



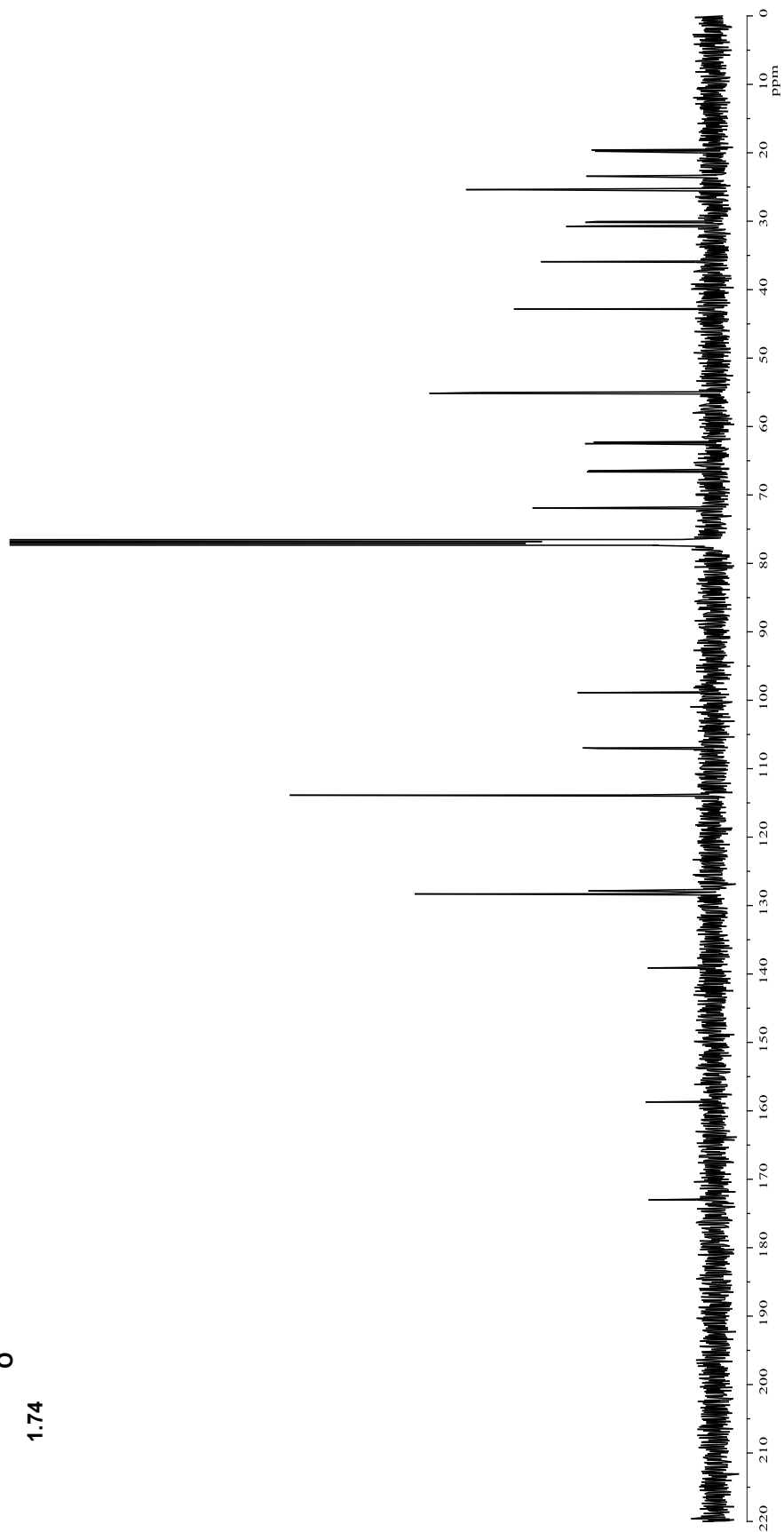
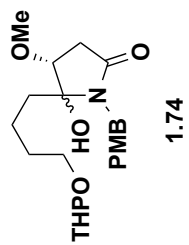
The 400 MHz ¹H NMR spectrum of compound **1.68** in CDCl₃.



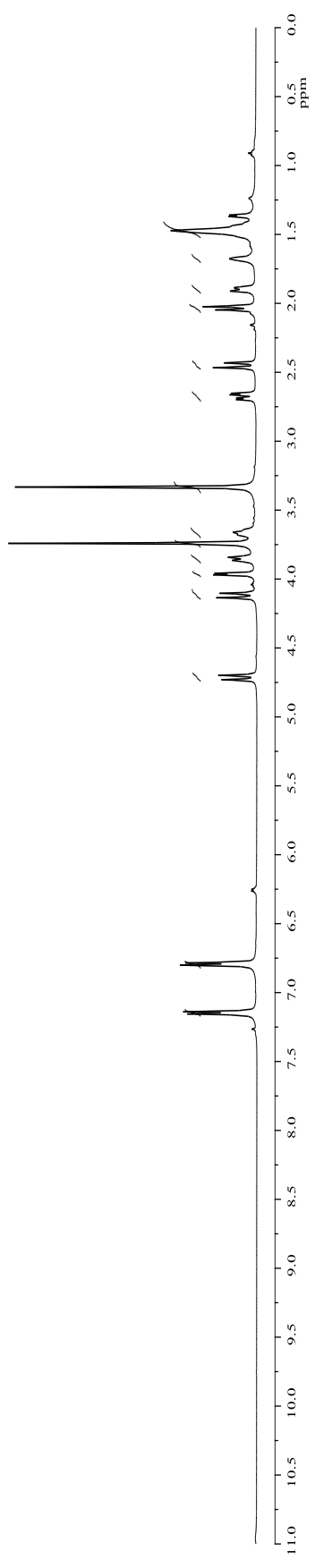
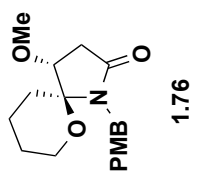
The 100 MHz ^{13}C NMR spectrum of compound **1.68** in CDCl_3 .



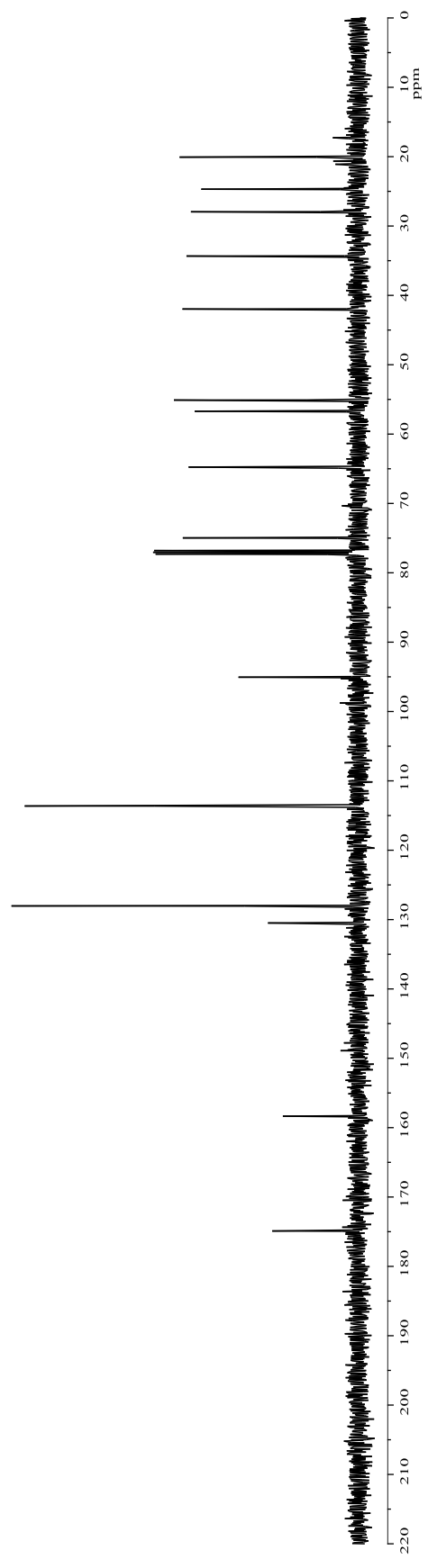
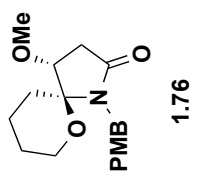
The 400 MHz ¹H NMR spectrum of compound **1.74** in CDCl₃.



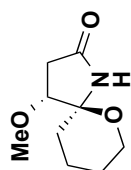
The 100 MHz ¹³C NMR spectrum of compound 1.74 in CDCl₃.



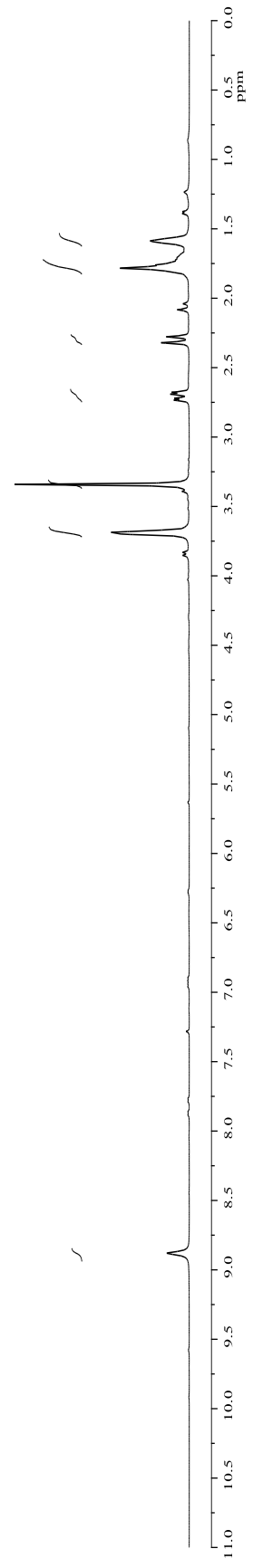
The 400 MHz ¹H NMR spectrum of compound **1.76** in CDCl₃.



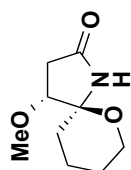
The 100 MHz ¹³C NMR spectrum of compound **1.76** in CDCl₃.



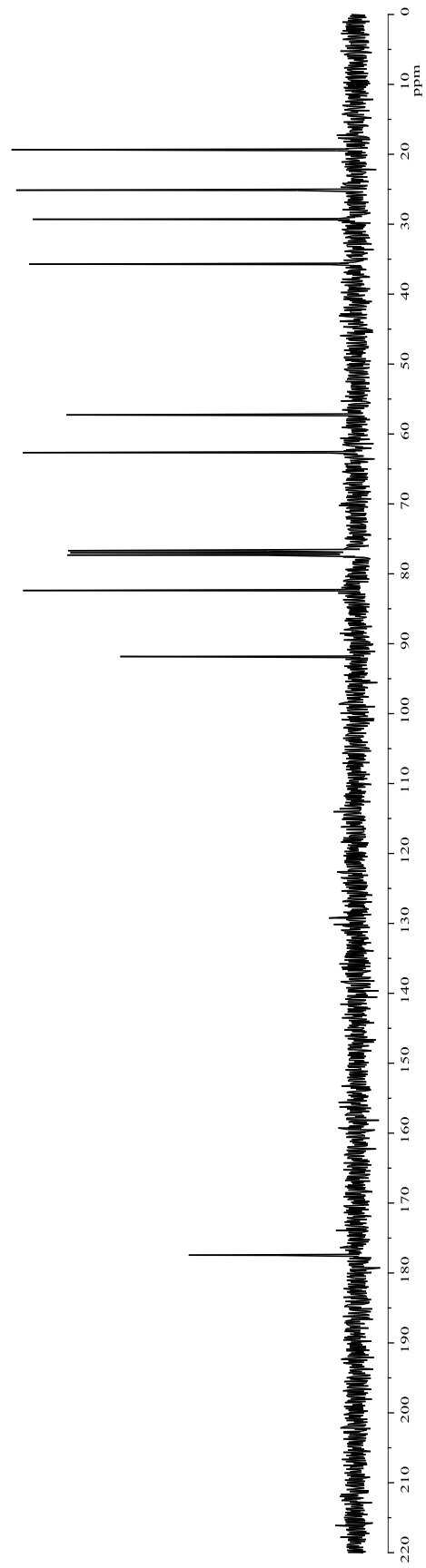
1.77



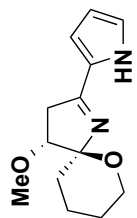
The 400 MHz ¹H NMR spectrum of compound **1.77** in CDCl₃.



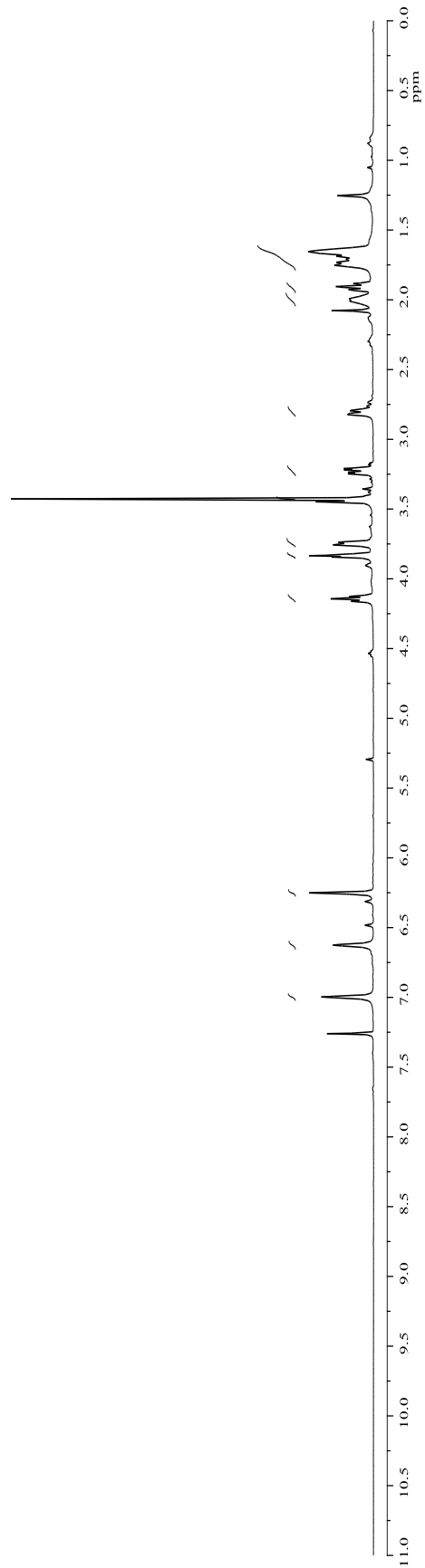
1.77



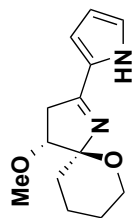
The 100 MHz ^{13}C NMR spectrum of compound 1.77 in CDCl_3 .



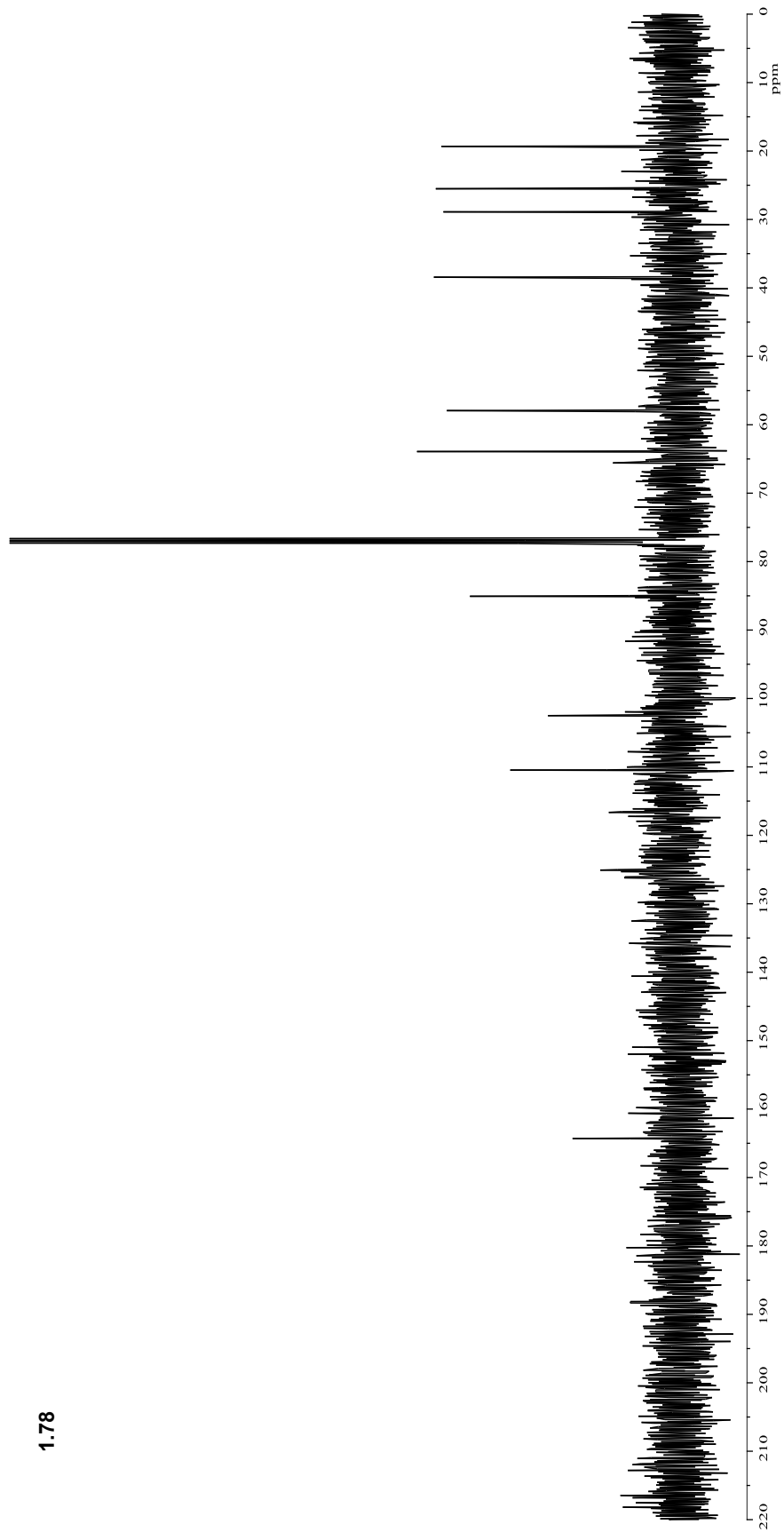
1.78



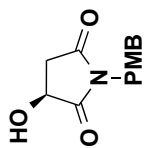
The 400 MHz ^1H NMR spectrum of compound 1.78 in CDCl_3 .



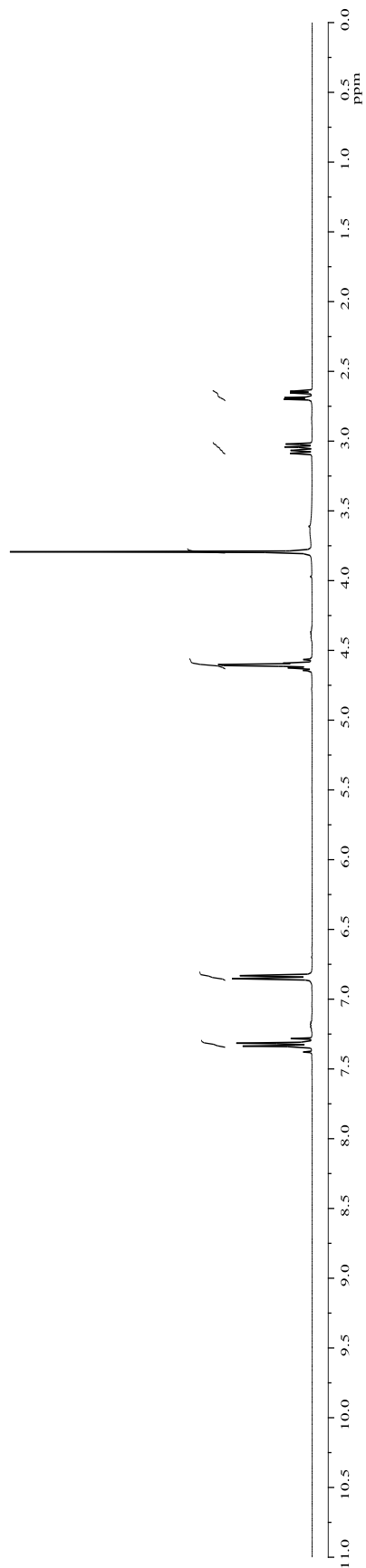
1.78



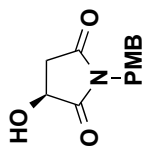
The 100 MHz ^{13}C NMR spectrum of compound 1.78 in CDCl_3 .



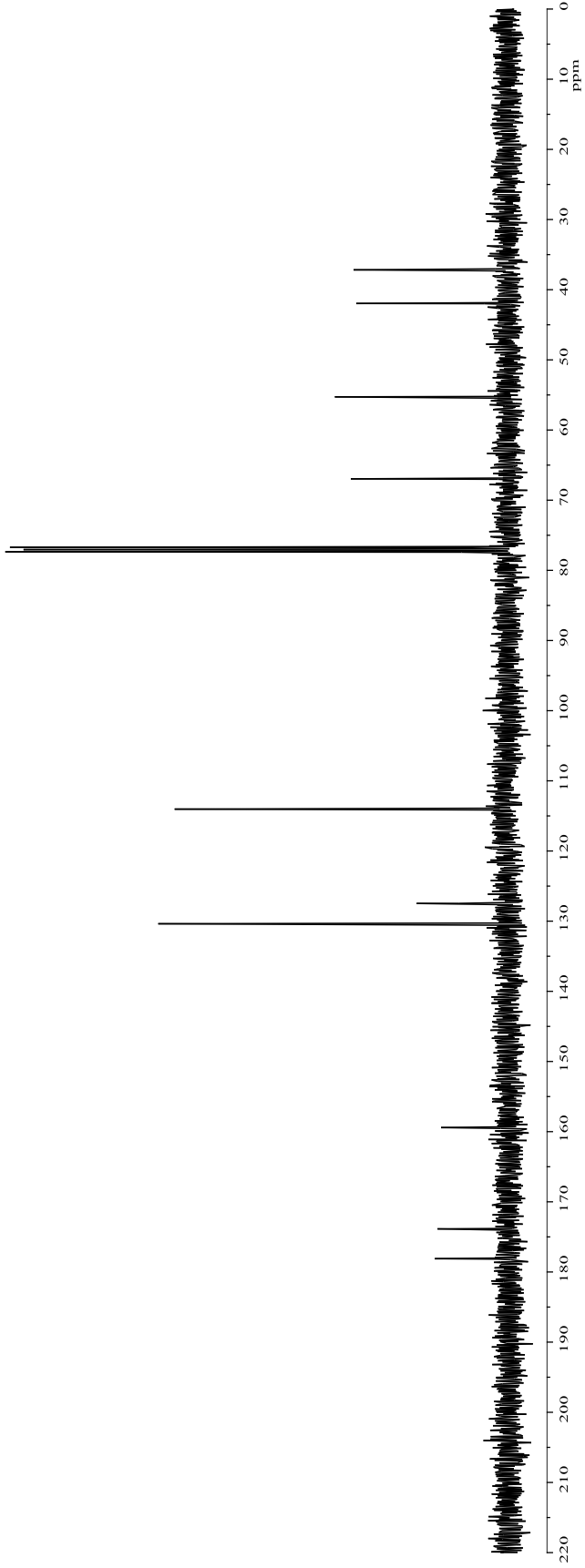
1.82



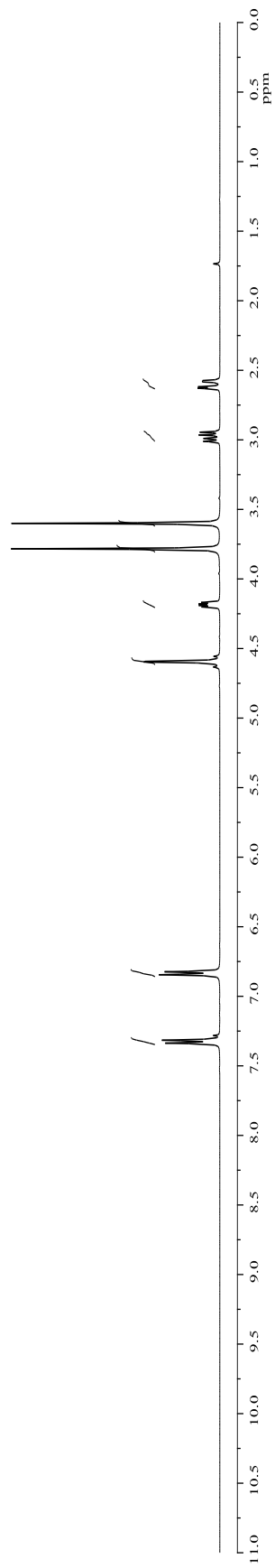
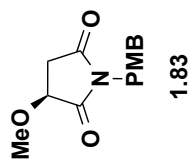
The 400 MHz ¹H NMR spectrum of compound **1.82** in CDCl₃.



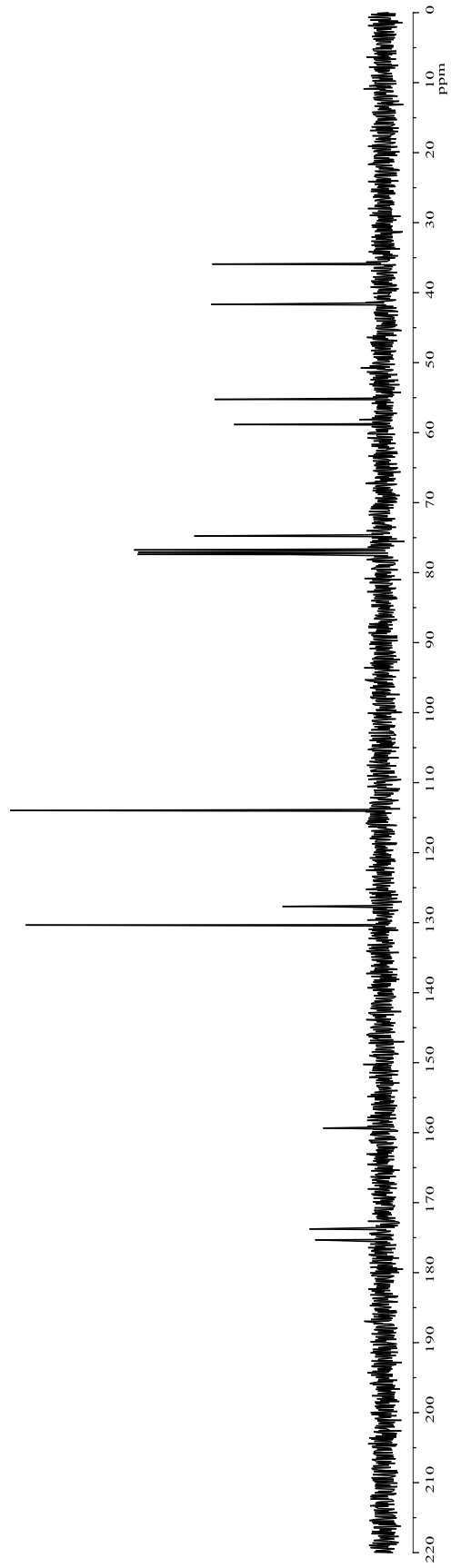
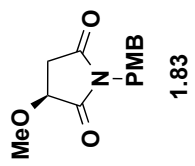
1.82



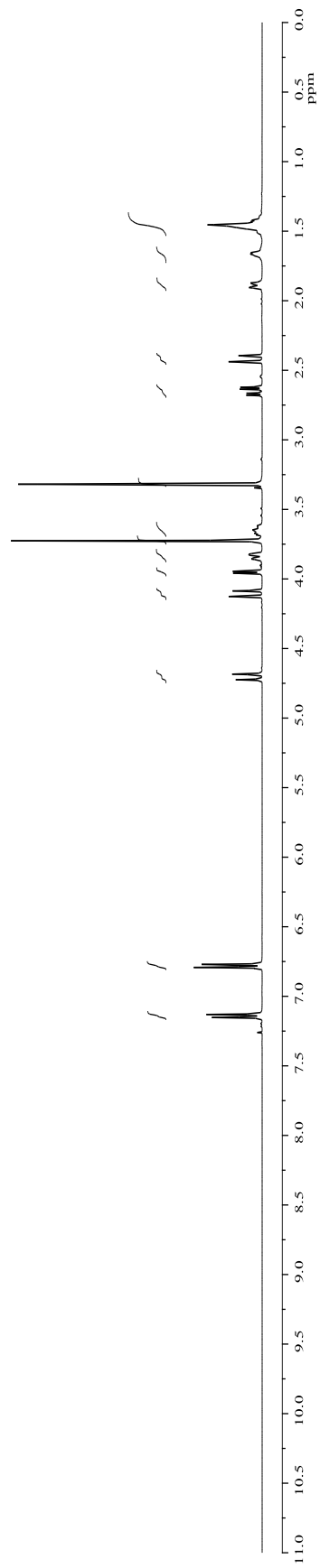
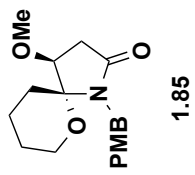
The 100 MHz ¹³C NMR spectrum of compound 1.82 in CDCl₃.



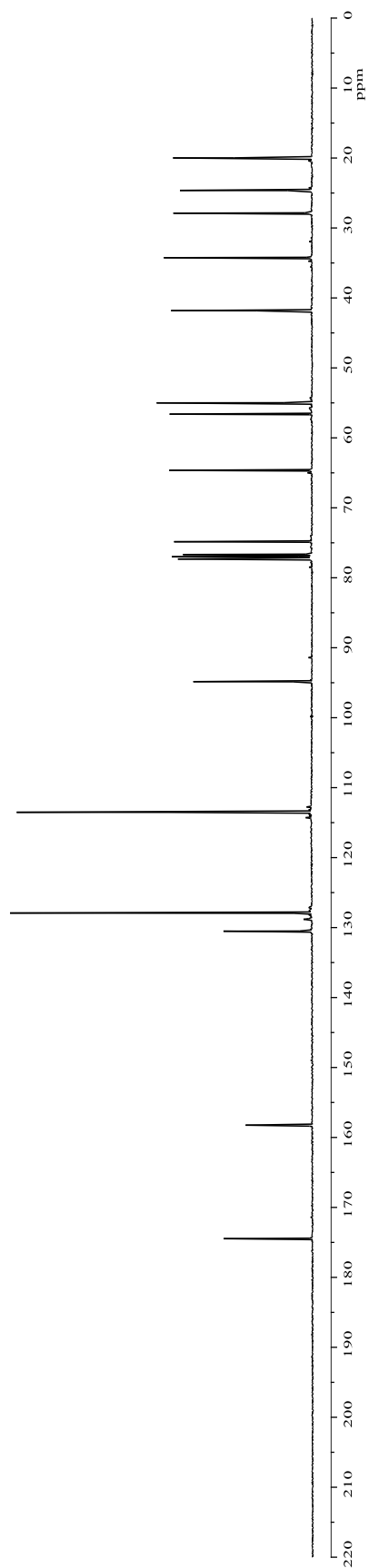
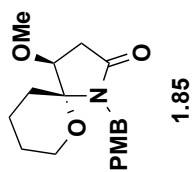
The 400 MHz ^1H NMR spectrum of compound **1.83** in CDCl_3 .



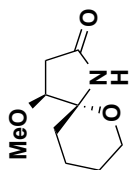
The 100 MHz ^{13}C NMR spectrum of compound **1.83** in CDCl_3 .



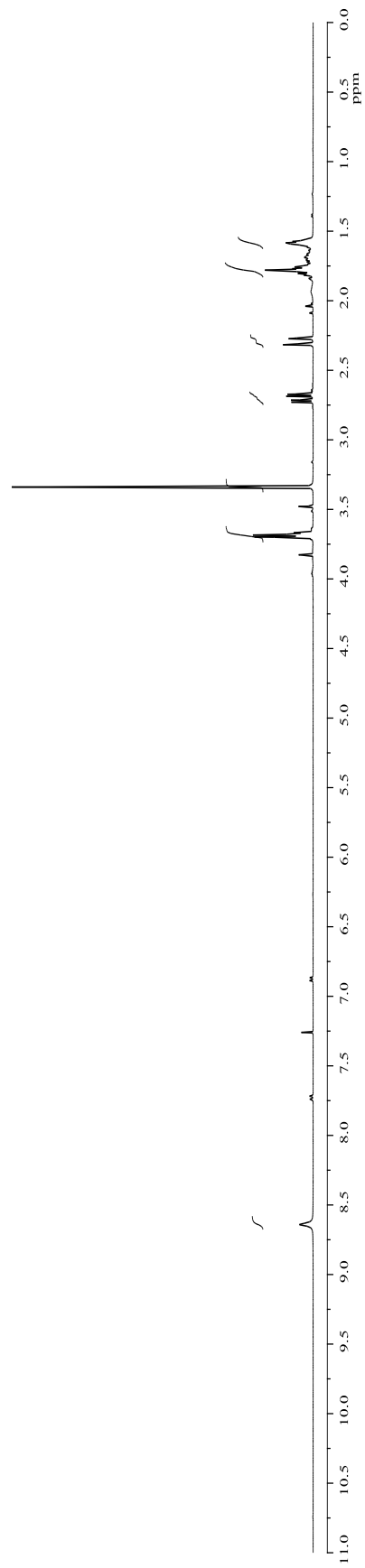
The 400 MHz ^1H NMR spectrum of compound **1.85** in CDCl_3 .



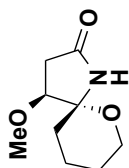
The 100 MHz ^{13}C NMR spectrum of compound **1.85** in CDCl_3 .



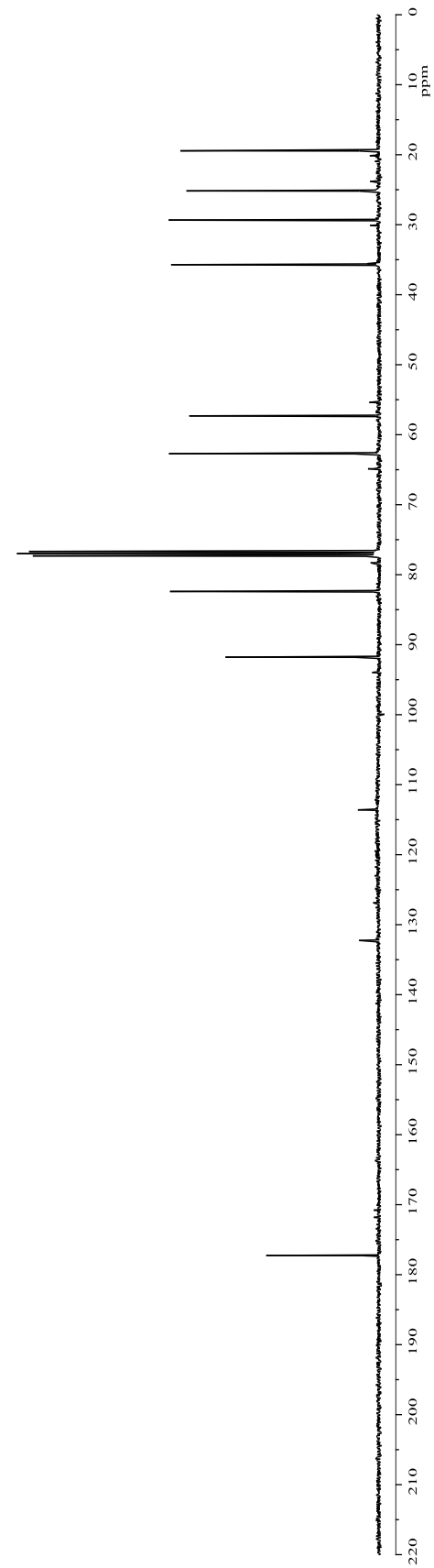
1.86



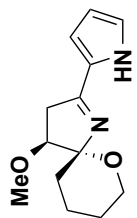
The 400 MHz ¹H NMR spectrum of compound **1.86** in CDCl₃.



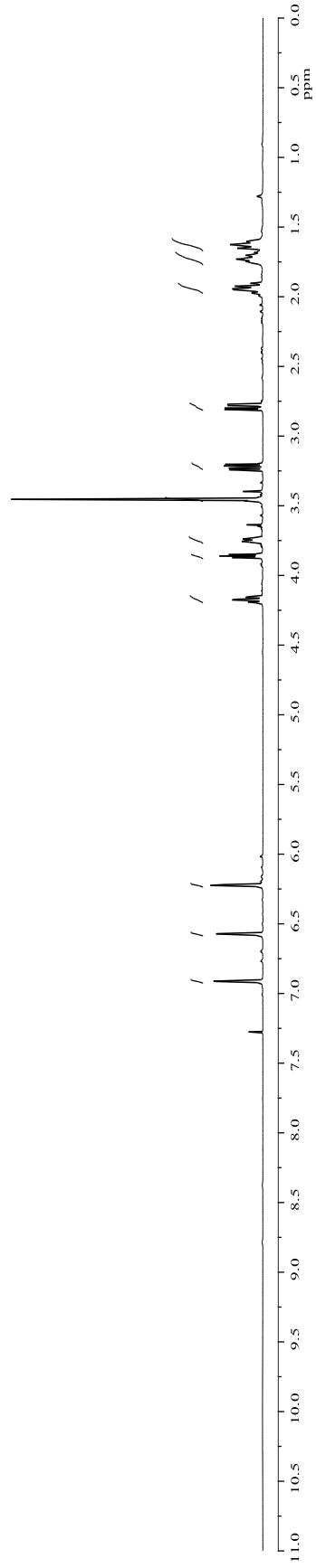
1.86



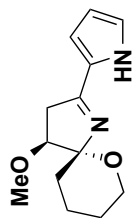
The 100 MHz ^{13}C NMR spectrum of compound **1.86** in CDCl_3 .



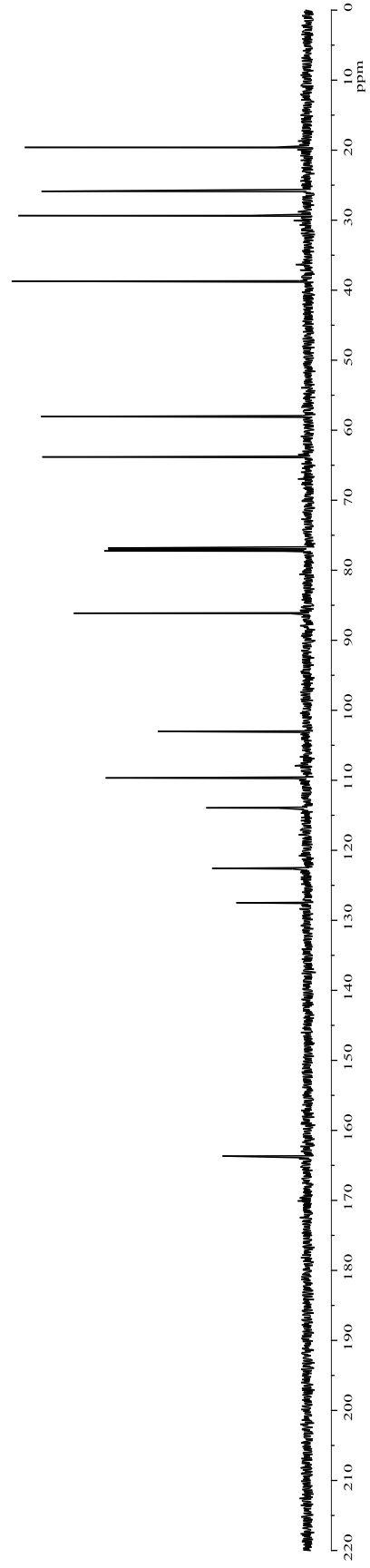
1.87



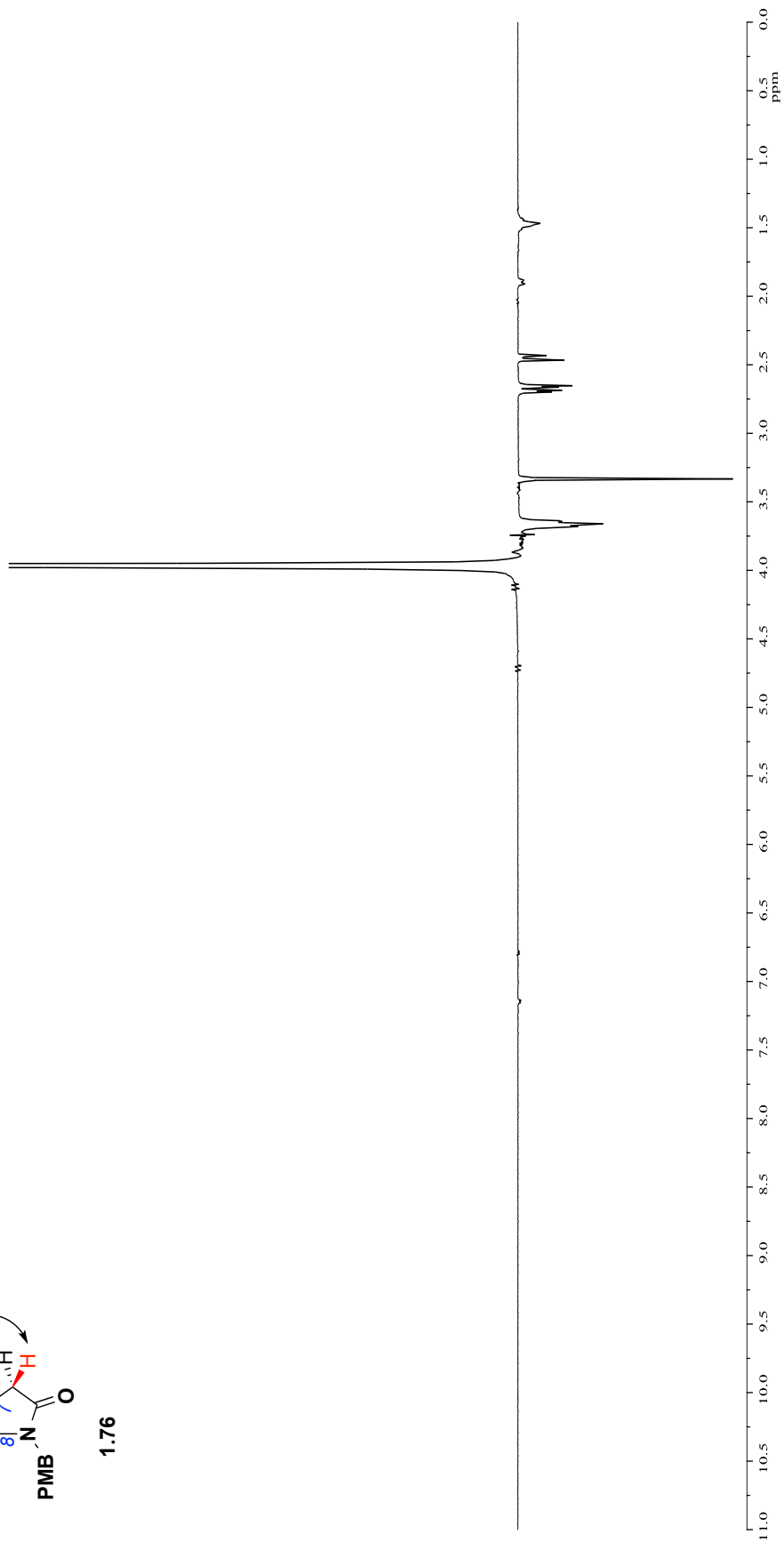
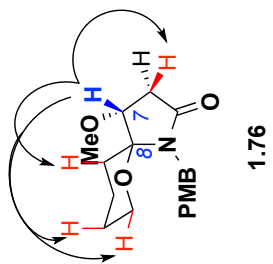
The 400 MHz ^1H NMR spectrum of compound **1.87** in CDCl_3 .



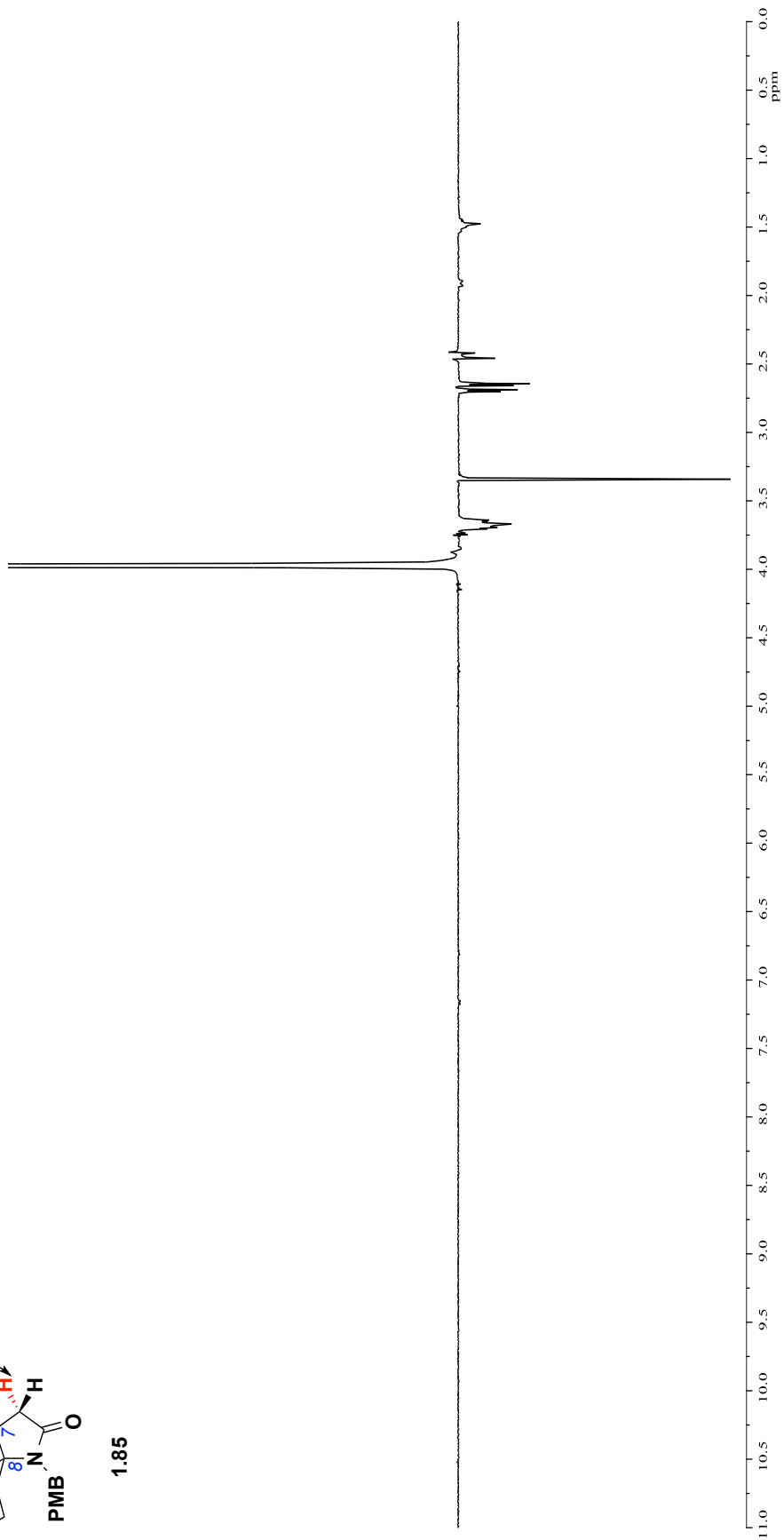
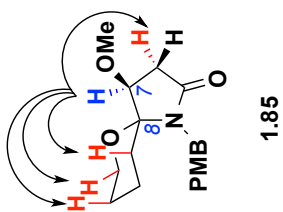
1.87



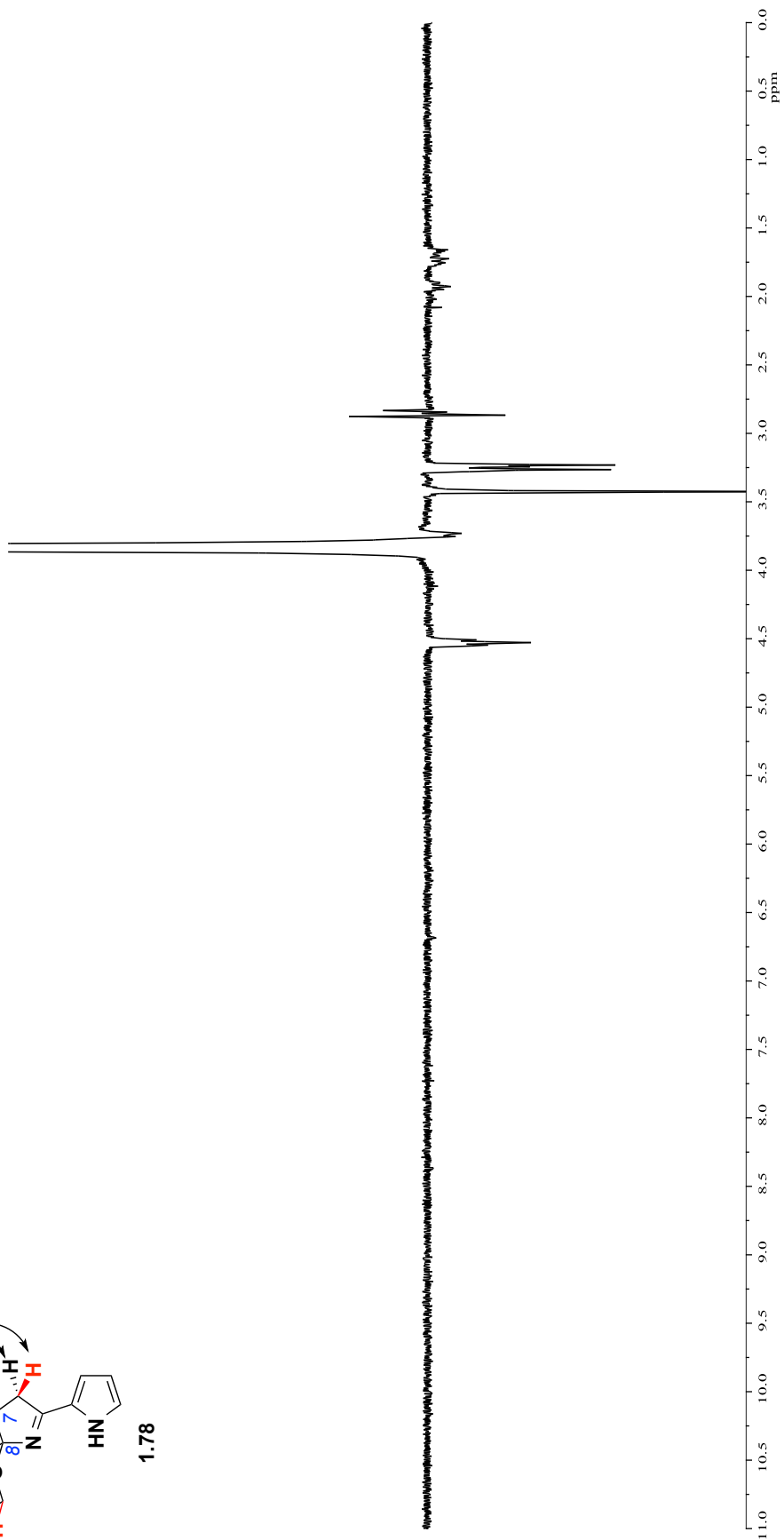
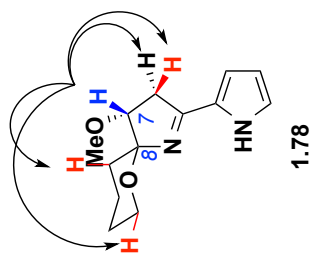
The 100 MHz ^{13}C NMR spectrum of compound 1.87 in CDCl_3 .



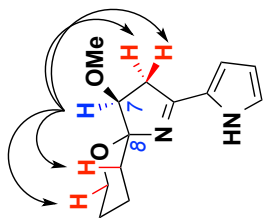
Diagnostic 1D nOe correlations in compound **1.76**.



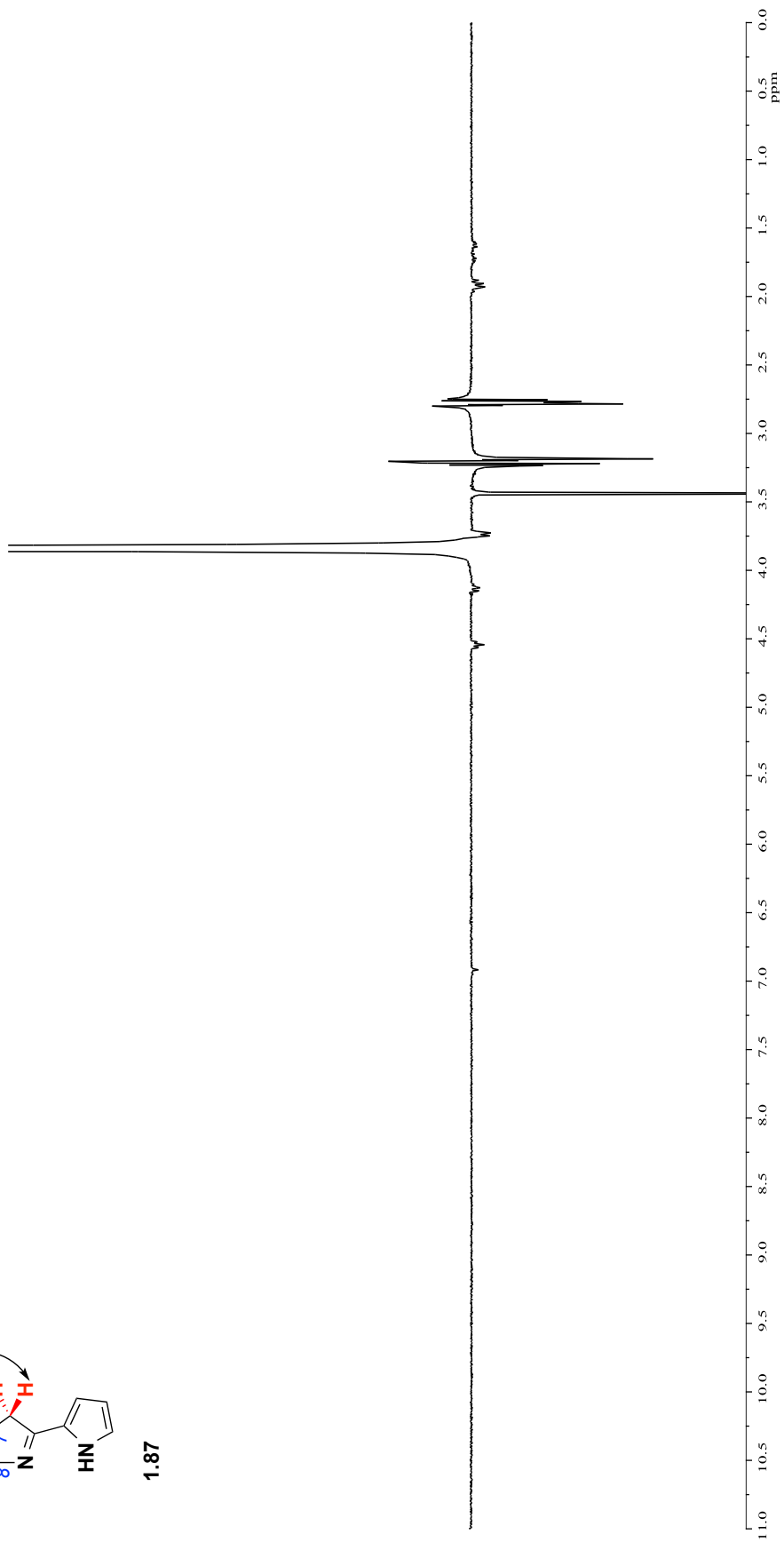
Diagnostic 1D nOe correlations in compound **1.85**.



Diagnostic 1D nOe correlations in compound 1.78.



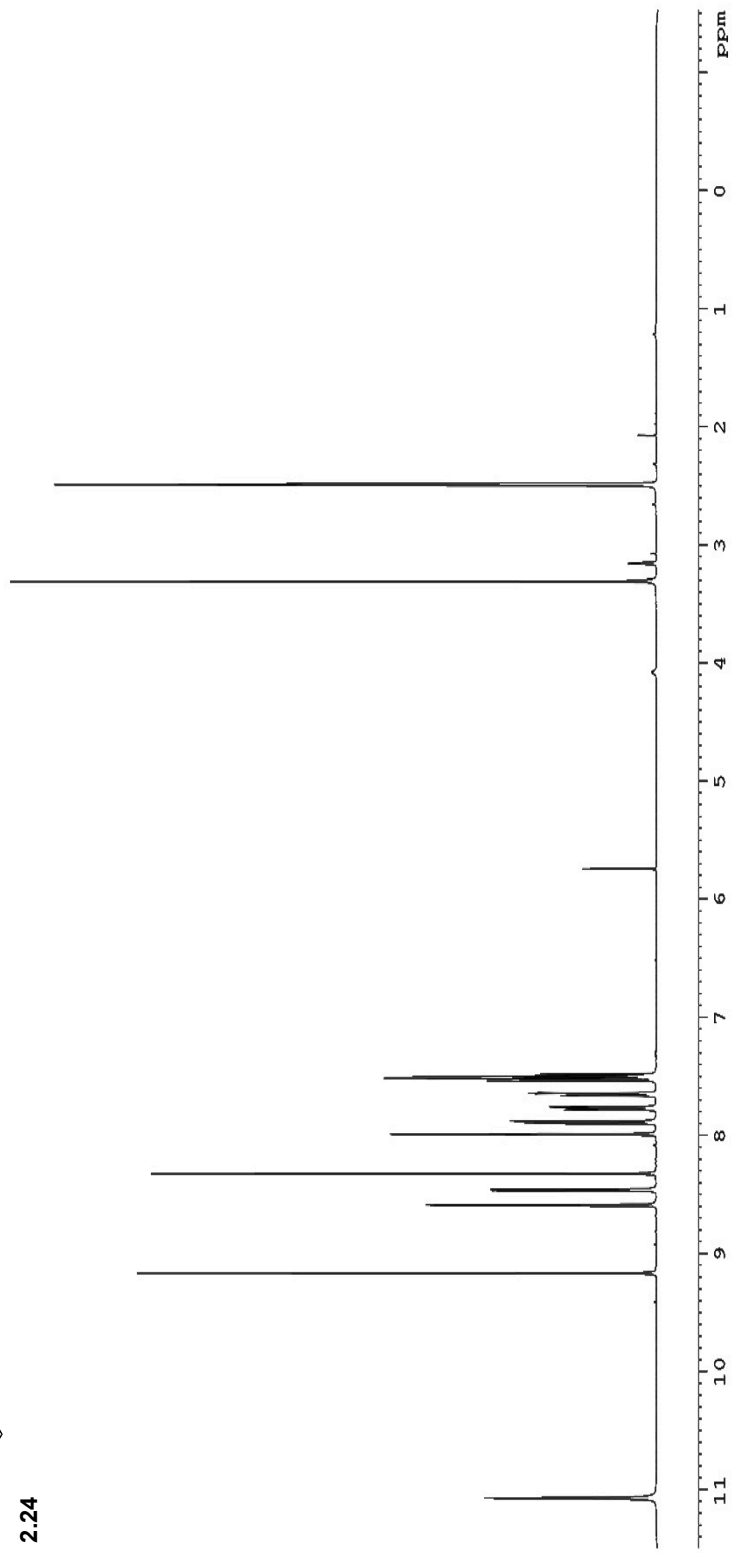
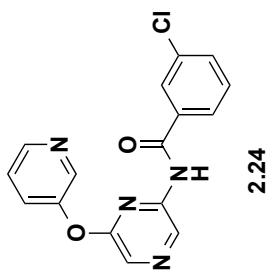
1.87



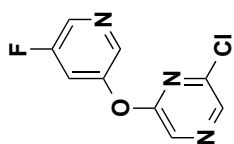
Diagnostic 1D nOe correlations in compound **1.87**.

Appendix B

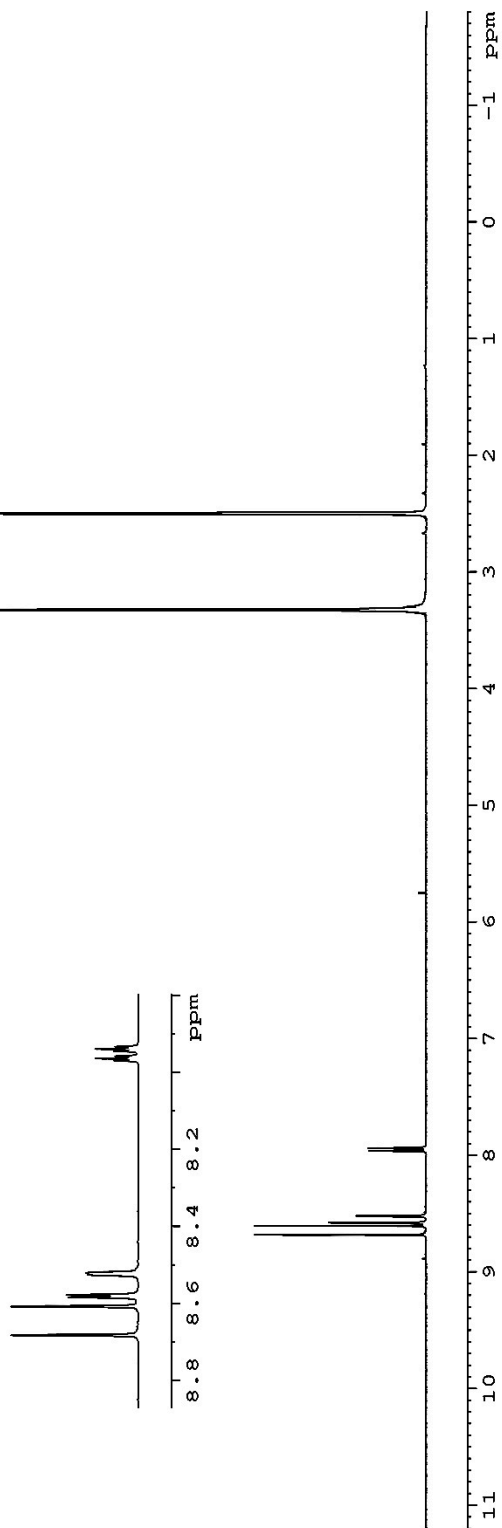
SPECTRA RELEVANT TO CHAPTER 2



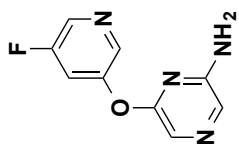
The 400 MHz ¹H NMR spectrum of compound 2.24 in DMSO-*d*₆.



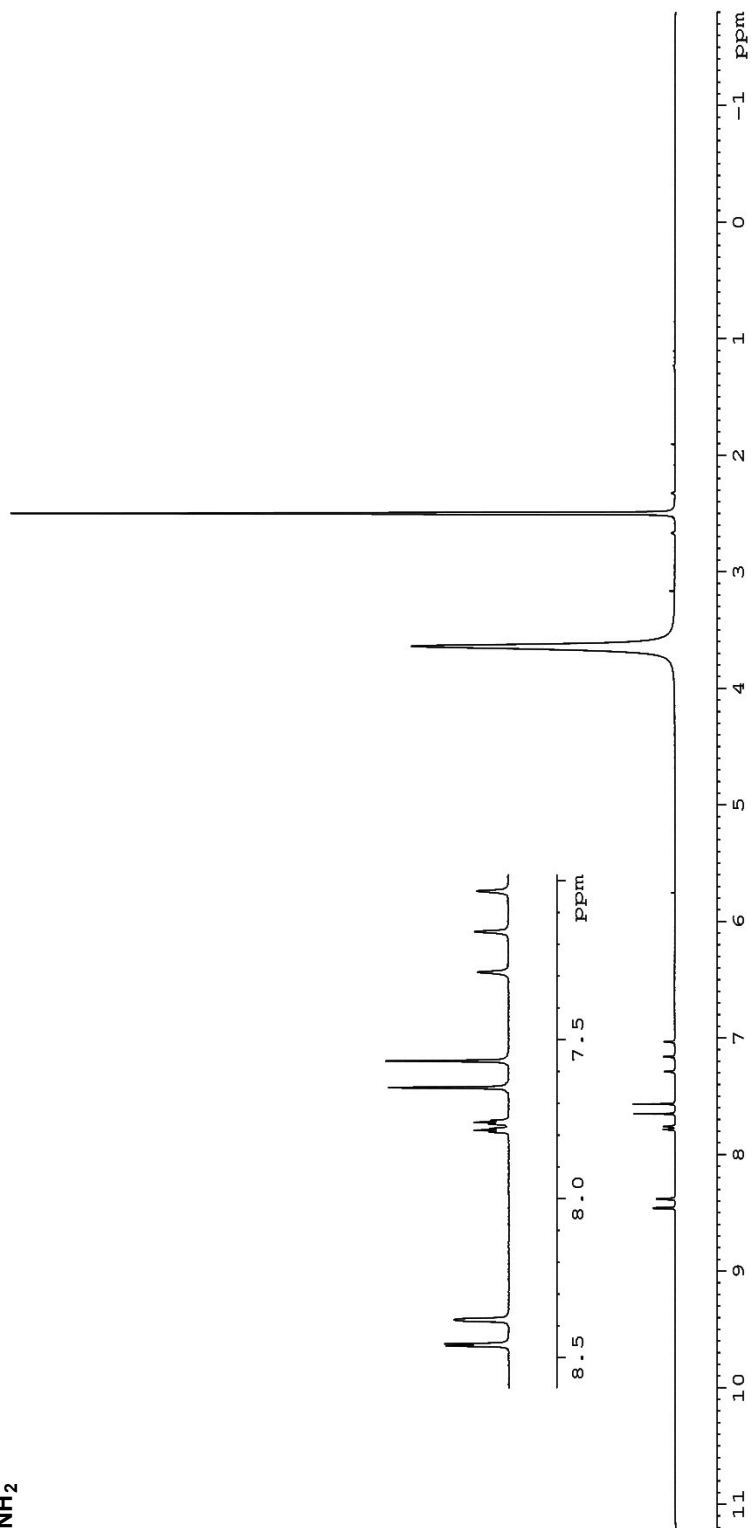
2.31a



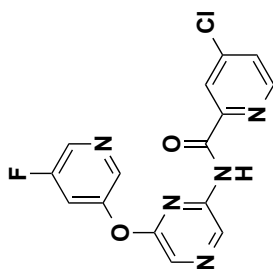
The 400 MHz ¹H NMR spectrum of compound 2.31a in DMSO-*d*₆.



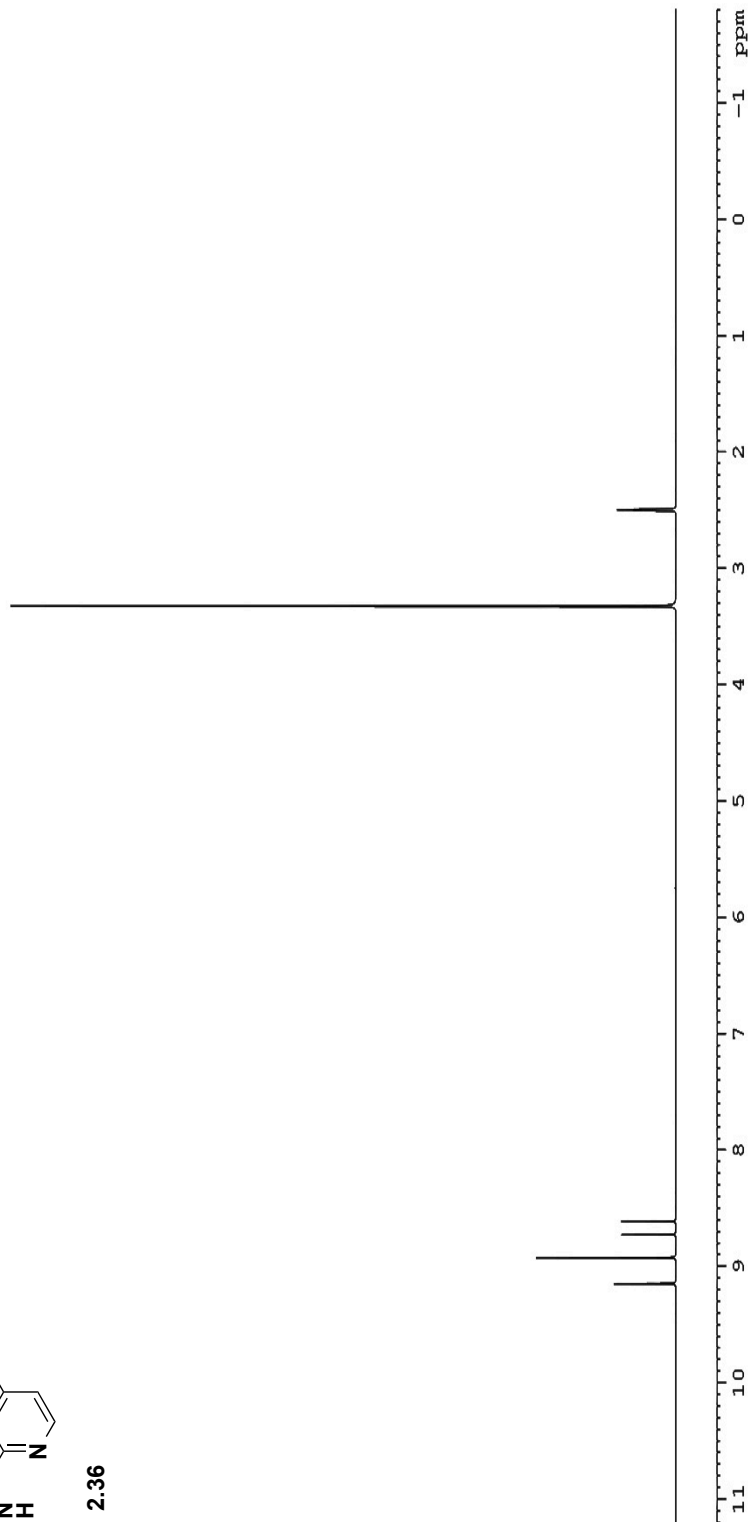
2.34a



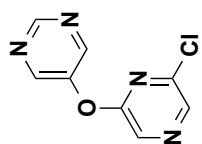
The 400 MHz ¹H NMR spectrum of compound 2.34a in DMSO-*d*₆.



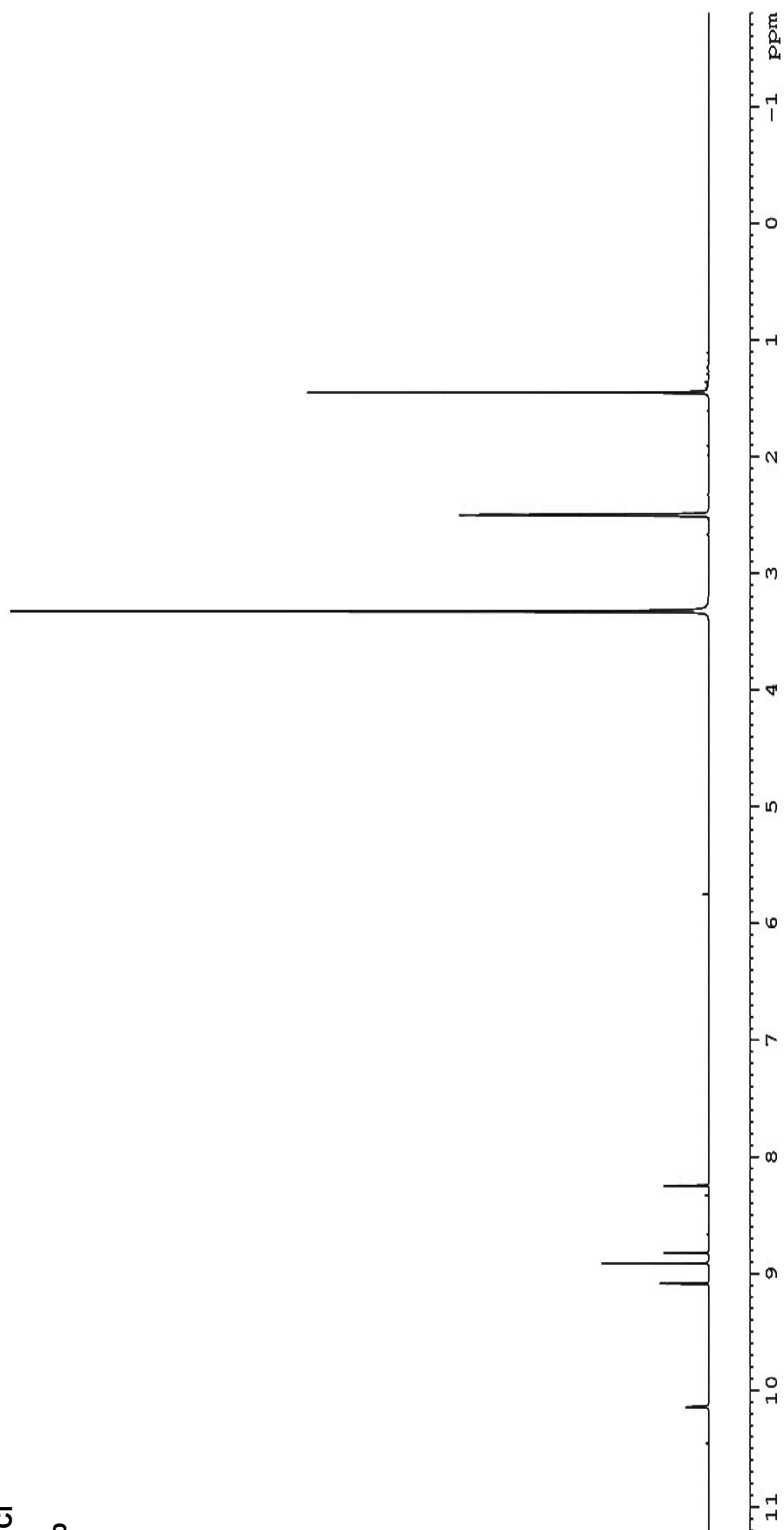
2.36



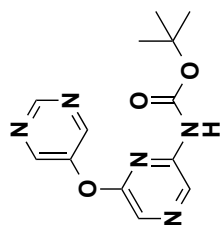
The 400 MHz ¹H NMR spectrum of compound 2.36 in DMSO-*d*₆.



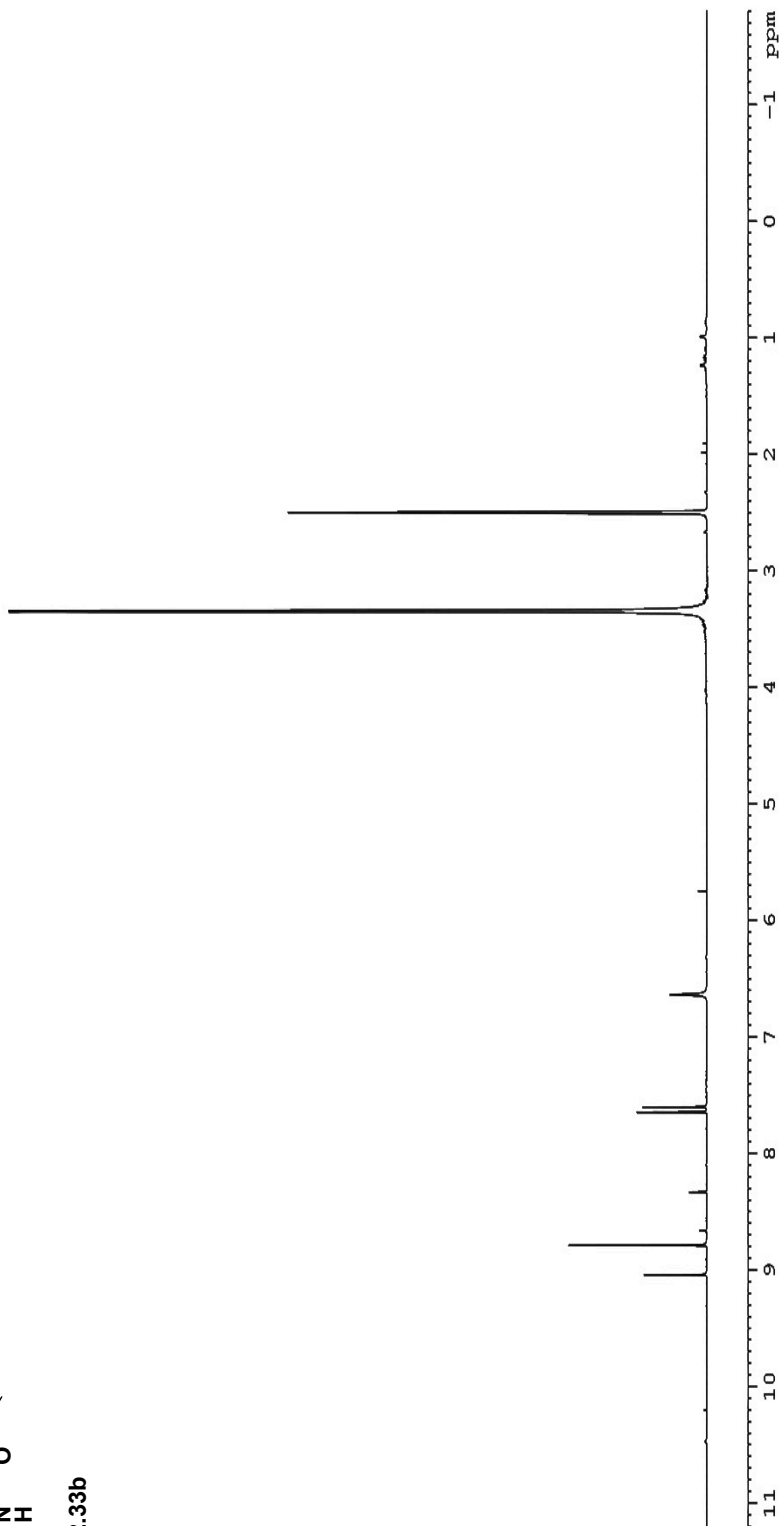
2.31b



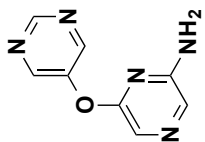
The 400 MHz ^1H NMR spectrum of compound **2.31b** in $\text{DMSO-}d_6$.



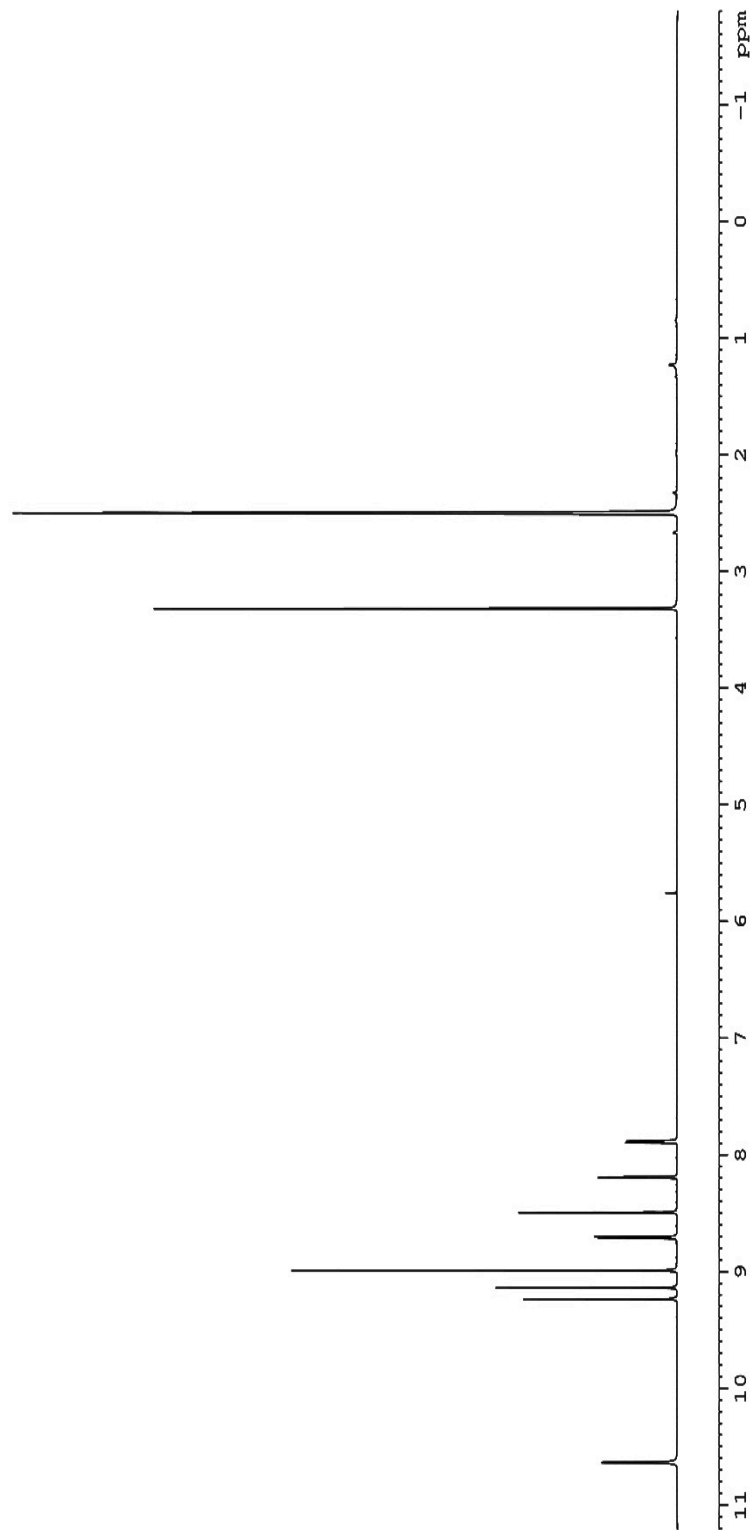
2.33b



The 400 MHz ^1H NMR spectrum of compound **2.33b** in $\text{DMSO-}d_6$.



2.34b



The 400 MHz ^1H NMR spectrum of compound **2.34b** in $\text{DMSO-}d_6$.

REFERENCES

1. Boonlarppradab, C., Kauffman, C. a, Jensen, P. R. & Fenical, W. Marineosins A and B, cytotoxic spiroaminals from a marine-derived actinomycete. *Org. Lett.* **10**, 5505–8 (2008).
2. Aldrich, L. N., Dawson, E. S. & Lindsley, C. W. Evaluation of the biosynthetic proposal for the synthesis of marineosins A and B. *Org. Lett.* **12**, 1048–51 (2010).
3. Aldrich, L. N. *et al.* Towards the Total Synthesis of Marineosin A: Construction of the Macrocyclic Pyrrole and an Advanced, Functionalized Spiroaminal Model. *European J. Org. Chem.* **2013**, 4215–4218 (2013).
4. Cai, X.-C. & Snider, B. B. Synthesis of the Spiroiminal Moiety and Approaches to the Synthesis of Marineosins A and B. *J. Org. Chem.* (2013). doi:10.1021/jo402178r
5. Fürstner, A. Chemistry and biology of roseophilin and the prodigiosin alkaloids: a survey of the last 2500 years. *Angew. Chem. Int. Ed. Engl.* **42**, 3582–603 (2003).
6. Fürstner, A., Grabowski, J. & Lehmann, C. W. Total Synthesis and Structural Refinement of the Cyclic Tripyrrole Pigment Nonylprodigiosin. *J. Org. Chem.* **64**, 8275–8280 (1999).
7. Fürstner, A., Grabowski, J., Lehmann, C. W., Kataoka, T. & Nagai, K. Synthesis and biological evaluation of nonylprodigiosin and macrocyclic prodigiosin analogues. *Chembiochem* **2**, 60–8 (2001).
8. Aldrich, L. N. Progress Toward the Total Synthesis of Marineosins A & B; Total Synthesis of Tambjamine K and Unnatural Analogs with Improved Anticancer Activity, and Discovery of Selective M1 Antagonists. *Diss. Theses* (2012).
9. Boger, D. L. & Patel, M. Total synthesis of prodigiosin, prodigiosene, and desmethoxyprodigiosin: Diels-Alder reactions of heterocyclic azadienes and development of an effective palladium(II)-promoted 2,2'-bipyrrole coupling procedure. *J. Org. Chem.* **53**, 1405–1415 (1988).
10. Boger, D. L. & Patel, M. Total synthesis of prodigiosin. *Tetrahedron Lett.* **28**, 2499–2502 (1987).
11. Clift, M. D. & Thomson, R. J. Development of a merged conjugate addition/oxidative coupling sequence. Application to the enantioselective total synthesis of metacycloprodigiosin and prodigiosin R1. *J. Am. Chem. Soc.* **131**, 14579–83 (2009).

12. Regourd, J., Ali, A. A.-S. & Thompson, A. Synthesis and anti-cancer activity of C-ring-functionalized prodigiosin analogues. *J. Med. Chem.* **50**, 1528–36 (2007).
13. Papireddy, K. *et al.* Antimalarial activity of natural and synthetic prodiginines. *J. Med. Chem.* **54**, 5296–306 (2011).
14. D'Alessio, R. *et al.* Synthesis and Immunosuppressive Activity of Novel Prodigiosin Derivatives. *J. Med. Chem.* **43**, 2557–2565 (2000).
15. Melvin, M. S., Calcutt, M. W., Noftle, R. E. & Manderville, R. A. Influence of the A -Ring on the Redox and Nuclease Properties of the Prodigiosins: Importance of the Bipyrrrole Moiety in Oxidative DNA Cleavage. *Chem. Res. Toxicol.* **15**, 742–748 (2002).
16. Parikh, S. A. *et al.* Phase II Study of Obatoclax Mesylate (GX15-070), a Small-Molecule BCL-2 Family Antagonist, for Patients With Myelofibrosis. *Clin. Lymphoma Myeloma Leuk.* **10**, 285–289 (2010).
17. Konopleva, M. *et al.* Mechanisms of antileukemic activity of the novel Bcl-2 homology domain-3 mimetic GX15-070 (obatoclax). *Cancer Res.* **68**, 3413–20 (2008).
18. Carter, G. T. Natural products and Pharma 2011: strategic changes spur new opportunities. *Nat. Prod. Rep.* **28**, 1783–9 (2011).
19. NCI Cancer Bulletin - National Cancer Institute. (2011). at <<http://www.cancer.gov/ncicancerbulletin/041911/page5>>
20. Panarese, J. D. *et al.* Spiroaminal Model Systems of the Marineosins with Final Step Pyrrole Incorporation. *Tetrahedron Lett.* **54**, 2231–2234 (2013).
21. Kelly, W. L. Intramolecular cyclizations of polyketide biosynthesis: mining for a “Diels-Alderase”? *Org. Biomol. Chem.* **6**, 4483–93 (2008).
22. Cai, X.-C., Wu, X. & Snider, B. B. Synthesis of the spiroiminal moiety of marineosins A and B. *Org. Lett.* **12**, 1600–3 (2010).
23. Sydor, P. K. *et al.* Regio- and stereodivergent antibiotic oxidative carbocyclizations catalysed by Rieske oxygenase-like enzymes. *Nat. Chem.* **3**, 388–92 (2011).
24. Salem, S. M. Biosynthesis of Marineosin, a Spiroaminal Undecylprodiginine Natural Product. *Diss. Theses* (2012). Paper 936. http://pdxscholar.library.pdx.edu/open_access_etds/936

25. Cai, X.-C. & Snider, B. B. Synthesis of the Spiroiminal Moiety and Approaches to the Synthesis of Marineosins A and B. *J. Org. Chem.* (2013). doi:10.1021/jo402178r
26. Zheng, J.-F., Chen, W., Huang, S.-Y., Ye, J.-L. & Huang, P.-Q. A divergent asymmetric approach to aza-spiropyran derivative and (1S,8aR)-1-hydroxyindolizidine. *Beilstein J. Org. Chem.* **3**, 41 (2007).
27. Huang, P. Q. *et al.* A new approach to (S)-4-hydroxy-2-pyrrolidinone and its 3-substituted analogues. *Tetrahedron: Asymmetry* **10**, 3309–3317 (1999).
28. Grieco, P. A. & Larsen, S. D. An intramolecular immonium ion variation of the Diels-Alder reaction: synthesis of (+-)-dihydrocannivonine. *J. Org. Chem.* **51**, 3553–3555 (1986).
29. Rapoport, H. & Castagnoli, N. 2,2''-Bipyrrole. *J. Am. Chem. Soc.* **84**, 2178–2181 (1962).
30. Baraznenok, I. L., Nenajdenko, V. G. & Balenkova, E. S. Chemical Transformations Induced by Triflic Anhydride. *Tetrahedron* **56**, 3077–3119 (2000).
31. Li, G., Zhang, X., Li, Q., Feng, P. & Shi, Y. A concise approach to the spiroiminal fragment of marineosins. *Org. Biomol. Chem.* **11**, 2936–8 (2013).
32. Parikh, J. R. & Doering, W. v. E. Sulfur trioxide in the oxidation of alcohols by dimethyl sulfoxide. *J. Am. Chem. Soc.* **89**, 5505–5507 (1967).
33. Bal, B. S., Childers, W. E. & Pinnick, H. W. Oxidation of α,β -unsaturated aldehydes. *Tetrahedron* **37**, 2091–2096 (1981).
34. Ley, S. V., Norman, J., Griffith, W. P. & Marsden, S. P. Tetrapropylammonium Perruthenate, Pr 4 N + RuO 4 - , TPAP: A Catalytic Oxidant for Organic Synthesis. *Synthesis (Stuttg)*. **1994**, 639–666 (1994).
35. Niswender, C. M. & Conn, P. J. Metabotropic glutamate receptors: physiology, pharmacology, and disease. *Annu. Rev. Pharmacol. Toxicol.* **50**, 295–322 (2010).
36. Conn, P. J., Christopoulos, A. & Lindsley, C. W. Allosteric modulators of GPCRs: a novel approach for the treatment of CNS disorders. *Nat. Rev. Drug Discov.* **8**, 41–54 (2009).
37. Julio-Pieper, M., Flor, P. J., Dinan, T. G. & Cryan, J. F. Exciting times beyond the brain: metabotropic glutamate receptors in peripheral and non-neural tissues. *Pharmacol. Rev.* **63**, 35–58 (2011).

38. Substituted heteroarylamine carboxamide analogs as mglur5 negative allosteric modulators and methods of making and using the same. (2011).
39. GPCR. at <<http://www.nature.com/scitable/topicpage/gpcr-14047471#>>
40. mGlu5 Receptor Antagonists: A Novel Class of Anxiolytics? at <http://journals.prous.com/journals/servlet/xmlxsl/pk_journals.xml_summary_pr?p_JournalId=3&p_RefId=473&p_IsPs=Y>
41. Felts, A. S. *et al.* Discovery of VU0409106: A negative allosteric modulator of mGlu5 with activity in a mouse model of anxiety. *Bioorg. Med. Chem. Lett.* **23**, 5779–5785 (2013).
42. Conn, P. J. & Pin, J. P. Pharmacology and functions of metabotropic glutamate receptors. *Annu. Rev. Pharmacol. Toxicol.* **37**, 205–37 (1997).
43. Varney, M. A. *et al.* SIB-1757 and SIB-1893: Selective, Noncompetitive Antagonists of Metabotropic Glutamate Receptor Type 5. *J. Pharmacol. Exp. Ther.* **290**, 170–181 (1999).
44. Laras, Y. *et al.* Substituted thiazolamide coupled to a redox delivery system: a new gamma-secretase inhibitor with enhanced pharmacokinetic profile. *Org. Biomol. Chem.* **3**, 612–8 (2005).
45. Sharma, S., Rodriguez, A. L., Conn, P. J. & Lindsley, C. W. Synthesis and SAR of a mGluR5 allosteric partial antagonist lead: Unexpected modulation of pharmacology with slight structural modifications to a 5-(phenylethynyl)pyrimidine scaffold. *Bioorg. Med. Chem. Lett.* **18**, 4098–4101 (2008).
46. Kalvass, J. C. & Maurer, T. S. Influence of nonspecific brain and plasma binding on CNS exposure: implications for rational drug discovery. *Biopharm. Drug Dispos.* **23**, 327–38 (2002).
47. Morrison, R. D. *et al.* The role of aldehyde oxidase and xanthine oxidase in the biotransformation of a novel negative allosteric modulator of metabotropic glutamate receptor subtype 5. *Drug Metab. Dispos.* **40**, 1834–1845 (2012).
48. Njung'e, K. & Handley, S. L. Effects of 5-HT uptake inhibitors, agonists and antagonists on the burying of harmless objects by mice; a putative test for anxiolytic agents. *Br. J. Pharmacol.* **104**, 105–12 (1991).
49. Broekkamp, C. L., Rijk, H. W., Joly-Gelouin, D. & Lloyd, K. L. Major tranquilizers can be distinguished from minor tranquilizers on the basis of effects on marble burying and swim-induced grooming in mice. *Eur. J. Pharmacol.* **126**, 223–229 (1986).

50. Deacon, R. M. J. Digging and marble burying in mice: simple methods for in vivo identification of biological impacts. *Nat. Protoc.* **1**, 122–4 (2006).
51. Lindsley, C. W. *et al.* (3-Cyano-5-fluorophenyl)biaryl negative allosteric modulators of mGlu(5): Discovery of a new tool compound with activity in the OSS mouse model of addiction. *ACS Chem. Neurosci.* **2**, 471–482 (2011).